Numerical Analysis of Loss and Performance Optimization Efforts for LP Steam Turbine Exhaust Hoods

Von der Fakultät Energie-, Verfahrens- und Biotechnik
der Universität Stuttgart zur Erlangung der Würde eines Doktors
der Ingenieurwissenschaften (Dr.-Ing.) genehmigte Abhandlung

Vorgelegt von
Dickson Katiwa Munyoki
aus Kitui, Kenia

Hauptberichter: Prof. Tekn. Dr. Damian Vogt
Mitberichter: Prof. Simon Hogg

Tag der mündlichen Prüfung: 02. März 2023

Institut für Thermische Strömungsmaschinen
und Maschinenlaboratorium der Universität Stuttgart

2024

Declaration

The work contained in this thesis was done by Dickson Katiwa Munyoki under the supervision of Prof. Tekn. Dr. Damian Vogt and technical guidance of Dr. -Ing. Markus Schatz, both of the Institute of Thermal Turbomachinery and Machinery Laboratory, University of Stuttgart. No part of this thesis has been submitted elsewhere for any other degree or qualification and all findings reported in this thesis is the author's own work. Relevant work carried out by other researchers and referred in this report is appropriately cited.

Acknowledgments

To the Almighty God, the creator of the universe, I give thanks for giving me peace of mind and good health in a far land away from my family for over three years. To my supervisor, Prof. Tekn. Dr. Damian Vogt and my technical advisor, Prof. Dr. -Ing. Markus Schatz, I thank you for assisting me throughout this project and for offering me the opportunity to undertake the research in the first place. I appreciate all the guidance, support and corrections throughout the course of my work. Thank you for the many hours spent reading my work and giving the so important feedback and always doing so in a timely manner. I thank you for the opportunities you accorded me to attend conferences and present my findings by giving both the authorization and financial support. These opportunities gave me a chance to travel to Poland, Norway and USA for the first time in my life. These memories will live on and am forever grateful. I am thankful to Dr. -Ing. Juergen F. Mayer and Dr. -Ing. Annemarie Paul for their guidance and assistance during my initial stages of PhD application. I would like to appreciate my masters thesis supervisor, Prof. Dr. -Ing. Eckehard Specht of Otto von Guericke University of Magdeburg, Germany and Prof. Dr. Eng. John M. Kihiu of Jomo Kenyatta University of Agriculture and Technology, Kenya for their recommendation letters which made it possible for me to be considered for this research work. I also appreciate Mr. Peketsa Mangi and Mr. Geoffrey Muchemi for their efforts when I was requesting for a study leave from my employer.

I would like to thank all my former fellow research engineers and PhD students at the Institute of Thermal Turbomachinery and Machinery Laboratory, University of Stuttgart for helping me at the initial stages of my research. I would like to sincerely thank Mr. Benjamin Kuschel for his help during the initial test rig setup and programming in LabVIEW. I would like to thank Dipl.-Ing. Fabian Mueller for helping me from time to time with my experiments. I would like to appreciate Mr. Christopher Fuhrer for his help in learning most of the softwares I used for the numerical simulations and analysis. My gratitute also goes to the Machinery Laboratory technical team members: Mr. Martin Brausewetter, Mr. Martin Krinn and Mr. Pavlos Tipsios for their assistance in fabrication of experimental parts and assembly of the test rig.

I take this opportunity to thank my employer, the Kenya Electricity Generating Co. Plc (KenGen) for giving me a study leave to undertake this research in Germany. Am very grateful to the German Academic Exchange Service (DAAD) for awarding me a scholarship to pursue this PhD research. I thank my mother, Joyce Wayua Munyoki, for bringing me up and educating me. Finally to my wife, Irene, thank you for being there for me throughout this journey. It was not easy because of the geographical distance between us but now we can look back and proudly say, "yes, we did it". Thank you for your love, support, encouragement and for taking care of our daughters, Shanice and Ariana, in my absence.

Publications

Findings of the work included in this thesis have been presented at ASME conferences and published as ASME conference proceedings:

1. Munyoki, D.; Schatz, M.; Vogt, D.M.: Detailed Numerical Study of the Main Sources of Loss and Flow Behavior in Low Pressure Steam Turbine Exhaust Hoods. ASME Turbo Expo 2017: Turbomachinery Technical Conference and Exposition, June 2017, Charlotte, North Carolina, USA, GT2017- 63269

2. Munyoki, D.; Schatz, M.; Vogt, D.M.: Numerical Investigation of the Influence of Hood Height Variation on Performance of Low Pressure Steam Turbine Exhaust Hoods. ASME Turbo Expo 2018: Turbomachinery Technical Conference and Exposition, June 2018, Oslo, Norway, GT2018- 76562

3. Munyoki, D.; Schatz, M.; Vogt, D.M.: Numerical Investigation of the Influence of Flow Deflection at the Upper Hood on Performance of Low Pressure Steam Turbine Exhaust Hoods. ASME Turbo Expo 2019: Turbomachinery Technical Conference and Exposition, June 2019, Phoenix, Arizona, USA, GT2019- 90391

Abstract

Most of the world's power is produced by large steam turbines using fossil fuel, nuclear and geothermal energy. The LP exhaust hoods of these turbines are known to contribute significantly to the losses within the turbine, hence a minor improvement in their performance, which results in a lower back-pressure and hence higher enthalpy drop for the steam turbine, will give a considerable benefit in terms of fuel efficiency.

This thesis is divided in two parts: In the first part, a detailed numerical analysis of sources of loss in LP exhaust hoods is carried out. The methodology used in doing this starts with a well known approach from literature where the diffuser inflow is divided into sectors and the streamlines originating from these sectors are used for flow field visualization. In the new approach, this existing procedure is developed further such that the flow properties of the various streamlines are analysed at predetermined evaluation surfaces within the flow domain. In so doing, this more advanced methodology shows clearly where most losses occur within the flow domain and makes it easier to make decisions for improving the exhaust hood performance. Using this approach, most losses are found to occur at the upper hood and are associated with the swirling flows resulting from the difficulty experienced by the flow in turning towards the condenser. At the lower side of the diffuser, the initial flow direction is more or less towards the condenser hence these flows contribute less to exhaust hood losses. The numerical results of the reference configuration based on a scaled axial-radial diffuser test rig operated by ITSM are thoroughly validated at both the design and overload operating conditions and at three tip jet Mach numbers (0, 0.4 and 1.2).

The second part of the thesis focuses on possible modifications of LP exhaust hoods to achieve better performance. Having identified that most losses occur at the upper hood and the reason for it well understood, the influence of changing the hood height above the diffuser is extensively investigated at design load. It is found that the hood height has huge impact on performance and that an optimum hood exists for a given tip jet Mach number. Deflector configurations at the upper hood are also investigated. They are found to redirect the flow at the upper hood and minimise the intensity of the swirling flows hence leading to improvement in performance of LP steam turbine exhaust hoods. The best performing deflector configuration, the double wall deflector, is found to give a considerable improvement in performance amounting to 20% at design load and 40% at overload both at tip jet Mach number of 0.4 (corresponding to shrouded last stage blades).

Kurzfassung

Der größte Anteil der weltweiten elektrischen Leistung wird von großen Dampfturbinen erzeugt, die mit fossilen und nuklearen Brennstoffen und Geothermie betrieben werden. Die Strömung im Abdampfgehäuse von Niederdruck-Dampfturbinen trägt signifikant zu den Gesamtverlusten von Dampfturbinen bei, so dass selbst eine relativ geringe Verbesserung der Strömungsführung in diesem Bereich beachtliche Auswirkungen auf den Wirkungsgrad der Anlage hat, da der Gegendruck am Austritt der Turbine absinkt und somit eine höhere Enthalpiedifferenz für die Expansion zur Verfügung steht.

Die vorliegende Arbeit ist in zwei Teile gegliedert: Im ersten Teil wird eine detaillierte numerische Analyse der Verluste in Abdampfgehäusen von Niederdruck-Dampfturbinen vorgenommen. Die dazu verwendete Methodik stützt sich auf einen in der Literatur bereits beschriebenen Ansatz, bei welchem die Einströmung in den Diffusor, der sich zwischen Turbinenaustritt und Abdampfgehäuse befindet, in Sektoren aufgeteilt wird. Von diesen Sektoren ausgehend werden Stromlinien genutzt, um das Strömungsfeld zu analysieren. Dieser Ansatz wird durch eine Auswertung der Strömungszustände entlang der Stromlinien an festgelegten Ebenen innerhalb des Gehäuses erweitert. Damit kann identifiziert werden, wo die höchsten Verluste auftreten, so dass Maßnahmen zur Verbesserung der Strömungsführung erarbeitet werden können. Aus der Auswertung geht hervor, dass die Strömung im Oberteil des Gehäuses auf Grund der mehrfachen Umlenkung auf dem Weg zum Kondensator stark verlustbehaftet ist. Die Abströmung aus dem unteren Teil des Diffusors muss nur wenig umgelenkt werden und trägt daher kaum zur Verlustentstehung bei.

Die numerischen Strömungssimulationen wurden an einer skalierten Referenzgeometrie durchgeführt, die auch experimentell im Auslegungspunkt sowie im Überlastzustand bei drei unterschiedlichen Spaltmachzahlen (0, 0.4 und 1.2) vermessen wurde. Mithilfe der Messdaten konnten die Ergebnisse der Simulationen umfangreich validiert werden.

Der zweite Teil der Arbeit befasst sich mit der Verbesserung der Strömungsführung durch geometrische Modifikationen am ND-Abdampfgehäuse. Basierend auf dem im ersten Teil gewonnenen Verständnis der Verlustmechanismen im Oberteil des Gehäuses wird zunächst der Einfluss der Haubenhöhe charakterisiert, wobei sich herausstellt, dass diese einen enormen Einfluss auf die Verluste im Abdampfgehäuse hat. Insbesondere zeigt sich, dass es für jede der untersuchten Spaltmachzahlen eine optimale Haubenhöhe gibt. Des Weiteren wird die Anordnung einfacher Umlenkbleche im Oberteil des Gehäuses untersucht, die die Strömungsführung verbessern und damit die Effizienz des Abdampfgehäuses deutlich erhöhen. Mit einem "double wall deflector", d.h. einer Umlenkung der Strömung in axialer Richtung und Umfangsrichtung, wird dabei eine signifikante Verbesserung erreicht. Bei einer Spaltmachzahl von 0.4 (entsprechend der Strömung bei Deckbandschaufeln) wird die Effizienz im Vergleich zur Referenzgeometrie um 20% im Auslegungspunkt und 40% bei Überlast erhöht.

Contents

List of Figures

List of Tables

Nomenclature

A_1	m^2	Blockage 1 area
A_2	m^2	Blockage 2 area
A_H	m^2	Hood area
A_T	m^2	Total blockage area
b	mm	Blockage 1 height
C_f	-	Skin friction coefficient
C_p	-	Pressure recovery coefficient for a given sector flow at a given evaluation surface
Cpk	-	Pressure recovery coefficient at condenser plane
d	mm	Diffuser outlet diameter
$d1, d2$	mm	Blockage 2 diameters
h	mm	Exhaust hood height measured from the half-joint plane upwards
L		Left
	m	Characteristic length
LHS		Left hand side
n		Number of streamlines used per sector flow
P		Evaluation plane
Pk	Pa	Area average of static pressure at condenser plane
P_{si}	Pa	Static pressure at point of intersection between a streamline and an evaluation surface
P_{sin}	Pa	Area average of static pressure at diffuser inlet
Ps	Pa	Average value of static pressure at an evaluation surface for a given sector flow
Ps_{in}	Pa	Average value of static pressure at diffuser inlet for a sector flow
P_{ti}	Pa	Total pressure at the point of intersection between a streamline and an evaluation surface
P_{tin}	Pa	Mass flow average of total pressure at diffuser inlet
Pt	Pa	Mass flow average of total pressure at an evaluation surface for a given sector flow
Pt_{in}	Pa	Mass flow average of total pressure at diffuser inlet for a sector flow
Re		Reynolds number
s	mm	Diffuser separation thickness
u	m/s	Velocity vector in the x-direction
u'	m/s	Velocity vector in the x'-direction
U_{fric}	m/s	Frictional velocity

v	m/s	Velocity vector in the y-direction
v_i	m/s	Velocity at point of intersection between a streamline and an evaluation surface
w	m/s	Velocity vector in the z-direction
	m	Exhaust hood width
x'	m	Transposed x-coordinate oriented along an inclined evaluation surface at the upper hood
(x, y, z)	m	Coordinates of the exhaust hood
y^+		Non-dimensional wall distance
Δy	m	Wall spacing

Greek Letters

α	-	Blockage area ratio
γ	-	Free area ratio
ζ	-	Dissipation coefficient for a given sector flow at a given evaluation surface
θ	[°]	Angle positioning the evaluation surfaces within the upper hood in Matlab
μ	kg/ms	Dynamic viscosity
ξ	-	Residual kinetic energy coefficient for a given sector flow at a given evaluation surface
ρ	kg/m^3	Free stream density
ρ_i	kg/m^3	Density at the point of intersection between a streamline and an evaluation surface
τ_{wall}	Pa	The wall shear stress

Subscripts

i	Streamline index
$norm$	Normalized
ref	Reference configuration

1 Introduction

1.1 Background

Large low-pressure steam turbines have enormous power output and are responsible for about 60% of the world's power generation [68]. The exhaust hoods of these turbines present major losses due to friction and inability of the hood to properly diffuse the flow. Their function and especially the diffuser downstream of the last turbine stage is to transfer the turbine leaving kinetic energy to potential energy while guiding the flow from the turbine exit plane to the condenser. Large scale steam turbines use an axial-radial exhaust diffuser where the condenser is situated below the turbine [68]. This reduces the axial length of the diffuser, hence lowers the cost of exhaust hood systems. Additionally, the space between the turbine and the generator is reduced resulting in a shorter shaft requirement between them hence lowering the risk of shaft vibration. Fig. 1.1 shows a steam turbine power plant with down-flow configuration exhaust hood structure where the condenser is located below the turbine.

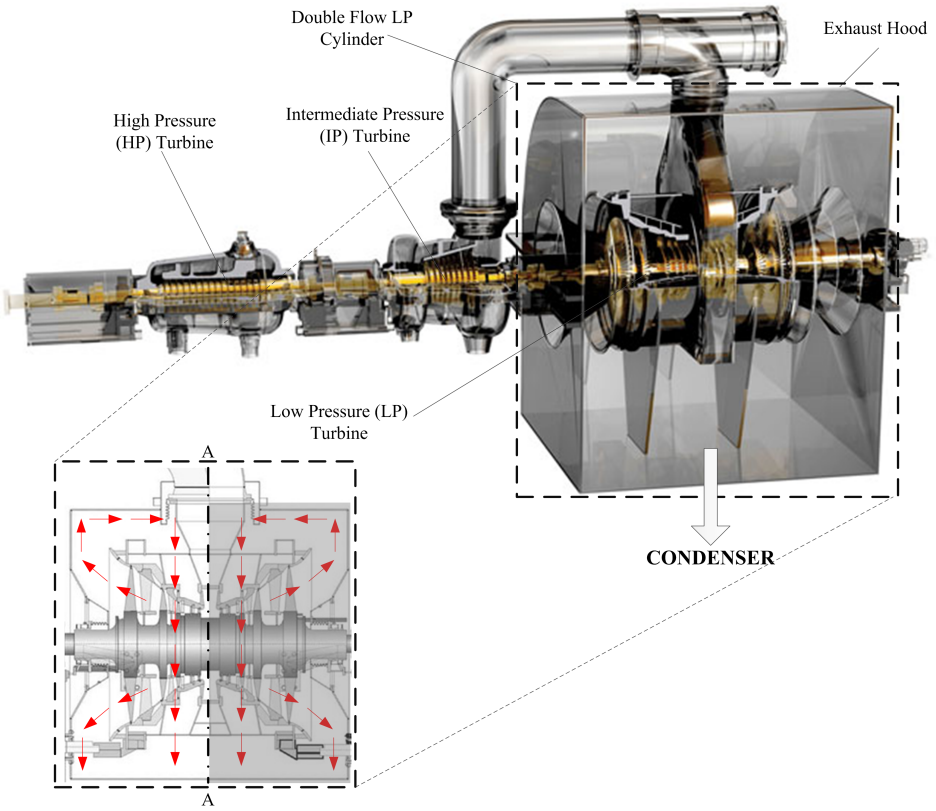

Figure 1.1 – Steam turbine power plant [7, 25]

However, the use of an axial-radial diffuser is not without problems. This is because the flow in such a diffuser is no longer rotational symmetric, since the flow in the top part of the diffuser stagnates at the turbine casing, while the flow in the bottom part does not encounter any obstacle. The rotational flow downstream of the last stage blades has non-uniform distributions of pressure, velocity and temperature. This, combined with the high flow turning of the compact axial-radial diffuser results in the formation of a series of separations within the diffuser [10]. Fig. 1.2 shows these separations occuring within the diffuser and the exhaust hood. Despite the vertical symmetry of the hood geometry, the flow structure within the exhaust hood is asymmetric because swirl is prevalent at the turbine exit [8]. While purely axial diffusers can achieve pressure recoveries in the range of 70 – 80%, the performance of axial-radial diffusers is often much worse with some diffusers exhibiting negative static pressure recovery coefficient values. This is because of the additional flow turning and the resulting highly dissipative swirling flows.

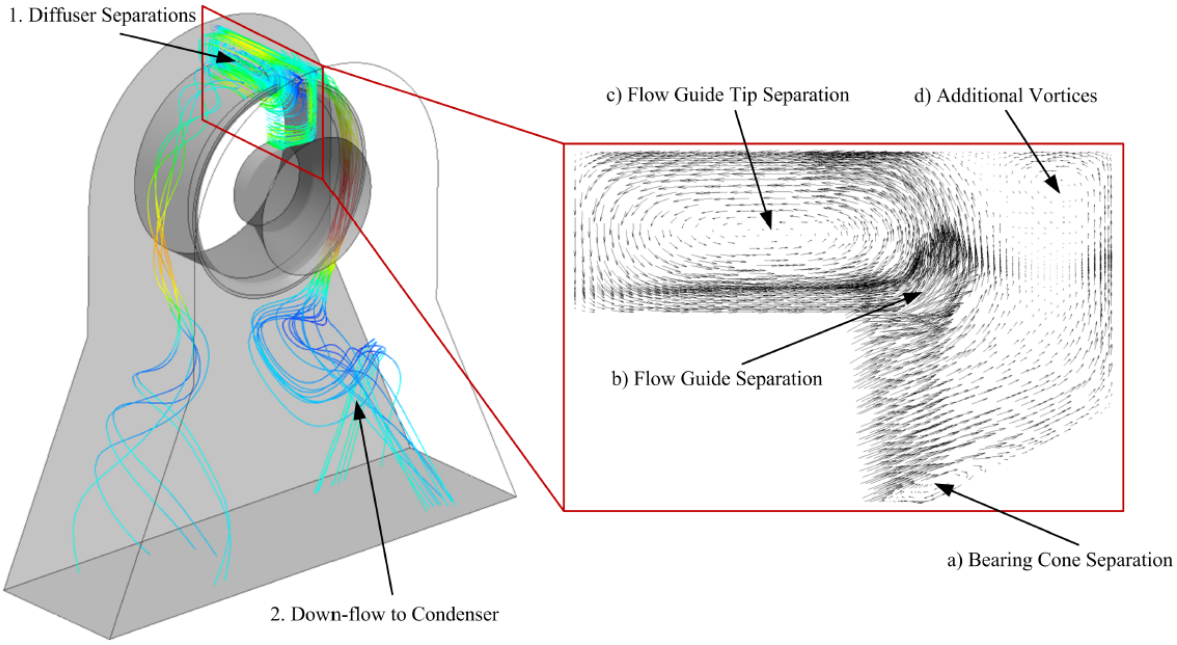

Figure 1.2 – Separations within the exhaust hood of LP steam turbine [7]

Efficiency is probably the most important performance parameter for most turbomachines. Present levels of efficiency have been achieved by an ever improving understanding of the fluid mechanics and thermodynamics of the flow which in turn has been obtained by a combination of improved experimental and theoretical methods applied both to whole machines and to individual components. In particular, the advent of modern numerical methods of flow calculation has greatly improved the ability to model the flow through a machine [14]. Understanding the various sources of loss in a steam turbine power plant is the first step in designing more efficient machines. Tanuma et al. [69] ranked the sources of loss in steam turbines as shown in Fig.1.3. In their ranking, the aerodynamic loss of LP steam turbines exhaust hoods was second with a magnitude almost equivalent to losses associated with stator and rotor blading of LP turbine which was ranked first. The current study focuses on identification of loss sources in exhaust

hoods and geometrical variations on hood outer casing aimed at improving their performance.

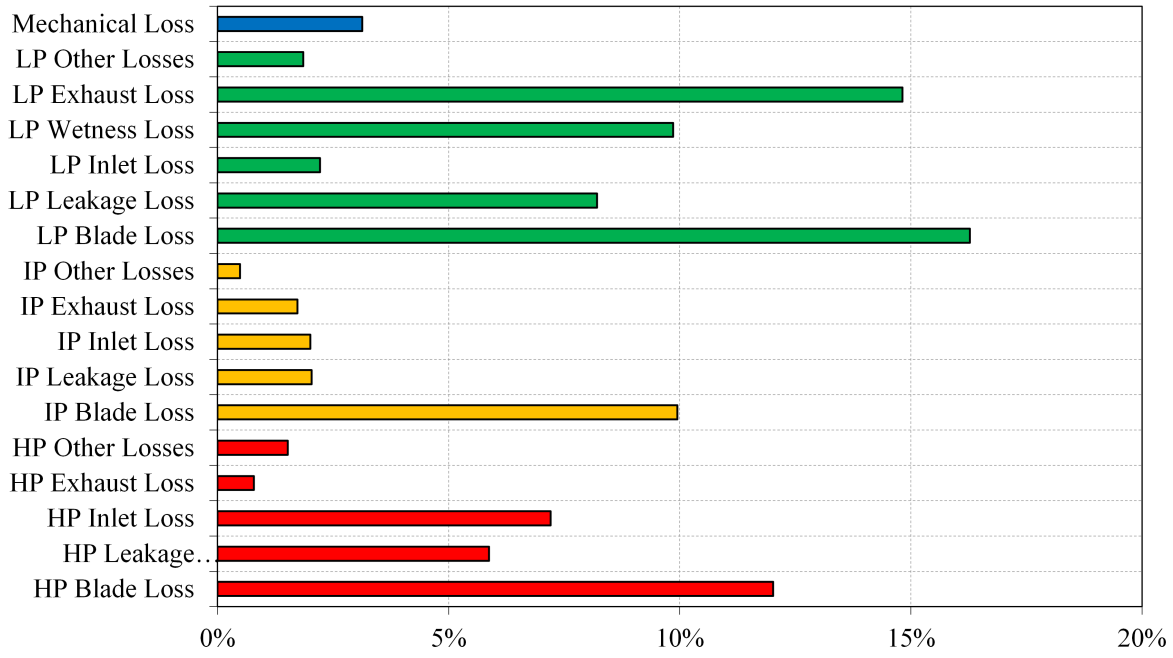

Figure 1.3 – Relative fraction of losses in steam turbines as reported by Tanuma et al. [69]

The exhaust hood of a large scale steam turbine significantly influences the overall performance of the steam power plant. An exhaust system with a high static pressure recovery produces a low back-pressure at the turbine exit hence increased work generated by the turbine. It is estimated that a pressure recovery improvement of 10%-points in the diffuser and exhaust hood translates into 1% of last stage efficiency [64].

1.2 Thesis objective

The main objective of the current research is to numerically study the sources of loss in exhaust hoods, devise geometrical interventions for loss reduction and hence suggest geometrical modifications to improve the overall performance of exhaust hoods.

Since large scale steam turbines have an enormous power output and are responsible for about 60% of the world's power generation [68], only a minor improvement of the exhaust hood, which results in a lower back-pressure and hence higher enthalpy drop for the steam turbine, will give a considerable benefit in terms of fuel efficiency. To decide on geometrical modifications for improving hood performance, a thorough understanding of loss sources is necessary. A detailed numerical investigation carried out revealed that swirling flows especially at the upper hood are the main contributors of losses in exhaust hood. Therefore, interventions suggested are aimed at reducing the intensity of vortices

formed within the top part of the exhaust hood. The following specific objectives are pursued:

- Experimental measurement of the reference hood configuration at two operating points (design- and overload with variation of tip jet Mach number) using a 1:15 scaled axial-radial diffuser test rig operated by ITSM. Numerical models were created from geometries of the test rig, solved and their results validated using the experimental data.
- Numerical investigation of sources of loss and flow behavior for the reference hood configuration. This was done for two loading conditions (design- and overload).
- Numerical investigation of influence of hood height variation on the pressure recovery coefficient of LP exhaust hoods.
- Numerical investigation of geometrical modifications of the exhaust hood outer casing. The loss study showed that swirling flows at the upper hood were the main causes of dissipation within the exhaust hood. Therefore, deflector portions were included in the outer casing to guide the flow and minimize vortex intensity at the upper hood and hence improve the exhaust hood performance.

1.3 Thesis scope and overview

The current research focus on performance improvement of LP exhaust hood of large scale steam turbines. To achieve this, Computational Fluid Dynamics (CFD) is used to analyze the flow structure within the exhaust hood in order to identify the main sources of loss which is known from literature to be significant [7, 19, 46, 68, 82]. The numerical models for the reference configuration used for this study are developed from an axial-radial diffuser test rig operated by the Institute of Thermal Turbomachinery and Machinery Laboratory (ITSM) of the University of Stuttgart. This test rig represents a scaled exhaust hood of a LP steam turbine with an exhaust area of $10m^2$ corresponding to a scaling factor of approximately 1:15. The simulations are performed in ANSYS CFX, Release 17 and meshes are created in ANSYS ICEM CFD. The most significant geometrical features of the test rig that have the highest impact on the exhaust hood performance are modeled. Results from experiments performed using this scaled test rig are used to validate the numerical results of reference configuration.

In order to perform a thorough analyses of the flow regime and identify the sources of loss occuring within the LP exhaust hoods, a well known flow visualization approach used by Mizumi et al. [46] and later by Yin et al. [82] is further developed so that the flow originating from the different diffuser inlet sectors can be compared in terms of losses not only qualitatively but also quantitatively. This new approach clearly showed that most losses were occuring within the flow originating from the upper diffuser inlet sectors. This knowledge meant that modifications would have more impact if performed on the upper part of the exhaust hood.

Geometrical modifications of the numerical model of the reference configuration is performed in ICEM CFD aimed at testing the effect of hood height variation. Further geometrical modifications are carried out to include flow deflectors as part of the outer casing to investigate their impact on the losses. The deflector location targeted the upper hood in order to influence the flow originating from the upper diffuser inlet sectors that had been identified to generate the highest losses.

Since large scale steam turbines have an enormous power output and are responsible for about 60% of the world's power generation [68], only a minor improvement of the exhaust hood, which results in a lower back-pressure and hence higher enthalpy drop for the steam turbine, will give a considerable benefit in terms of fuel efficiency.

2 Theory and Literature Review

2.1 Introduction

The main objective of engineering research is to advance technology safely and make processes more efficient. Advancing any technology requires the researcher to understand well the fundamental principles of the target technology. Most engineering achievements however were made without complete understanding of underlying principles. Engineers were and still are forced to develop theories of their own, which would be generalised by scientists only later[17, 57, 65].

The current research focuses on losses found in exhaust hood of low-pressure steam turbine and how these devices can be optimized for efficient performance of the overall steam turbine. The exhaust hood can be subdivided into two main parts: the diffuser and the collector/outer casing. The exhaust diffuser comprises of the flow guide and the bearing cone, the purpose of which is to slow down the flow converting part of the kinetic energy of the flow leaving the last stage steam turbine blades into potential energy, a process mainly referred to as static pressure recovery. Because of the fixed condenser pressure, this static pressure recovery at the diffuser generates a lower static pressure at the turbine exit which means lower back-pressure at the turbine exit and hence resulting in higher power output of the turbine. The flow exiting the diffuser is guided by the collector and exhaust hood outer casing to the condenser[7]. Most optimization effort of the exhaust hood focuses on the size and shape of the diffuser, as it is often assumed that the diffuser has the most important role in the reduction of losses. However, from design practice, the diffuser is only one of the main factors that determine the performance of the exhaust hood [82].

Research focusing specifically on steam turbine exhaust hoods has stretched over the last 30 years but currently the understanding of the flow physics in the exhaust hood is not yet mature. Small scale experimental tests in the 1980s showed the potential improvements possible with the exhaust hood design, but it is only since the rise of CFD simulations from the mid-1990s that a more detailed understanding of the complexities of the flow has been gained. [7].

This thesis presents exhaust hood performance improvement achieved by introducing deflector surfaces as integral parts of the exhaust hood outer casing. The proposed modifications for performance improvements presented were made possible by a thorough understanding of the flow behavior and loss mechanism detailed in Chapter 3. The current research work utilizes computational fluid dynamics to thoroughly understand the flow behavior and losses in exhaust hoods of low-pressure turbines. The numerical models used for the reference configuration are developed from an Axial-radial diffuser test rig operated by the ITSM. The numericals results for the reference configuration are val-

idated using experimental results obtained using the test rig. Details of test rig, the numerical models and the operating conditions are given in Chapter 3.

2.2 Computational Fluid Dynamics

Computational Fluid Dynamics (CFD) is arguably the most practiced branch of fluid mechanics with many researchers in academic, research and industrial organizations using it extensively in different applications e.g aerospace, automotive, power generation sector, etc. It is an established industrial design tool, helping to reduce design time scales and improve processes throughout the engineering world. CFD provides a cost-effective and accurate alternative to scale model testing, with variations on the simulation being performed quickly, offering obvious advantages [2]. Ongoing research yields softwares that improves the accuracy and speed of complex simulation scenarios such as transonic or turbulent flows. The fundamental basis of almost all CFD problems is the Navier-Stokes equations, which define many single-phase fluid flows. These governing equations of fluid flow represent mathematical statements of the conservation laws of physics:

- the mass of a fluid is conserved
- the rate of change of momentum equals the sum of the forces on a fluid particle (Newton's second law)
- the rate of change of energy is equal to the sum of the rate of heat addition to and the rate of work done on a fluid particle (first law of thermodynamics).

For ease of use, all commercial CFD packages include sophisticated user interfaces to input flow problem parameters and to inspect the results. All codes contain three main elements: a pre-processor, a solver and a post-processor. Pre-processing consists of the input of a flow problem to a CFD program by means of an user-friendly interface and the subsequent transformation of this input into a form suitable for use by the solver. The user activities at the pre-processing stage involve:

i. definition of the geometry of the region of interest (the computational domain)
ii. grid generation - the sub-division of the domain into a number of smaller, non-overlapping sub-domains: a grid (or mesh) of cells (or control volumes or elements)
iii. selection of the physical and chemical phenomena that need to be modelled
iv. definition of fluid properties
v. specification of appropriate boundary conditions at cells which coincide with or touch the domain boundary.

The solution to a flow problem (velocity, pressure, temperature, etc.) is defined at nodes inside each cell. The accuracy of a CFD solution is governed by the number of cells in the grid. In general, the larger the number of cells, the better the solution accuracy. Both the accuracy of a solution and its cost in terms of necessary computer hardware and computation time are dependent on the fineness of the grid. Optimal meshes are often non-uniform: finer in areas where large variations occur from point to point and coarser in regions with relatively little change. At present, it is up to the skills of the CFD user to design a grid that is a suitable compromise between desired accuracy and solution cost. Over 50% of the time spent in industry on a CFD project is devoted to the definition of the domain geometry and grid generation [76].

There are three distinct streams of numerical solution techniques: finite difference, finite element and spectral methods. The finite volume method, a special finite difference formulation is central to most well-established CFD codes: ANSYS CFX , FLUENT, PHOENICS and STAR-CD. The numerical algorithm consists of the following steps: integration of the governing equations of fluid flow over all the (finite) control volumes of the domain, conversion of the resulting integral equations into a system of algebraic equations (discretization) and solution of the algebraic equations by an iterative method [76].

The first step, the control volume integration, distinguishes the finite volume method from all other CFD techniques. The resulting statements express the (exact) conservation of relevant properties for each finite size cell. This clear relationship between the numerical algorithm and the underlying physical conservation principle forms one of the main attractions of the finite volume method and makes its concepts much more simple to understand by engineers than the finite element and spectral methods. As in preprocessing, a huge amount of development work has taken place in the post-processing field. Due to the increased popularity of engineering workstations, many of which have outstanding graphics capabilities, the leading CFD packages are now equipped with versatile data visualisation tools. These include: domain geometry and grid display, vector plots, line and shaded contours, 2D and 3D surface plots, particle tracking, particle view manipulation, colour postscript output, alphanumeric output and data export capabilities for further manipulation external to the code [76].

2.2.1 Boundary layer and boundary layer theory

A boundary layer refers to a region of fluid in the immediate vicinity of a bounding surface where the effects of viscosity are significant. The thickness of the velocity boundary layer is normally defined as the distance from the solid surface to the point at which the viscous flow velocity is 99% of the freestream velocity (U_∞). Flows at high Reynolds numbers can be divided up into two regions. In the bulk of the flow region away from the walls, the viscosity can be neglected, and the flow corresponds to the inviscid limiting solution. This is called the inviscid outer flow. The second region is the very thin boundary layer at the wall where the viscosity must be taken into account [56]. Fig. 2.1 is a schematic of boundary layer at a flat plate at zero incidence. It illustrates a subdivision of flow by a broken line into two regions: one near the bounding surface where the viscous effects are taken into account and the other where these effects are neglected i.e the

flow is considered inviscid. This constitutes the so called boundary layer concept which is so important in modern CFD.

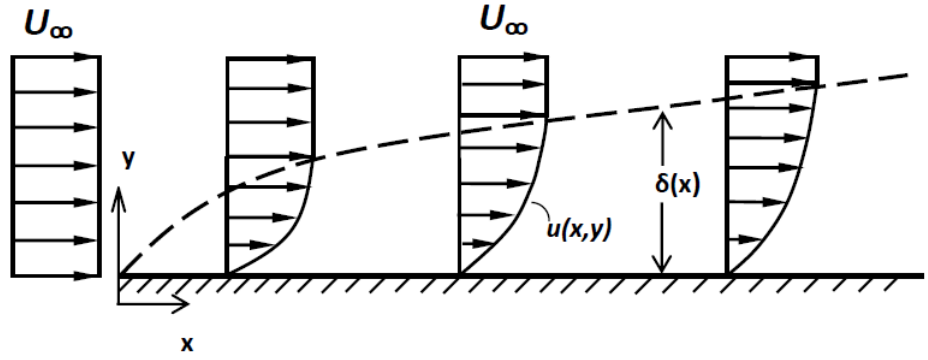

Figure 2.1 – Schematic of boundary layer at a flat plate at zero incidence [56]

Experiments and mathematical analysis have shown that the near-wall region can be subdivided into two layers. In the innermost layer, the so-called viscous sublayer where the flow is almost laminar-like, and the (molecular) viscosity plays a dominant role in momentum and heat transfer. Further away from the wall, in the logarithmic layer, turbulence dominates the mixing process. Finally, there is a region between the viscous sublayer and the logarithmic layer called the buffer layer, where the effects of molecular viscosity and turbulence are of equal importance [2]. Fig. 2.2 illustrates these subdivisions of the near-wall region.

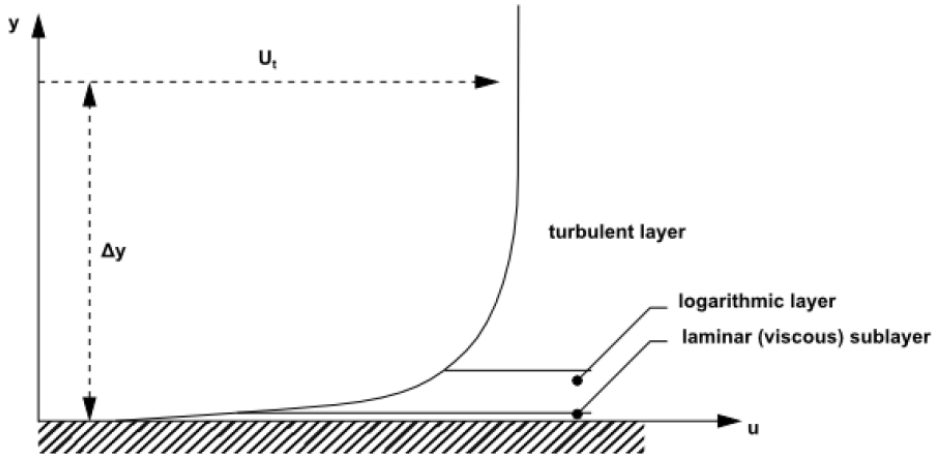

Figure 2.2 – Subdivision of the boundary layer [2]

Prof. Ludwig Prandtl was the first to show that in the case of most technically important flows, one may treat the flow, as a whole as frictionless and utilize the simplifications for the calculations thus made possible but that in the immediate neighbourhood of the solid walls one always had to take friction into consideration. Thus Prandtl subdivided for purpose of calculation, the flow surrounding a body into two domains: A layer subject to friction in the neighbourhood of the body and a frictionless region outside of this layer. This theoretical approach of Prandtl commonly referred to as the Prandtl friction or boundary layer has proved to be very fruitful in modern flow theory [56].

Many considerations of aerodynamics are based on the ideal fluid i.e a frictionless incompressible fluid. By neglecting compressibility and friction, the extensive mathematical theory of the ideal fluid (potential theory) has been made possible. Actual liquids and gases satisfy the condition of incompressibility rather well if the flow Mach number is not extremely high. The hypothesis of absence of friction is not satisfied by any actual fluid, however it is true that most technically important fluids, for instance air and water, have a very low coefficient of friction and therefore behave in many cases almost like the ideal frictionless fluid [56].

Under certain circumstances (e.g adverse pressure gradient), a reverse flow occurs in the immediate proximity of the surface (separation of the boundary layer). This separation contributes to formation of vortices in the flow. Thus, a considerable change in pressure distribution results. Boundary layer separation is very important in exhaust hood flows because separation can occur at both the diffuser lip and the bearing cone. A number of authors have associated the losses in LP turbine exhaust hoods with these flow separations and the resulting vortices [46, 48, 82].

2.2.2 y^+ value

The y^+ value is a non-dimensional distance (based on the local velocity) from the wall to the first mesh node. Fig. 2.3 is a pictorial definition of the y^+ value in terms of the first cell height in a mesh grid. Equations 2.1 to 2.5 are used to compute the height of the first cell off the wall required to achieve a desired y^+ using flat-plate boundary layer theory.

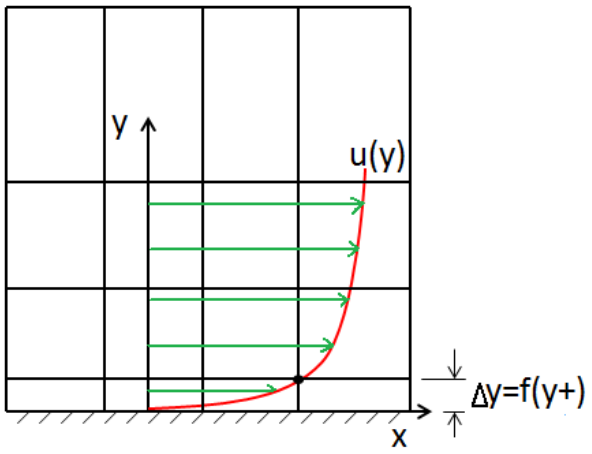

Figure 2.3 – y^+ definition

$$Re_x = \frac{\rho u L}{\mu} \tag{2.1}$$

$$C_f = \frac{0.026}{Re_x^{1/7}} \tag{2.2}$$

$$\tau_{wall} = \frac{C_f \rho u^2}{2} \tag{2.3}$$

$$U_{fric} = \sqrt{\frac{\tau_{wall}}{\rho}} \tag{2.4}$$

$$\Delta y = \frac{y^+ \mu}{\rho U_{fric}} \tag{2.5}$$

In turbulence modeling, it is very important to check if the boundary layer profile is being resolved. This is because in turbulent flows, the velocity fluctuations within the boundary layer can be a significant percentage of the mean flow velocity. A Reynolds averaging approach using turbulence models provide an estimate of the increased level of stress within the boundary layer, termed the Reynolds stresses.

In the laminar sub-layer region ($y^+ < 5$) inertial forces are less dominant and the flow exhibits laminar characteristics. Low-Re turbulence models (e.g the SST) aim to resolve this area and therefore require an appropriate mesh resolution to do this with accuracy. This is most critial for flows with changing pressure gradient where separation is expected e.g in diffuser flows [2].

When using Low-Re models or any models with enhanced wall treatment, the average y^+ value should be on the order of 1 to ensure that the laminar sub-layer is captured. When using wall function models, the y^+ value should ideally be above 15 to avoid erroneous modeling in the buffer layer and the laminar sub-layer. High quality numerical results for the boundary layer will only be obtained if the overall resolution of the boundary layer is sufficient. The minimum number of cells to cover a boundary layer accurately is around 10 but values of 20 are desirable [2].

Use of the standard wall function (ϵ-based models) implies that the boundary layer mesh lies entirely within the log-law region of the boundary layer. For industrial applications, this in fact might be difficult to achieve due to varying geometrical and velocity scales involved and therefore grids are inherently designed with arbitrary refinement. The use of the scalable wall function, available in ANSYS CFX, offers an elegant solution to this ambiguity often encountered. This wall function virtually displaces the mesh to a y^+ approximately equal to 11.225 (transition to the log-law composite layer) irrespective of the level of refinement, thereby avoiding the erroneous modeling of the laminar sub-layer and buffer region. For grids designed with $y^+ > 11.225$, the scalable wall function will provide identical results to the standard wall function [2].

2.2.3 Turbulence and turbulence modeling

Most regions of LP exhaust hood flow experience flow turbulence. As opposed to laminar flow, turbulent flow exhibits a chaotic and random state of movement in which the velocity and pressure vary continuosly with time within a substantial region of flow. The flow motion becomes intrinsically unsteady even with constant imposed boundary conditions [76]. A turbulent flow is characterized in terms of mean values of flow properties and some statistical properties of their fluctuations in the so called Reynolds decomposition. Visualization of turbulent flows reveal rotational flow structures (turbulent eddies).

The largest turbulent eddies interact with and extract energy from the mean flow by a process called vortex stretching. Among the simplest flows of significant engineering importance are those in the category of free turbulent flows: mixing layers, jets and wakes. A mixing layer forms at the interface of two regions: one with fast and the other with slow moving fluid. In a jet, a region of high-speed flow is completely surrounded by stationary fluid. A wake is formed behind an object in a flow, so here a slow moving region is surrounded by fast moving fluid. Transition to turbulence occurs after a very short distance in the flow direction from the point where the different streams initially meet; the turbulence causes vigorous mixing of adjacent fluid layers and rapid widening of the regions across which the velocity change takes place. In LP turbine exhaust hood flows, wakes due to rotating last stage rotor blades extend past the diffuser inlet. A jet flow in LP turbine exhaust hood occurs due to the tip leakage jet through the gap between the last stage rotor blades and the turbine casing. Mixing layers dominate the flow in the exhaust hood outer casing as flow originating from different diffuser inlet sectors meet each other within the exhaust hood downstream of the diffuser outlet at different flow velocities [48].

Turbulence intensity is a measure of the turbulent velocity fluctuations that are dependent on upstream flow. Turbulent kinetic energy is the mean kinetic energy per unit mass in the fluctuating velocity field. As an inlet condition, turbulence intensity defines how well-developed the velocity profile is in terms of quantifying the Reynolds stresses. Low turbulence intensity, Tu < 1% occurs for external flow across aerodynamic objects and higher turbulence, Tu > 10% is present inside complex geometries and flow inside rotating machinery. For flow in not-so-complex devices like large pipes, the typical range is 1% < Tu < 5% [11].

Given the importance of the avoidance or promotion of turbulence in engineering applications (e.g the radial component of turbulence is beneficial in diffusers since it transfers energy towards the walls, which delays separation and improves the radial velocity profile [29]), a lot of research is dedicated on numerical methods to capture the important effects due to turbulence. The methods can be grouped into the following three categories:

- Turbulence models for Reynolds-averaged Navier-Stokes (RANS) equations: In order to be able to compute turbulent flows with the RANS equations, it is necessary to develop turbulence models to predict Reynold stresses and the scalar transport terms and close the system of mean flow equations. Attention is focused on the mean flow and the effects of turbulence on mean flow properties. Prior to the application of numerical methods, the Navier-Stokes equations are time averaged (or ensemble averaged in flows with time-dependent boundary conditions). Extra terms appear in the time-averaged (or Reynolds averaged) flow equations due to the interactions between various turbulent fluctuations. These extra terms are modeled with classical turbulence models: among the best known ones are the k-ϵ model and the Reynolds stress model. The computing resources required for rea-

sonably accurate flow computations are modest, so this approach has been the mainstay of engineering flow calculations over the last three decades [76].

- Large eddy simulation: this is an intermediate form of turbulence calculations which tracks the behaviour of the larger eddies. The method involves space filtering of the unsteady Navier-Stokes equations prior to the computations, which passes the larger eddies and rejects the smaller eddies. The effects on the resolved flow (mean flow plus large eddies) due to the smallest, unresolved eddies are included by means of a so-called sub-grid scale model. Unsteady flow equations must be solved, so the demands on computing resources in terms of storage and volume of calculations are large [76].

- Direct numerical simulation (DNS): these simulations compute the mean flow and all turbulent velocity fluctuations. The unsteady Navier-Stokes equations are solved on spatial grids that are sufficiently fine that they can resolve the Kolmogorov length scales at which energy dissipation takes place and with time steps sufficiently small to resolve the period of the fastest fluctuations. These calculations are highly costly in terms of computing resources [76].

For most engineering purposes, it is unnecessary to resolve the details of the turbulent fluctuations. CFD users are almost always satisfied with information about the time-averaged properties of the flow (e.g. mean velocities, mean pressures, mean stresses, etc.). Therefore, the vast majority of turbulent flow computations has been and for the foreseeable future will continue to be carried out with procedures based on the Reynolds-averaged Navier-Stokes (RANS) equations. A description of the effects of turbulence on the mean flow is nevertheless needed because the time-averaging operation on the momentum equations discards all details concerning the state of the flow contained in the instantaneous fluctuations [76]. For purposes of the current study, three turbulent models are described: k-ϵ, k-ω and the SST turbulence models.

The k-ϵ turbulence model

In this turbulence model, two transport equations (PDEs), one for the turbulent kinetic energy k and another one for the rate of dissipation of turbulent kinetic energy ϵ are solved along with the RANS flow equations. The underlying assumption for this model is that the turbulent viscosity is isotropic: i.e the ratio between Reynolds stress and mean rate of deformation is the same in all directions. This assumption fails in many complex flows where it leads to inaccurate predictions [76]. Within ANSYS CFX, this turbulence model uses the scalable wall-function approach to improve robustness and accuracy when the near-wall mesh is very fine. The scalable wall functions enable solutions on arbitrarily fine near-wall grids, which is a significant improvement over standard wall functions. While standard two-equation models, such as the k-ϵ model, provide good

predictions for many flows of engineering interest, there are applications for which these models may not be suitable [2]. Among these are:

- flows with boundary layer separation
- flows with sudden changes in the mean strain rate
- flows in rotating fluids
- flows over curved surfaces.

Problems in k-ϵ turbulence model can be summarized as follows [76]:

- It predicts excessive levels of turbulent shear stress, particularly in the presence of adverse pressure gradients (e.g. in curved shear layers) leading to suppression of separation on curved walls.
- It predicts excessive levels of turbulence in stagnation/impingement regions giving rise to excessive heat transfer in attachment regions.

It is expected that the k-ϵ model, and all other models that are based on Boussinesq's isotropic eddy viscosity assumption, will have problems in swirling flows and flows with large rapid extra strains (e.g. highly curved boundary layers and diverging passages) that affect the structure of turbulence in a subtle manner [76].

The k-ϵ model is by far the most widely adopted turbulence model for exhaust hood flow simulation [13, 30, 55, 59, 81, 85], despite its poor performance in predicting highly separated flows [7].

The k-ω turbulence model

In this turbulence model, two transport equations (PDEs), one for the turbulent kinetic energy (k) and a further one for the turbulent frequency (ω) are solved along with the RANS flow equations. The models assume that the turbulence viscosity is linked to the turbulence kinetic energy and turbulent frequency via the relation of equation 2.6.

$$\mu_t = \rho \frac{\kappa}{\omega} \tag{2.6}$$

One of the advantages of the k-ω formulation is the near wall treatment for low-Reynolds number computations. The model does not involve the complex nonlinear damping functions required for the k-ϵ model and is therefore more accurate and more robust. The main problem with the k-ω model is its well known strong sensitivity to freestream conditions [2]. Depending on the value specified for ω at the inlet, a significant variation in the results of the model can be obtained, which is undesirable.

The Shear Stress Transport (SST) turbulence model

The k-ω based SST model accounts for the transport of the turbulent shear stress and gives highly accurate predictions of the onset and the amount of flow separation under adverse pressure gradients [2]. Menter [38] noted that the results of the k-ϵ model are much less sensitive to the assumed values in the free stream, but its near-wall performance is unsatisfactory for boundary layers with adverse pressure gradients. This led him to suggest a hybrid model using a transformation of the k-ϵ model into a k-ω model in the near-wall region and the standard k-ϵ model in the fully turbulent region far from the wall [38–41]. The Reynolds stress computation and the k-equation are the same as in Wilcox's original k-ω model, but the ϵ-equation is transformed into an ω-equation by using the relationship of equation 2.7.

$$\epsilon = k\omega \tag{2.7}$$

In the year 2003, Menter [37, 42–44] did a lot of work on turbulence modeling. He summarized a series of modifications to optimize the performance of the SST k-ω model based on experience with the model in general-purpose computation. The main improvements are:

- revised model constants
- numerical instabilities may be caused by differences in the computed values of the eddy viscosity with the standard k-ϵ model in the far field and the transformed k-ϵ model near the wall. Blending functions are used to achieve a smooth transition between the two models. Blending functions are introduced in the equation to modify the cross-diffusion term and are also used for model constants
- limiters - the eddy viscosity is limited to give improved performance in flows with adverse pressure gradients and wake regions, and the turbulent kinetic energy production is limited to prevent the build-up of turbulence in stagnation regions.

The Mentor's SST model is superior to the k-ϵ and k-ω models in simulation of turbulence in separated flows which is a common phenomena in LP turbine exhaust hoods. It was developed primarily to overcome the weaknesses of these models while utilizing their strengths. Because of this, the SST model is used to model turbulence throughout the current research. A few simulations were run using the k-ϵ model for the reference configuration in order to check if it under-predicts flow separation and hence over-predicts the exhaust hood performance as highlighted in literature [10, 76].

2.3 Flow Structure and Flow Separation in LP Exhaust Hoods

The flow in LP Steam turbine exhaust hoods is known to be a complex 3D, unsteady, transonic wet steam. Numerically modeling such a flow accurately poses a challenge due to

the impractically high computational power requirement. Various calculation simplications to reduce the computational demand have been successfully verified with experimental data although to date there is no best-practice approach to reduce the computation time for routine design exercises [7].

The rotational flow at the interface between the exit of the last stage blades and the diffuser inlet has varying distributions of pressure, velocity and temperature. The flow separations within the diffuser and vortices have been investigated and classified in studies over the last 15 years as bearing cone separation, flow guide separation,flow guide tip separation and additional vortices [81, 84]. As the flow progress downstream, the vortices formed within the diffuser combine to a single vortex stretching downstream into the condenser. The flow structure reverses across the meridional plane, hence two counter-rotating vortices are found at the condenser neck. Despite the vertical symmetry of the hood geometry, the flow structure is asymmetric because of the direction of rotation of the turbine and horizontal asymmetry of the hood casing [7]. Owczarek et al. [53] was the first researcher to observe a separation along the bearing cone in the form of a horseshoe vortex. The researchers used lampblack oil flow visualisation technique to identify this separation. The flow was attached at the diffuser inlet but separated along the bearing cone, with the separation extending into the collector. Numerical simulations by Tindell et al. [74] assigned the horseshoe vortex which forms from this separation to be one of the major contributors 15-20% of the loss found typically in exhaust hoods. The importance of the horseshoe vortex within the diffuser has been identified by numerous researchers including Xu et al. [81] and Fan et al. [18]. Zhang et al. [84] underscored the fact that the very nature of a diffuser makes it prone to separation, with the adverse pressure gradient increasing the potential for the low kinetic energy boundary layer fluid to separate from the bearing cone wall as the flow velocity decreases. The steam turbine exhaust diffuser is particularly susceptible due to large swirl of the inlet flow, highlighted by Fan et al. [18]. The components of the inlet velocity in the axial and tangential directions, act against the curvature of the bearing cone, encouraging boundary layer separation. This was corroborated by Fu and Liu [22] who found out that a large swirl angle at the hub resulted in the separation along the bearing cone, with the magnitude of the separation reducing with decreasing swirl. Numerical analysis by Tindell et al. [74] with representative inlet conditions indicated that the separation point was depended upon the operating point of the turbine. Beevers et al [4] observed that accurate prediction of the separation point is vital,the earlier the separation the less pressure the diffuser can recover. Liu et al. [32] investigated the effect of hood inlet conditions, comparing uniform with distorted inflow, and found the bearing cone separation was only present with non-uniform distributions at inlet to the diffuser. This was corroborated by Fan et al. [18]. The losses resulting from this vortex can be large because of its magnitude. Xu et al.[81] estimated that the vortex can occupy up to two-thirds of the diffuser height. The blockage effect (reduction in the effective flow area) reduces the ability of the diffuser to recover pressure.

Static pressure distribution along the flow guide is important in predicting the static pressure recovery [4]. This region is of particular importance in exhaust hood studies as it is the most likely to have boundary layer separation where the effects of flow deceleration due to flow area expansion and streamline curvature are superimposed [52].

Two separations are present in the flow guide region, namely, Flow guide tip separation and Separations along the length of the flow guide. Owczarek et al.[53] was the first researcher to note the separation in the step region behind the tip of the flow guide. This separation was attributed by Zhang et al. [84] to be due to a phenomena they referred to as backward-facing step expansion. With progression downstream, the magnitude of the vortex increases, as the pressure decreases when approaching the condenser neck. The separation along the length of the flow guide is highly dependent on the flow guide geometry and the modelling of the tip leakage jet. A sharp kink angle changing the flow from the axial direction to 30°, was found by Yoon et al. [83] to lead to separation along the flow guide. Previous research has shown that optimization of the flow guide geometry can suppress this separation [77, 80, 83]. Research has also indicated [19, 28, 66] the positive influence of modelling the tip leakage jet.

There has been little research on additional vortices which form within the diffuser due to the comparatively small losses associated with them. Xu et al. and Fu and Liu [22, 81] have attempted to categorise the vortices, with Xu et al. observing an endwall vortex in the collector and a separation vortex on the outer guide wall. Both noted that with progression downstream, the magnitude of the vortices decreases and by inlet to the condenser neck all vortices combine to form the outlet vortex.

One important aspect characterising the exhaust hood flow structure is its asymmetry. This asymmetry is present between both the radial and meridional planes of the exhaust hood due to two different mechanisms. The asymmetry of the exhaust hood geometry in the radial plane results in a flow asymmetry between the top and the bottom of the exhaust hood. According to Benim et al. [5], this characteristic plays an important role in the formation of vortices in the diffuser. The geometry causes the flow downstream of the rotor to develop a circumferentially non-uniform distribution , which couples the exhaust hood to the last stage. This important observation adds to the complexity of any exhaust hood numerical simulation.

2.4 Application of CFD in LP Exhaust Hoods Flows

Tindell et al. [73] highlighted the usefulness of CFD for accurately assessing the performance of low-pressure steam turbine exhaust hoods. The most advanced CFD models take into account flow unsteadiness [62] but comparatively few studies are available due to high computational demand of the simulation. Tanuma et al. [69] used unsteady numerical analysis for simulation of diffuser flows in LP exhaust hoods. Compressible Navier-Stokes equations were solved using the high-order high-resolution finite-difference method including the wet steam condensation model. The complexity of the unsteady, transonic, wet steam flow regime within the exhaust hood is too time-consuming for currently available computational power. Due to this, various simplification methodologies must be adopted to reduce the computational demand [7]. In their optimization efforts of steam turbine exhaust hoods, Mizumi et al. [46] utilized a commercially available CFD code STAR-CD. They adjusted beforehand one of the parameters of the k-ϵ based turbulent flow model so that the experimental result and the analysis re-

sult match each other well. In the estimation of Cp, the absolute errors between the CFD results and their corresponding test results were less than 0.02 for all different models tested. In this work, they were able to propose a new exhaust hood structure with special ducts which separate the flow from the uppermost part of the exhaust hood from the one with different origin and can smoothly turn the flow downwards towards the condenser. They were able to show high pressure recovery improvement of 12% with the refined model. They were able to propose this new exhaust hood model following flow field visualization approach that showed them where most of the losses were being generated. Yin et al. [82] utilized ANSYS CFX as the CFD solver for their simulations aimed at identifying flow losses within the exhaust hood and analysing modified exhaust hoods obtained by varying various geometrical parameters that they investigated. They used the k-ϵ turbulence model for turbulence treatment. They concluded that the interaction of swirls is the main factor to influence the static pressure recovery. They further concluded that for good performance of exhaust hoods; the cylinder should be large enough, the diffuser should turn and expand the flow well and that swirling flows which negatively impact the exhaust hood performance should be avoided in the improved exhaust hood design. For turbulence modeling, the k-ϵ model is by far the most widely adopted turbulence model for exhaust hood flow simulation [13, 30, 55, 59, 81, 85], despite its poor performance in predicting highly separated flows [7]. Both SST [69] and $k-\omega$ [61] models are used, although infrequently. Becker et al. [3] investigated the influence of tip clearance on a swirling flow in an axial-radial diffuser. Their comparison of experimental data to numerical results based on k-ϵ and Shear Stress Transport (SST) turbulence model showed that the pressure recovery at design load is fairly well predicted by both models. A study by Cordova and Stoffel [12] of six turbulence models in a channel diffuser found acceptable level of accuracy for all models examined. Ris et al. [55] found a change of no more than 5% in hood losses was observed when varying the turbulence models. Industry studies by Beevers et al. [4] found no significant difference shown between the k-ϵ and k-ω SST turbulence models. The Reynolds Stress model predicted a larger separation region in the diffuser, but the turbine efficiency calculated was less than 0.1% lower than the alternative, less computationally expensive turbulance models. This produced "no large appreciable differences in the diffuser and exhaust hood flow field [7]. Irrespective of the CFD methodology or turbulence model used, one main shortcoming of numerical simulations is the over-prediction of the hood static pressure recovery coefficient compared with experimental data. This can sometimes vary by up to 7% [32], with the discrepancy increasing with increasing vortex size. Typical values of exhaust hood Cp range between 0.2 to 0.4 [18, 19, 23, 32, 34, 80]. Discrepancies between experimental and numerical results are primarily attributed to unrepresentative boundary conditions [63], inaccuracies in turbulence and transitional modelling [15] and simplification of the exhaust hood geometry [4].

2.5 Pressure, Swirl Angle Distribution and Tip Leakage Jet Downstream of the Turbine

The total pressure distribution at the inlet to exhaust hood diffuser was shown by Fu et al. [22] to have a significant influence on the flow structure and vortex formation in the exhaust diffuser. Ideally, the total pressure distribution downstream of the last stage blades would be uniform, however, this is not the case, in reality [7]. Liu et al. [33] were the first to observe that the high pressure region at the hub of the blade has a positive impact on the diffuser performance as it can help suppress the separation region along the bearing cone. Fu and Liu [22] carried out a comprehensive evaluation of the total pressure gradient and magnitude on exhaust hood flows. An adverse pressure gradient, as expected, encouraged bearing cone separation whereas a favourable pressure gradient helped suppress the separation region.

Fu and Liu [23] concluded that inlet swirl angle is a primary factor influencing losses in the exhaust hood. The effect of swirl angle on the pressure recovery of annular diffusers has been widely explored in the works of McDonald et al. and Kumar et al. [31, 35]. Swirl was shown to have a positive impact on the performance of a separated diffuser flow by suppressing the separation, however, this positive effect deteriorates at high swirl angles. Research has shown that it is difficult to translate the early annular diffuser work to the steam turbine exhaust hood, due to the highly non-uniform flow structure downstream of the turbine blade [79]. Fu and Liu carried out extensive studies [22, 23] on the effect of swirl angle distribution on the separations forming within the diffuser and concluded that the swirl angle at the hub has the greatest influence on losses. A high swirl angle at the hub of the blade facilitates the formation of a large vortex along the bearing cone, reducing the effective area of the diffuser and hindering the pressure recovery potential. Tajc et al. [67] noted that although flow swirl can act to stabilize the boundary layer in some regions, high swirl at the hub can cause separation along the bearing cone. Although the flow mechanisms behind this separation were not considered in depth by either researcher, Fan et al. [18] attributed this to the tangential component of the velocity acting against the curvature of the bearing cone.

Musch et al. [52] through analysis of a range of studies concluded that the main first order effects on the diffuser flow field are the tip jet and the swirl of the last stage. Benim et al. [5] was one of the first researchers to acknowledge the favourable effect that the rotor tip leakage jet has on the boundary layer along the flow guide in the exhaust hood. This has since been investigated in a variety of published work [19, 28, 67]. The rotor tip typically has a shrouded cover with a seal segment on top. The jet which results from the seal clearance gives kinetic energy to the flow guide wall helping to prevent flow separation [47]. Experimental work by Tajc et al. in 2006 and 2009 [28, 67] successfully suppressed the separation along the flow guide, and reduced the losses by up to 20% by using a synthetic jet to tangentially blow in steam, simulating the tip jet. The high adverse pressure gradient in the flow guide region encourages flow separation but the tip jet adds momentum to the boundary layer suppressing or reducing the flow separation. The separation point was shown by Finzel et al. [19] to move further downstream with increasing jet strength until completely suppressed. Despite the widely accepted positives of the tip

leakage jet on the diffusser flow field, there are also disadvantages. The presence of the tip jet results in turbine leakage losses and hence a lower turbine efficiency; an effect which increases with increase in jet strength [19]. Maier and Wachter [36] studied the effect of the unsteady shock induced separations which can form at the flow guide as a result of the supersonic jet. The self-excited nature of this effect within the diffuser was found to induce potentially dangerous oscillations in the rotor blade itself.

2.6 Experimental techniques

Until the first half of the 1990s, many scale tests were conducted to develop and redesign the exhaust hoods of LP turbines in order to decrease the pressure loss and increase the static pressure recovery. Since the latter half of 1990s, CFD studies have been initiated, where the goal is to optimize the aerodynamic design of the diffusers and structures in exhaust hoods [69]. Even with the advancement in CFD, experimental methods have continued to play a central role in development of exhaust hoods of LP turbines. Denton [15] notes that CFD is a prediction tool and must always be used together with experimental testing to validate results.

Experimental testing mainly uses scaled models, due to the financial limitations of full-scale testing. Gray et al. [26] stated in 1989 that typical scale factors used in such models range from 1:20 to 1:30 depending on the length of the last row blade in the actual turbine. However, over the past 20 years the scale of models has increased to between 1:15 [32, 84] and 1:10 [4, 83] more closely matching the Reynolds number to that of the actual turbine [10]. To attempt true dynamic simulation, Beevers' facility in 2010 [4], used R134a gas mixed with air as the working fluid in their 1:10 scale model. Most researchers use air as the working fluid in their scale models.

Static or rotating devices are used for creating representative pressure, swirl and velocity distributions at the diffuser inlet in LP exhaust hood tests [10]. Static devices have remained relatively unchanged over the past 30 years with the multiple wire mesh screens and stationary vane used by Gray in 1989 [26] to generate radial distributions of pressure and swirl angle adopted right up until Liu's testing in 2003 [32]. Alternative methods include a row of narrow plates and stationary row of blades used by Tajc in 2007 [66]. Static devices are a simple way of giving representative conditions at inlet but fail to capture the unsteady effects [24]. Because of the missing turbine stage, the results obtained using stationary devices are not transferable one to one from the test rig to a real turbine but generic studies of the effects of different parameters have proven to be reliable [19].

Rotating devices have scarcely been explored in scaled experimental testing of exhaust hoods. Application of even a large 1:4 scaling to a 50Hz machine increases the rpm from 3000 to 12,000, introducing issues concerning structural integrity and absorbing generated power. Typically rotating devices have taken two forms; wheels with varying diameter spokes or scaled rotating blades [10]. Spoked wheels were used by Sieker in 2008 [58] to generate the high level of turbulence, energizing the boundary layer. A larger diameter spoke was used to reduce the separation region because of the increased turbulence from the wakes. Zhou in 2008 has been one of the few researchers to include scale model

of rotating blades, using resistors to absorb the power generated by the 1:15 scale turbine [10]. Majority of published work using rotating devices has been carried out by large industrial suppliers with custom test facilities such as those used by Beevers in 2010 and Yoon in 2011 [4, 83]. Rotating devices have been found to challenge experimental instrumentation due to the unsteady flow, with both Xu and Sieker [58, 81] finding repeatable experimental results difficult to achieve with a 5-hole probe because of unsteady instabilities [10]. Probe traverses may enable the validation of CFD results but usually fail to provide enough information in order to understand the flow details and finally improve the design approaches [33]. Particle image velocimetry (PIV) offers an alternative, a reliable method for capturing instantaneous whole field velocity measurements used to determine the kinetic energy loss, turbulence characteristics, and consequently the performance of the hood [85]. Although this approach allows a more detailed flow structure to be measured, common seeders such as oil require regular cleaning from the clear acrylic hood models and there can be restrictions in the size of the flow field which can be captured in a single traverse. In 2008, Sieker [58] recommended laser Doppler velocimetry (LDV) as a method for recording velocity profiles as it is non intrusive, requires no calibration and allows stagnant and reverse flow (such as in vortices) to be accurately captured [10].

Experimental results are very important in validation of numerical results which offers a better insight into the flow regime and better possibilities of detailed analysis. Experimental methods are more expensive and time consuming compared to modern numerical simulations.

2.7 Optimization Efforts for LP Exhaust Hoods

The exhaust hood of a steam turbine is an important area of power plant design. This is because the performance of the exhaust hood influences the efficiency of the low pressure (LP) turbine [10]. Academic and industrial research in steam turbine exhaust hood field has increased over the last two decades due to the high potential gains in last stage blades of the low pressure turbine and the accompanying exhaust diffuser and hood [7].

A number of researchers have associated losses occurring in exhaust hoods with diffuser flow separation and the resulting vortices [46, 48, 82]. Tindell's numerical simulations [72] attributed the horseshoe vortex which forms from a separation along the bearing cone to be one of the major contributors of the loss found typically in exhaust hoods. Later in 2001, the significance of the horseshoe vortex was highlighted by Xu [81]. In 2010, Beevers [4] observed that accurate prediction of the separation point is vital, the earlier the separation the less pressure the diffuser can recover. The blockage effect and the subsequent reduction of the effective flow area reduces the ability of the diffuser to recover pressure. The separation along the length of the flow guide is highly dependent on the flow guide geometry and the modeling of the tip leakage [10].

Previous research has shown that optimization of the flow guide geometry can suppress this separation [77, 83]. Research has also indicated the positive influence of modeling the tip leakage jet [19]. The counter-rotating outlet vortices in the condenser neck have

a detrimental effect on the condenser efficiency, as it is desirable to have a uniform distribution of the steam across the heat transfer surface [9]. Reverse flow at the core of each vortex has been noted by multiple researchers including Stastny in 2000 [63]. Different experimental and 3D numerical studies have been conducted on exhaust hoods of LP steam turbines aimed at optimizing their performance. In 1967, Sovran and Klomp [60] introduced experimentally determined optimum diffuser geometry charts that are still used by many turbomachinery manufacturers. They had already considered that the inlet flow conditions affect the optimum diffuser geometry [69]. Becker et al. [3] investigated the influence of tip clearance on a swirling flow in an axial-radial diffuser. Their comparison of experimental data to numerical results based on k-ϵ and Shear Stress Transport (SST) turbulence model showed that the pressure recovery at design load is fairly well predicted by both models. Xu et al. [81] showed good agreement between their numerical simulations of low pressure exhaust casings and experimental data without upstream turbine stages. Fu et al. [21] presented a comparison between steam turbine exhaust hood tests with one-stage turbine (stator and rotor blades rows) and numerical results. Experimental investigations performed by Finzel et al. [19] with systematic variations of geometrical parameters of a model steam turbine exhaust hood with two axial-radial diffuser configurations demonstrated that there was a large influence of their investigated geometrical exhaust hood parameters (exhaust hood area, flow area in the horizontal joint plane and location of the steam inlet) on the diffuser flow, especially when the area available for the flow is strongly restricted. Epiphanov et al. [16] studied the effect of deflector vane geometry on the performance of a large-scale turbine exhaust hood at transonic flow conditions using air-test experiments and 3D numerical simulation. After numerous experiments on a 1:25 scale model under realistic Mach number conditions, they were able to select an optimized configuration of an exhaust hood which had a vaned axial-radial diffuser. Although this design resulted in a significant reduction of pressure loss compared to the original design under moderate Mach numbers, the loss coefficient rose drastically when approaching the design flow rate hence necessitating further optimization. Gray et al. [26] evidenced flow interactions between the turbine stage and exhaust hood in full-scale tests and improved the hood performance by redesigning the last row of blades. Kreitmeier and Greim [30] optimized the interaction zone between the last turbine stage and the diffuser to improve the turbine performance. From their experiments and numerical simulation, Fu et al. [20] established that the swirl angle profile and total pressure profile due to the upstream turbine stage at the diffuser inlet have an unfavorable effect on the exhaust hood performance. Stein et al. [64] underscore the importance of accurate prediction of the pressure recovery for the overall turbine performance determination, as a 10%− points improvement in pressure recovery roughly translates into a 1% improvement in last stage efficiency. Taylor et al. [70], through varying different important dimensions of an exhaust hood, found out that their designs are far more sensitive to changes in box size at higher stage loading when the leaving energy from the last blade increases. They additionally noticed that a reduction in the available flow area, regardless of whether this is achieved through changing hood width, axial length to the hood back wall or hood height, resulted in a decrease in the diffuser recovery performance.

Tanuma et al. [68] reported that the aerodynamic loss of LP exhaust hoods is almost the same as that of stator and rotor blading of the LP turbine, hence making losses in the LP exhaust hood a very important factor in the overall power plant optimization efforts. Finzel et al. [19] reported that three-dimensional inhomogeneous flow in the exhaust hood of LP steam turbines is a major cause of losses and design of a low-loss exhaust hood remains a challenge especially in retrofit units.In the case of a complete retrofit of LP turbine an optimum design of the axial-radial diffuser and exhaust hood may often be impossible because of geometric limitation. In these cases, Finzel et al. observes that it is important to know the influence of the geometrical parameters of the exhaust hood on the pressure recovery factor to provide an appropriate design. Zoe Burton [7] in her PhD thesis explains that in 1950's and 60's turbine blades were designed using simple radial equilibrium theory resulting in an aerodynamically inefficient design for both last stage blades (LSBS) and exhaust hood [1]. Although retrofitting (installing modern blading into an existing exhaust hood casing) can significantly improve the efficiency of the last stage turbine, the exhaust hood is typically not optimized for the retrofitted blades and subsequently the aerodynamic shortcomings are mainly found in the exhaust hood system. As the exhaust hood casing and condenser can rarely be modified in retrofits, it is the exhaust diffuser that has the most potential for improvement. Yin et al. [82] clarifies that most optimization effort of the exhaust hood focuses on the size and shape of the diffuser, as it is often assumed that the diffuser has the most important role in the reduction of losses. However, from design practice, the diffuser is only one of the main factors that determine the performance of the exhaust hood. Only two groups of researchers, Finzel et al. [19] and Taylor et al. [70] were found to performed extensive investigation on the influence of varying the exhaust box dimensions. Mizumi et al. [46] proposed an optimized exhaust hood with flow separation ducts that was aimed at minimizing the impact of the dissipative swirling flows.

Understanding the flow field and the loss mechanisms within the exhaust hood of LP steam turbines is key to developing better optimized exhaust hood systems. Mizumi et al. [46] examined the vortex structure of the exhaust hood flow by streamline visualization and found out that the origins of the swirling flows with strong vorticity were all found to be from the upper part of the exhaust hood. With this knowledge, they proposed a new, more optimized exhaust hood which after verification in their scale model test rig showed a high pressure recovery improvement of 12%. More recently, Yin et al. [82] rigorously analyzed the influence of swirl flows in exhaust hoods and concluded that the interaction of swirling flows is the main factor to influence the static pressure recovery. In this PhD thesis, a detailed analysis of the losses within the exhaust hood based on numerical results and the importance of swirl flows in loss generation in exhaust hoods of LP turbines is presented in Chapter 3. In order to allow the localization of the sources of loss, the existing approach of examining streamlines originating from various sectors at the diffuser inlet, first used by Mizumi [46] and later by Yin [82], has been developed further. Based on results of sources of loss, improved exhaust hood geometries are proposed in the current thesis incorporating flow deflectors (as integral parts of the outer casing) at the upper part of the exhaust hood. Results on influence of hood height on performance of LP turbine exhaust hoods are also presented. Munyoki et al. [48–50] have published three scientific papers as conference proceedings with the American Society of Mechan-

ical Engineers (ASME) focusing on different areas of this PhD thesis whose overall goal is to propose modification of exhaust hood to achieve better performance.

2.8 Conclusion

Optimizing the flow path of exhaust hoods of LP steam turbines is an important problem that has to be solved for achieving better performance of the low-pressure parts used in large steam turbines. These diffusers and hoods are among the bulkiest and the most metal-consuming parts of the turbines. Engineers who develop the designs of hoods construct them on the basis of data obtained from tests of model hoods carried out on static installations (without the preceding turbine stage) with uniform axial supply of air or with simulation of flow swirling at the inlet. In recent years, calculated simulation methods with the use of modern 3D computation codes have been widely and successfully used for practical application [27].

Flow separation occurring within the axial-radial diffuser and the exhaust box has been identified by a number of researchers as the main causes of loss occuring within the exhaust hood [7, 46, 82] however there is need to go deeper in the understanding of the loss mechanism within the exhaust hood and try to propose an optimized exhaust hood. Most optimization efforts from literature was found to focus on the size and shape of the diffuser, as it is often assumed that the diffuser has the most important role in the reduction of losses. Yin et al. [82] however notes that from design practice, the diffuser is only one of the main factors that determine the performance of the exhaust hood.

Until the first half of the 1990s, many scale tests were conducted to develop and redesign the exhaust hoods of LP turbines in order to decrease the pressure loss and increase the static pressure recovery. Since the latter half of 1990s, CFD studies have been initiated, where the goal is to optimize the aerodynamic design of the diffusers and structures in exhaust hoods [69]. Even with the advancement in CFD, experimental methods have continued to play a central role in development of exhaust hoods of LP turbines. Denton [15] notes that CFD is a prediction tool and must always be used together with experimental testing to validate results. Most experimental testing uses scaled models because of the high cost associated with full scale turbines however a few researchers especially those working with turbine manufacturers have used full scale models in the recent past.

The most advanced CFD models take into account flow unsteadiness [62] but comparatively few studies are available. Because of the high computational power and computational time requirement for unsteady simulations, many researchers use steady state simulation with turbulence modeled by the k-ϵ turbulence model. Interestingly, good agreement between experimental results and numerical simulations have been observed. It was also noted from literature that the k-ϵ model is by far the most widely adopted turbulence model for exhaust hood flow simulation [13, 30, 55, 59, 81, 85], despite its poor performance in predicting highly separated flows [7]. Both SST [69] and $k-\omega$ [61] models are used, although infrequently. Becker et al. [3] investigated the influence of tip clearance on a swirling flow in an axial-radial diffuser. Their comparison of experimental data to numerical results based on k-ϵ and Shear Stress Transport (SST) tur-

bulence model showed that the pressure recovery at design load is fairly well predicted by both models.

Using the correct boundary conditions at the inlet and outlet of a numerical model was found from literature to be very critical for proper prediction of the flow structure through the model and overall performance. The total pressure, static pressure, total temperature, swirl angle and turbulence intensity were the common parameters applied at the model boundaries. Mostly, static pressure was used at the model outlet to get the desired mass flow rate while a turbulence intensity of 5% was commonly applied at the diffuser inlet together with the appropriate total pressure profile, total temperature and the swirl angle profile.

Based on the literature review undertaken for the current work, the scope for the following areas of research was provided:

1. Further development of an existing methodology in literature [46] for flow field visualization in LP steam turbine exhaust hoods to enable not only the qualitative analysis but also a quantitative analysis of loss in exhaust hoods
2. Detailed numerical analysis of sources of loss in LP steam turbine exhaust hoods at design- and overload conditions for a reference configuration operated with three tip jet Mach numbers (0, 0.4, 1.2)
3. Detailed numerical investigation of influence of hood height variation on the performance of LP exhaust hoods.
4. Numerical evaluation of impact of including deflector walls as integral parts of the exhaust hood outer casing.

3 Detailed Numerical Study of the Main Sources of Loss and Flow Behaviour in Low Pressure Steam Turbine Exhaust Hoods

3.1 Introduction

While the design of axial-radial diffusers has been the object of quite many studies, the flow phenomena occurring within the exhaust hood have not received much attention in recent years. However, major losses occur due to dissipation within vortices and inability of the hood to properly diffuse the flow. Flow turning from radial to downward flow towards the condenser, especially at the upper part of the hood is essentially the main cause for this. This chapter presents a detailed analysis of the losses within the exhaust hood flow for two operating conditions based on numerical results. In order to identify the underlying mechanisms and the locations where dissipation mainly occurs, an approach is followed, whereby the diffuser inflow is divided into different sectors and pressure recovery, dissipation and finally residual kinetic energy coefficients of the flow originating from these sectors are calculated at different locations within the hood. Based on this method, the flow from the topmost sectors at the diffuser inlet is found to cause the highest dissipation for both investigated cases. Upon hitting the exhaust hood walls, the flow from the upper part of the diffuser is deflected, forming complex vortices which stretch into the condenser and interact with flow originating from other sectors, thereby causing further swirling and generating additional losses. The detailed study of the flow behavior in the exhaust hood and the associated dissipation presents an opportunity for designing optimized LP exhaust hoods to improve the flow and hence the overall pressure recovery coefficient.

3.2 Experimental Facility used for this Study

The current research is based on an axial-radial diffuser test rig operated by the ITSM of the University of Stuttgart. The reference configuration of the numerical model used is developed from the geometry of this test rig. The experimental data used to validate the numerical results at design load and overload both operated with three different tip jet Mach numbers (0, 0.4 and 1.2) are obtained by carying out experiments using this test rig and analysing the data obtained.

This axial-radial diffuser test rig experimental facility shown in Fig. 3.2 is used to model steam flow in the exhaust system of LP steam turbines. The axial-radial diffuser test rig represents a scaled exhaust of a LP steam turbine with an exhaust area of $10m^2$ corre-

sponding to a scaling factor of approximately 1:15. Two axial-radial diffusers are available for use with this test rig which differ in the size and shape of the outer shell. The two diffuser outer shells use the same inner shell to form the diffuser channel. The inner shell rotates to facilitate measurements at different locations. These diffusers are identified as KW21 and V3. Fig. 3.1 illustrates the two diffusers available for use with the test rig.

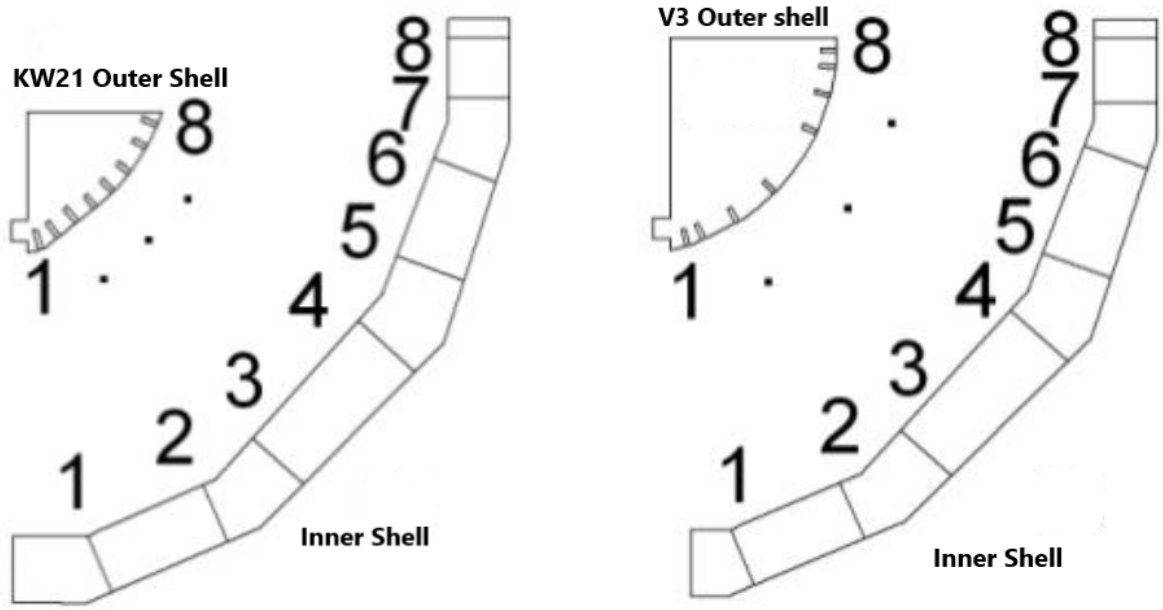

Figure 3.1 – Diffusers KW21 and V3 available for use with the test rig. They use the same inner shell but different outer shells. The numbered pressure taps represent static pressure measurement points

For this study, V3 diffuser was chosen for it had shown a better performance compared to KW21 diffuser from a previous research conducted in 2011 by Finzel et al. [19] where they investigated experimentally the influence of the exhaust hood area, the flow area in the horizontal joint plane and the location of the steam inlet using the same experimental facility used in the current research. This diffuser has an annular area of $0.0421 m^2$ at the diffuser inlet and a cylindrical curved surface area of $0.0701 m^2$ at the diffuser outlet. The condenser plane on the other hand has a rectangular surface area of $0.1337 m^2$. The diffuser channel V3, the diffuser inlet (E2), diffuser outlet (E3) and the condenser plane (C) are illustrated in Fig. 3.14.

The test rig is operated with air from two separate compressors which operate under suction for the main flow and pressure for the tip jet. The main flow is produced through suction by a radial compressor while the tip jet is produced by a screw compressor. The main flow in the test rig represents the steam flow through the rotor blade row using a simplified swirl body to model the radial swirl distribution of the last turbine blade row. Because of the missing turbine stage, the results are not transferable one to one from the test rig to a real turbine but generic studies of the effects of different parameters have proven to be reliable. The compressor has sufficient capacity to operate the rig at the same Mach numbers as real steam turbines. The compressor induced tip jet models the tip clearance flow of the turbine rotor blades. The total pressure of this tip jet can be

adjusted independently from the main flow allowing to simulate the leakage flow over shrouded and unshrouded blades. To eliminate the effect of the ambient test conditions, the operating point is defined by a constant reducing mass flow, which means adjusting of the main flow into the test rig. The main flow is measured with an inlet bellmouth nozzle. The ambient pressure and temperature are simultaneously determined. There are five groups of measurements at the axial-radial diffuser test rig namely; operating point measurements, probe measurement at the diffuser inlet, probe measurement at the diffuser outlet, wall pressure measurements of the diffuser outer shell and wall pressure measurements of the diffuser inner shell. The operating point dermination occurs through the measurement of different pressures and temperatures. The tip jet and the atmospheric temperature are measured using Pt100 thermometers.

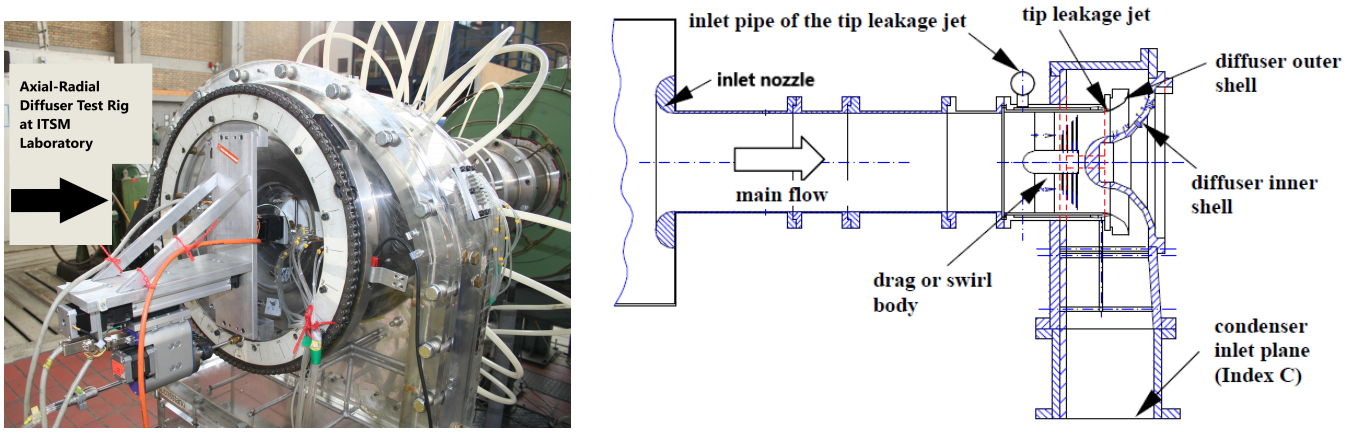

Figure 3.2 – Axial-radial diffuser test rig operated by ITSM. A photo and a longitudinal section through the test rig are presented.

The static pressure along the diffuser wall is measured by several pressure taps in the outer and inner diffuser shell. There are eight pressure taps along the wall at eight different circumferential positions on the outer diffuser shell. The inner diffuser shell which also contains the probe traverses can be rotated. There is one row of eight pressure taps along the inner diffuser wall. The wall pressures are not discussed in this thesis since emphasis is on the global performance of the exhaust hood.

There are two measurement planes for probe traverses, E2 and E3 (see Fig. 3.14b) at the diffuser inlet and the diffuser outlet respectively. In both measurement planes, conical pneumatic probes are used with five holes to determine total pressure, static pressure and flow angles. In the diffuser inlet plane E2, the flow field is measured at 96 discrete measurement points, six points on one radial stream at each 22.5° around the circumference. Similarly at the diffuser outlet plane E3, the flow field is measured at 96 discrete measurement points, six points on one axial stream at each 22.5° of rotation of the diffuser inner shell. The static pressure in the condenser plane is measured with eight pressure taps around the casing and directly pneumatic averaged (i.e. direct momentum averaging of the static pressure). A measurement tool based on LabView is used to control the traverse system and to store all data of interest. The analysis of the measurement data is done using a Matlab program after completion of measurements.

The 5-hole conical probes are calibrated in a free jet stream at Mach numbers as expected during the various experiments at the test rig. The pressure values obtained during calibration are used to calculate dimensionless flow coefficients (yaw angle, pitch angle, Mach number, total pressure and dynamic pressure coefficients) which are necessary to calculate actual pressure values from the measured probe pressures by means of linear interpolation. These calculations are performed by a FORTRAN code referenced by the LabVIEW program. The interpolated static and total pressures are further standardized in LabVIEW by being multiplied by a pressure factor equal to the quotient of the standard pressure (101.325kPa according to ISO 13443) and the atmospheric pressure. Similarly, all temperature values measured are standardized in LabVIEW by being multiplied by the quotient of the standard temperature (288.15K according to ISO 13443) and the atmospheric temperature. This standardization of pressure and temperature is done to ensure that measurement results are comparable with results from different tests performed on different dates when the prevailing atmospheric conditions are different. This standardization also enables comparison of results with results from other test facilities performed at different ambient conditions.

Although many parameters are measured at the axial-radial diffuser test rig to enable determination of the operating point and calculation of the exhaust hood performance, Table 3.1 summarizes operating parameters measured and others calculated from the measurements from the axial-radial diffuser test rig (the reference configuration) at different operating points in experiments that form the basis of the numerical simulation boundary conditions at the same operating points.

Table 3.1 – Main mass flow rate, tip jet mass flow rate, total pressure, static pressure and Mach number at the diffuser inlet, combined mass flow rate and static pressure at the condenser plane at different operating points

Operating point	**Mass flow rate (main, tipjet) [kg/s]**	**(Total pressure[Pa], Static pressure [Pa], Mach number) at diffuser inlet**	**(Mass flow rate [kg/s],Static pressure [Pa]) at Condenser plane**
Design load,tip jet Ma=0	(6.67, 0)	(97253, 80497, 0.5)	(6.67, 84054)
Design load,tip jet Ma=0.4	(6.67, 0.041)	(97446, 80471, 0.5)	(6.711, 83600)
Design load,tip jet Ma=1.2	(6.67, 0.071)	(97379, 80798, 0.5)	(6.741, 88614)
Overload,tip jet Ma=0	(7.55, 0)	(96227, 71471, 0.72)	(7.55, 75210)
Overload,tip jet Ma=0.4	(7.55, 0.041)	(96179, 71307, 0.72)	(7.591, 74716)
Overload,tip jet Ma=1.2	(7.55, 0.071)	(95942, 71937, 0.72)	(7.621, 80630)

In the current study, the choice to use tip jet Mach number of 0.4 to represent shrouded last stage blades and tip jet Mach number of 1.2 to represent unshrouded last stage blades is based on a previous study by Finzel et al. [19] in 2011 who used the same axial-radial diffuser test rig to experimentally study the influence of the exhaust hood area, the flow area in the horizontal joint plane and the location of the steam inlet. In their study, the researchers used the design load for the main flow with two tip jet flow configurations, one representing the shrouded blade with an isentropic tip flow Mach number

of 0.4 while the other tip jet flow representing the unshrouded blade with an isentropic tip flow Mach number of 1.2. It is understood that different turbines operate at different tip jet flow Mach numbers depending on the tip gap size and the turbine operating conditions but it was important to focus mainly on these two tip jet flow cases for ease of comparison of experimental results data for the reference configuration with results from the previous study performed on the same experimental facility.

The axial-radial diffuser test rig is designed for investigation of various effects on the performance of axial-radial diffusers, and some earlier results from this rig (without swirl at inlet) have been reported in 2002 by Thiemann et al. [71], in 2003 by Messner [45] and in 2004 by Polklas in his PhD thesis [54]. This test rig was used by Becker et al. [3] in 2005 to investigate the complex flow field together with numerical simulations aimed at optimizing the exhaust system. These researchers focused on the effect of the supersonic tip leakage jet over the last stage rotor blades on the diffuser flow and the diffuser performance at overload conditions. Finzel et al. [19] in 2011 used the same axial-radial diffuser test rig to experimentally study the influence of the exhaust hood area, the flow area in the horizontal joint plane and the location of the steam inlet. Their experimental measurements for all exhaust configurations studied were performed on two axial-radial diffuser geometries (KW21 and V3 already mentioned) at two different load points, which represent the outflow in the design point of a last stage rotor with and without shrouds.

The ITSM also operates a 3-stage model steam turbine in which extensive flow-field measurements downstream of the last stage have been made (e.g. by Zimmermann [86] in 1995, Truckenmueller [75] in 1997 and Voelker et al. [78], in 2005). The flow-field measurements have been used in earlier studies to define the inlet conditions for the flow in the axial-radial diffuser test rig. In particular two aspects of the real steam turbine flow can be modeled by the diffuser test rig. Firstly, the span-wise distribution of swirl velocity at the exit of the steam turbine rotor can be approximately modeled at different operating points by the use of fixed swirl vanes to generate swirling flow at the diffuser inlet. The approximation arises because these swirl vanes are of relatively simple geometry and only give a global representation of the highly complex real swirl distribution. In addition, the vanes are stationary so that the wakes remain in a fixed circumferential position and do not precisely model the rotating wakes from the rotor. Furthermore, there are 22 blades in comparison with approximately 40 blades in the real turbine. The detail of the secondary flows of the swirl vanes is also different from the actual secondary flows in the real machine. Fig. 3.3 shows part load, design load and overload stationary swirlers installed upstream of the diffuser inlet for the test rig depending on the operating point. Part load was not investigated in the current study. Secondly, the measurements performed in earlier studies in the steam turbine have identified a strong supersonic jet at the casing caused by the tip leakage flow over the rotor tip clearance gap. In the real turbine, the jet occurs over each rotating blade tip and is therefore periodic. The overall effect of the momentum of these jets is modelled by a uniform annular jet in the axial-radial diffuser test rig. The tip jet has been introduced into the rig by a special separate annular inlet at the outer diffuser shell with separate control over the flow to change the strength of the tip jet [3].

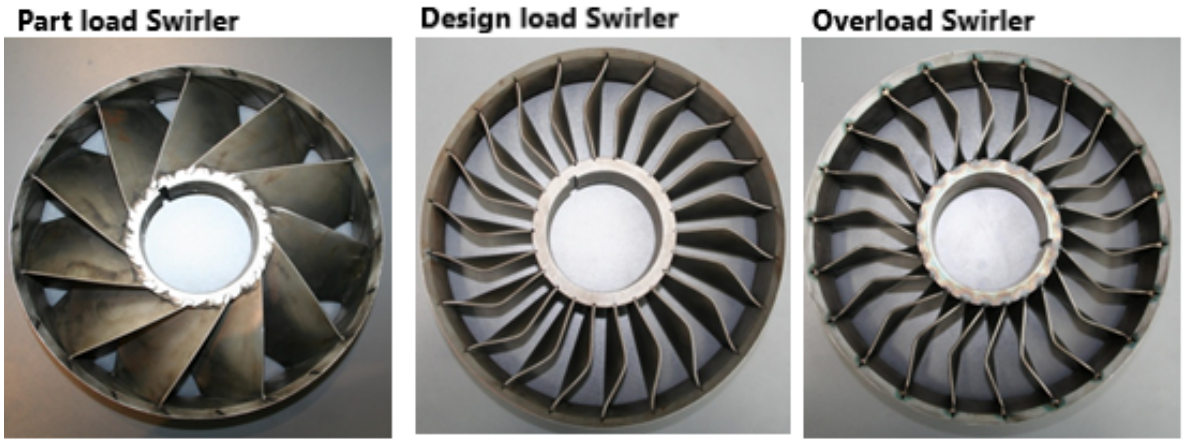

Figure 3.3 – Swirl bodies for Part -, design- and over- load opearting conditions respectively

3.3 Methodology

A numerical approach is used in this study to understand the flow behavior and the mechanisms of loss generation at design and overload operating points. In order to have confidence with the numerical flow fields which are key in understanding the loss mechanism, a mesh independency study is carried out and a validation of numerical results is further performed using experimental data obtained from an axial-radial diffuser test rig operated by the Institute of Thermal Turbomachinery and Machinery Laboratory (ITSM) of the University of Stuttgart. The numerical models used for this study are developed from this test rig which represents a scaled exhaust of a LP steam turbine with an exhaust area of $10m^2$ corresponding to a scaling factor of approximately 1:15. The simulations are performed in ANSYS CFX, Release 17 and meshes are created in ANSYS ICEM CFD. The most significant geometrical features of the test rig that have the highest impact on the exhaust hood performance are modeled. These features are:

- A swirl generator (one swirl generator for each operating point, design-, part- and overload)
- The tip jet geometry
- The axial-radial diffuser and the exhaust hood outer casing.

3.3.1 CFD model

Fig. 3.4 shows the various swirl generators for different operating points. These swirler numerical models are created from the geometry of the test rig's stationary swirlers (see Fig. 3.3) installed upstream of the diffuser inlet to simulate the diffuser inlet swirl generated by the turbine last stage rotor blades. In this study, the design and the overload operating points are considered.

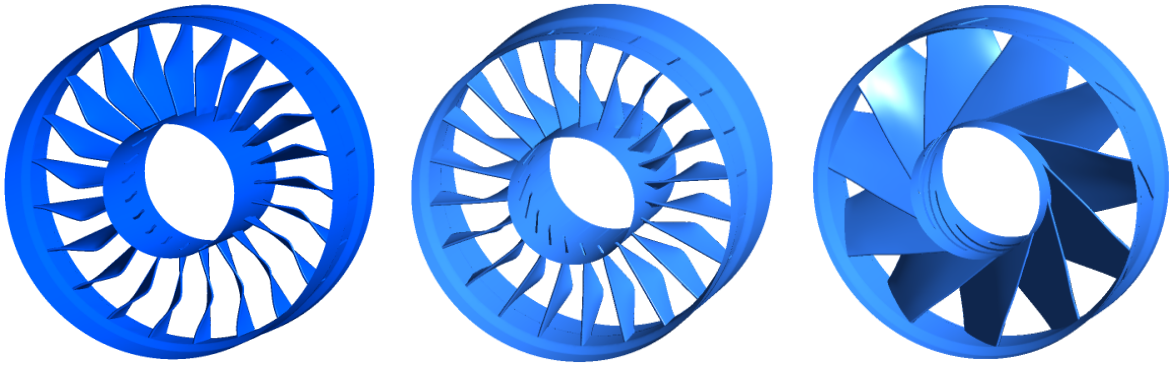

a) Design load swirler b) Overload swirler c) Part load swirler

Figure 3.4 – Numerical models of the stationary swirl generators for various operating points

Fig. 3.5 shows the tip jet, the axial-radial diffuser and the exhaust hood outer casing numerical models. The tip jet model comprises of an annular volume for the tip jet flow and a centre volume for the main flow. It is designed such that it connects both the swirler outlet and the diffuser inlet while providing a tip jet flow around the main flow at the diffuser inlet.

The main flow travels through the swirler, the tip jet model and then into the diffuser in that order while the tip jet flow injects around the diffuser inlet through the tip gap. The swirler, the tipjet model and the diffuser inlet are connected to each other using fluid/fluid interfaces.

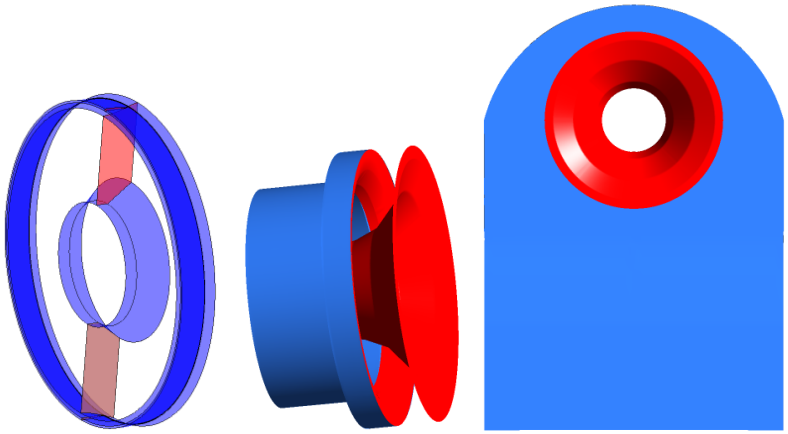

Figure 3.5 – The tip jet, the axial-radial diffuser and the exhaust hood outer casing numerical models (not to scale)

Fig. 3.6 shows the main dimensions of the axial-radial diffuser and the exhaust hood model. Fig. 3.7 on the other hand shows the position of the tip jet model outlet at the diffuser inlet plane and includes a sketch of the tip jet outlet ring with annular diameters of 261mm and 260.5mm resulting to a tip gap height of 0.25mm.

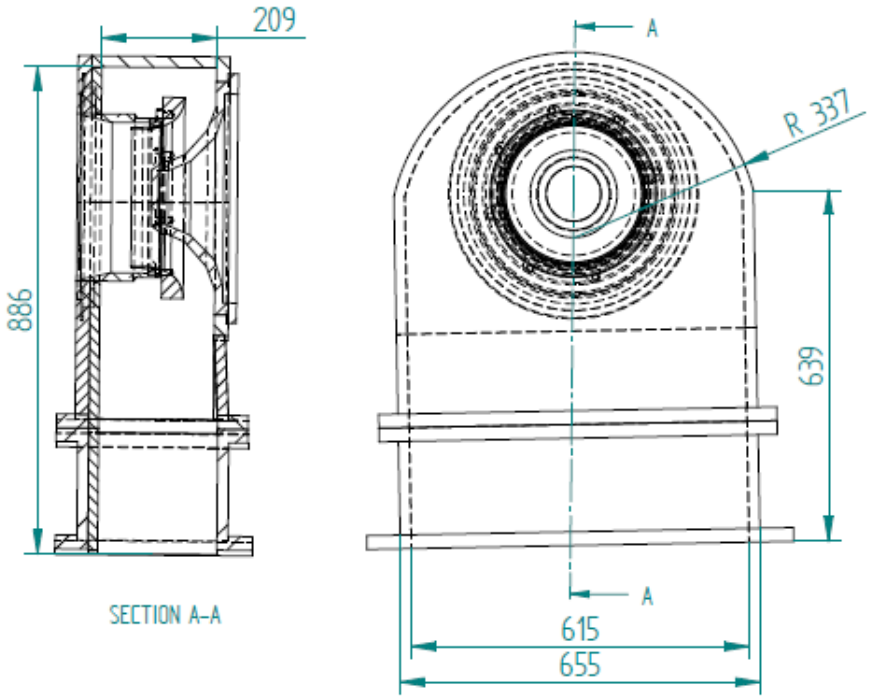

Figure 3.6 – The axial-radial diffuser and exhaust hood model main dimensions in mm

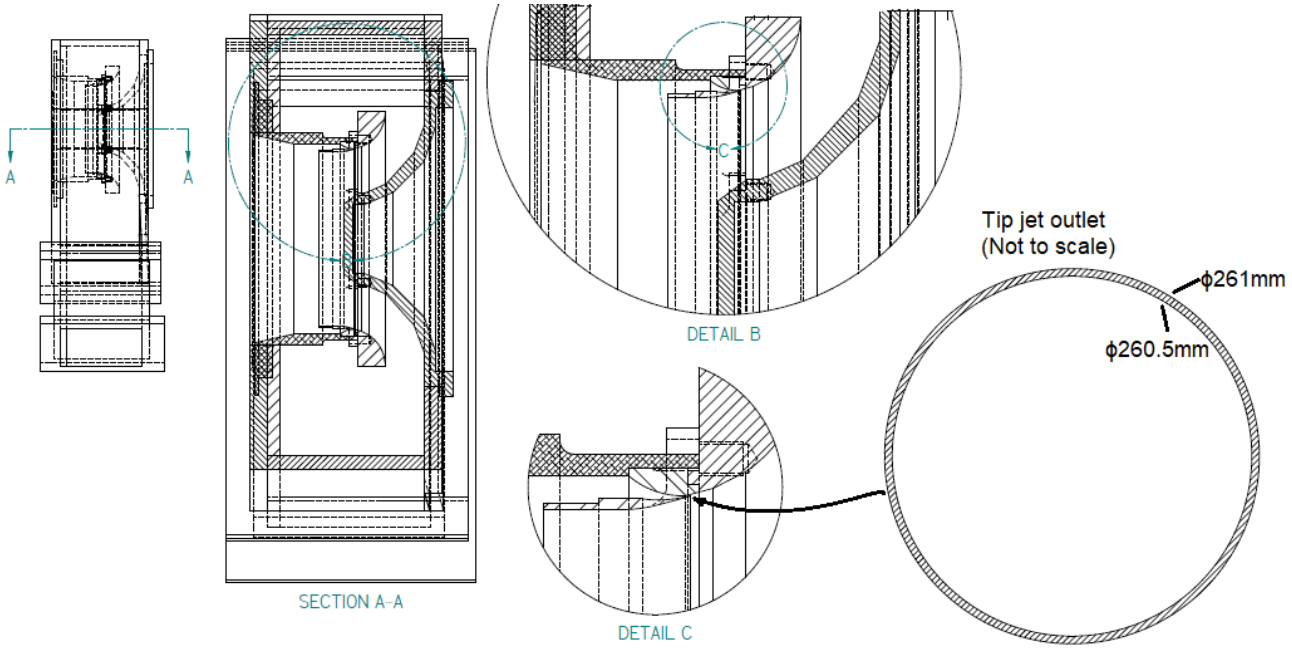

Figure 3.7 – Tip jet model outlet location at diffuser inlet including a not to scale sketch of the tip jet outlet ring

3.3.2 Mesh generation in ICEM CFD

The CAD model of a geometry of interest is first created in Solid Edge modelling software. This model is then imported into ICEM CFD. Visualizing and blocking of the 3D axial-radial diffuser channel connected to the hood volume was the most time consuming. The advantage though was that once the reference configuration was meshed, model modification for new configurations was relatively easy and quick. Structured mesh was created for all configurations. Near wall blocks were included in order to create very small cell heights next to the walls with subsequent cells increasing progressively in height away from the walls. These small near wall cells are essential in boundary layer flow calculations. The Shear Stress Transport (SST) turbulence model used in this study requires a small cell height next to the walls in order to ensure that the y^+ value is kept below 1. In order to obtain acceptable y^+ values within the diffuser and exhaust hood walls during simulation, the first cell next to diffuser and exhaust hood walls is created with a cell height of 0.002mm. This first cell height is estimated using equations 2.1 to 2.5 given in chapter 2 for calculation of the first cell height for a desired y^+ value. The small first cell height of 0.002mm allowed the y^+ values to be kept below 1 for all operating points in the current study. For the swirl generator and tip jet model, near wall blocks are not created, hence the y^+ values for walls of these geometries are not monitored during simulation. In the loss analysis, only the reference configuration is investigated, operated at two operating points i.e design and overload both at tip jet Mach number of 0.4. Fig. 3.8a shows blocks for the axial-radial diffuser (red) and those of exhaust hood inner- and outer casing (blue). Blocks are generated for one-half of the geometry since the geometry is symmetrical. Reflection is done in ANSYS CFX-Pre to obtain the full geometry. Fig. 3.8b shows a section of the generated axial-radial diffuser and the exhaust hood outer casing mesh. Table 3.2 shows the mesh size for the three components of the flow domain.

Table 3.2 – Number of mesh elements used

Model	**Number of elements**
Swirl generator	7 Million
Tip-Jet geometry	0.32 Million
Axial-radial diffuser/exhaust hood outer casing	5 Million
Total number of mesh elements	**12.32 Million**

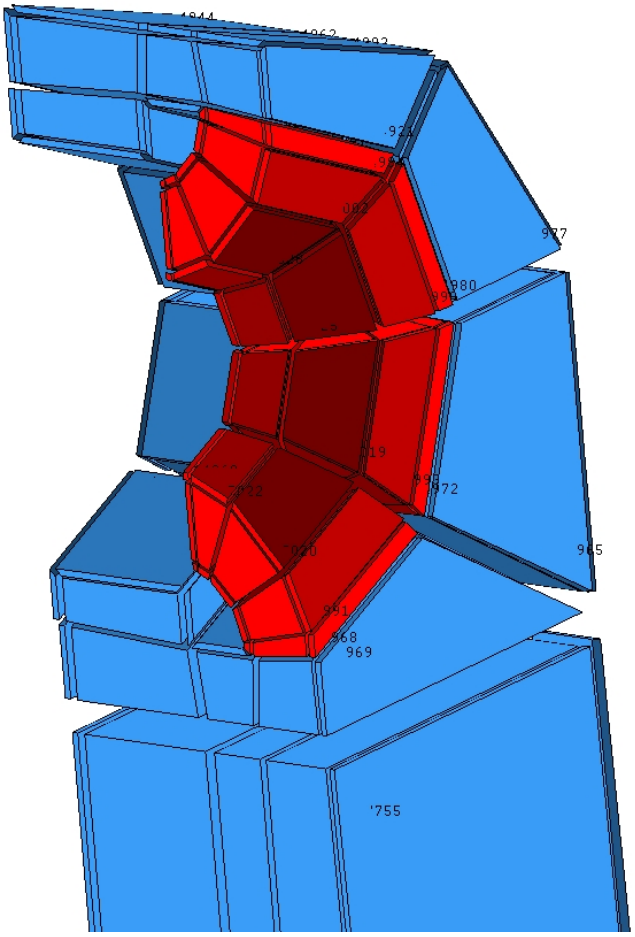

a) Blocks for hood and its axial-radial diffuser

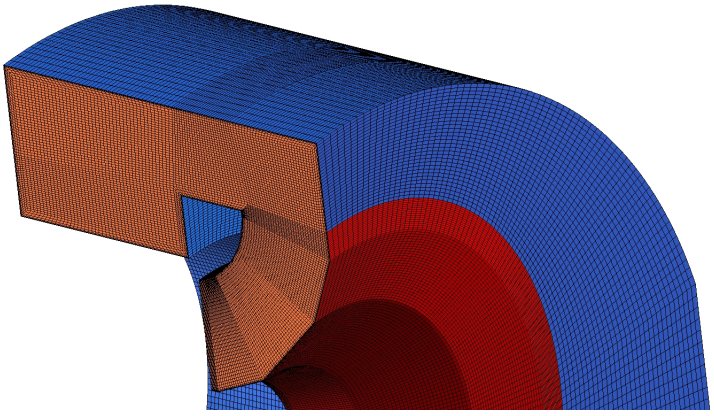

b) A section of mesh

Figure 3.8 – Hood/axial-radial diffuser blocks and a section of mesh

3.3.3 Numerical simulations

Steady state simulations are performed using ANSYS CFX Solver Release 17. The Shear Stress Transport (SST) turbulence model is used. In deciding which turbulence model to use, it was established from literature that the k-ϵ turbulence model underpredicts flow separation and hence is not well suited for use in axial-radial diffuser flows where flow seperation has a great influence on performance of the diffuser and the exhaust hood [7]. A few simulations were though performed using the k-ϵ turbulence model to confirm this fact and as expected, it was found to underpredict the diffuser separation and hence overstate the pressure recovery coefficient. In the numerical simulation, air modeled as ideal gas is selected in ANSYS CFX solver since the test rig used for this study uses air as the working fluid. A mesh independency study was carried out on individual meshes before deciding on the optimal number of mesh elements adequate for this study. Fig. 3.9 shows results of the mesh independency study for the axial-radial diffuser/exhaust hood outer casing mesh. Although 4 million elements were adequate for this model as seen in Fig. 3.9, 5 million elements were used as shown in Table 3.2.

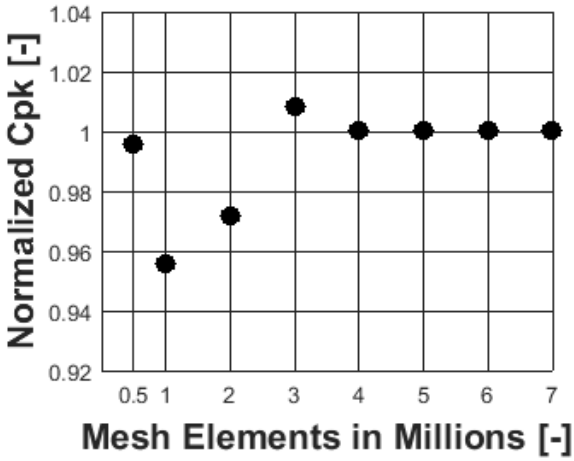

Figure 3.9 – Mesh independency study for the axial-radial diffuser/exhaust hood outer casing at design load and Ma_{tip}=0.

3.3.4 Justification for use of steady state simulation and the ideal gas model

Denton [15] notes that CFD is a prediction tool and must always be used together with experimental testing to validate results. For the current study, values of pressure recovery coefficient obtained using steady state simulation and the ideal gas model utilizing the shear stress transport (SST) turbulence model related well with values calculated from experimental data. Expected trends from literature was observed from both numerical and experimental values e.g. the improved pressure recovery coefficient at supersonic tipjet flow compared to subsonic tipjet flow or no tipjet. This validation of numerical results and the expected trends in literature are shown in Fig. 3.18. Since the experimental

test rig used in this study use air as the working fluid, air modeled as ideal gas was used in numerical simulation.

The most advanced CFD models take into account flow unsteadiness [62] but comparatively few studies are available in the literature [6]. Sieker in 2008 [58] stated that, a highly efficient turbine exhaust diffuser cannot be designed without taking into account the unsteady interactions, but at present, the enormous CPU hours requirement for a full 3D unsteady CFD calculation (10,000 CPU hours on parallel four processor machine for 65,000 iterations [62]) means that this remains a research method rather than a daily design tool. As computational power increases, it is expected that many future numerical studies in this area will include unsteady calculations [6].

Because of the high computational power and computational time requirement for unsteady simulations, many researchers use steady state simulation with turbulence modeled by the k-ϵ turbulence model. Interestingly, good agreement between experimental results and numerical simulations have been observed. Mizumi et al. [47] used commercially available CFD code STAR-CD. Standard turbulence models for STAR-CD are k-ϵ based models. However this model is known to perform poorly for separated flows. In order to overcome this shortcoming, they had to adjust one of the parameters of the k-ϵ turbulence model beforehand so that the experimental results and numerical results matched each other well. These researchers used the ideal gas approximation to estimate the steady flow in the exhaust hood. However, they considered the real gas effect of moist steam by adjusting flow rate, the ratio of specific heat (1.135: the value widely used to represent wet steam condition) and related quantities. Majority of the researchers assume an ideal gas [52, 55] with a specific heat ratio for wet steam [6]. For the current study, specific heat ratio for wet steam was not used because the entire study is based on a test rig operated by air as the working fluid. To be able to validate the numerical results with experimental data obtained from a test rig operated by air, it was necessary for the working fluid in simulation to have the properties of air. Earlier research work performed on this same test rig by Finzel et al. [19] and Becker et al. [3] were very reliable. Although the results from this test rig are not transferable one on one to a real turbine, they have proved reliable in picking expected influences and trends seen by other researchers using different facilities in different geographical locations. For example, Taylor et al. [70] in their parametric study of exhaust hoods in 2016 using the in-house GE's EDS (Exhaust Design System) method and a scaled model test rig at GE found out that reducing the exhaust box width relative to the diffuser lip diameter causes a drop off in diffuser recovery performance. For the narrowest exhaust box they analyzed, they saw a significant fall in performance at higher stage pressure ratios. This was consistent with results presented by Finzel et al. [19] in 2011 using the same test rig as used in the current study, who also saw decreasing diffuser performance as box width reduced. The GE's in-house method (EDS) is a popular method in the exhaust hood design field which was used by Benim et al. [5] in 1995 and Beevers [4] in 2010. The GE's in-house method (EDS) is a steady state RANS calculations which take the form of two parts: First, a single passage calculation from stator inlet to the exit of collector box downstream of the diffuser is modeled. The second step in the EDS calculation models the full exhaust hood and diffuser and uses the database to setup the diffuser inlet boundary profiles. This is done by iteratively

adjusting the inlet boundary conditions based on the calculated flow profiles at the coupling plane.

Numericals results from Taylor et al. [70] done using the GE's in-house EDS system compare quite well with their experimental results which were obtained from a test rig approximately 1/10 scale model of a last stage LP blade and the exhaust box with diffuser, located at GE Power in Rugby, UK. The test rig rotational speed and mixture ratio of the working fluid, R134a and air, are selected to give the required specific heat ratio which ensures the blade tip Mach number is the same as the full-scale machine.

In 2010, Fu et al. [23] did extensive investigations of influential factors on the aerodynamic performance of a steam turbine exhaust system. To evaluate the effect of fluid properties, the fluids for the full-scale exhaust hood were considered as wet steam and air. The thermodynamic properties for the wet steam were calculated based on the Redlich-Kwong equation. The thermodynamic properties for air were calculated by the perfect gas equation. Equilibrium phase change model was chosen to simulate the phase change occuring in the exhaust hood. Distributions of the total pressure, total temperature, flow direction (i.e. pitch angle and swirl angle) and turbulence intensity of 5% were specified at the domain inlet. Calculations for the 1/15 scale model were run with fluid properties of air while calculations for the full-scale geometry were run with properties for both steam and air. Using steady state simulations and the k-ϵ turbulence model utilizing CFX-5 commercial software, these researchers concluded that the numerical results were reliable for they showed similar trends to experimental results with few discrepancies e.g. at swirl angle of zero. These researchers found out that the trends of influence imposed by the inlet swirl distributions on the pressure recovery coefficient, total pressure loss coefficient, and circumferential non-uniformity coefficient are consistent for simulations with air and steam. compared with the performances simulated with air, with steam as the working fluid,the pressure recovery coefficient reduce a little, the total pressure loss coeffient increase slightly. Fig. 3.10 shows plots of pressure recovery coefficient and the total pressure loss coefficient calculated by Fu et al. [23] using different swirl profiles (used to simulate different loading conditions) showing similar trends of coefficient values for air and steam and very minor differences in the coefficient values. They concluded that changing the flow medium from air to steam seems to expand the flow separation located at the diffuser outer end-wall and slightly increase the total pressure loss. Meanwile, the pressure recovery coefficient change very little.

Zoe Burton, who did a thorough literature review in exhaust hood research and publised a paper on literature review, in her PhD thesis [7] in 2014 states that the majority of exhaust hood features can be reasonably well predicted with steady state simulations. However many future publications are expected to include unsteady CFD hood calculations as computational power increases.

3.3.5 Boundary conditions

Choosing the correct boundary conditions at the inlet and outlet of a simulation model is key to obtaining reliable results in CFD simulations. The boundary conditions used in the current study are based on measured values during experiments. Since the main flow

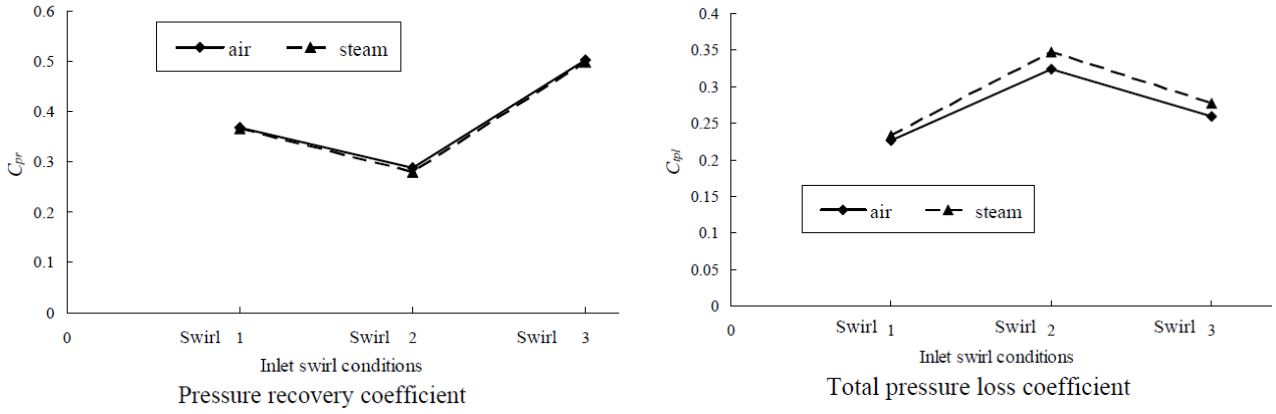

Figure 3.10 – Pressure recovery coefficient and Total pressure loss coefficient calculated by Fu et al.[23] using different swirl profiles showing comparable coefficient values when Air or Steam was used as working fluid in Simulation

inlet of the numerical simulation model is at the swirl generator inlet (see Fig.3.2 and Fig. 3.4) and there is no corresponding measurement plane at the test rig for this location, the total pressure set at the model inlet is adjusted while monitoring the total pressure at the diffuser inlet (Plane E2) until the value at this location corresponds closely to the experimentally determined mass flow averaged total pressure at diffuser inlet. The total pressure at the tipjet inlet is varied while monitoring the tipjet Mach number and mass flow at the tip gap until the desired Mach number is achieved. Once adjustment of total pressure at tipjet inlet and main model inlet are completed, the simulations are allowed to run to completion. In addition to the total pressure inlet boundary condition at main model inlet and the tipjet inlet, total temperature and turbulence intensity at both inlets is set at 296 K and 5% respectively. This value of the total temperature was approximated from the atmospheric temperature during the various experiments done for different operating conditions (carried out on different dates) which was close to this value. The turbulence intensity value was obtained from literature [11]. In 2010, Fu et al. [23] did extensive investigations of influential factors on the aerodynamic performance of a steam turbine exhaust system. In their numerical simulations using commericial software CFX-5, also specified a turbulence intensity of 5% at the diffuser inlet. The outlet boundary condition for simulations is set as the mass flow rate as determined during experiments. See Table 3.1 which summarizes operating parameters measured in experiments and others calculated from the measurements from the axial-radial diffuser test rig (the reference configuration) at different operating points that form the basis of the numerical simulation boundary conditions at the same operating points. The Mach number at diffuser inlet of 0.5 at design load as shown in Table 3.1 is consistent with real turbine Mach number at diffuser inlet. For example, Mizumi et al. [46] used a load condition of a typical power generation plant (60HZ/40"). In this condition, the averaged inflow Mach number of the corresponding actual turbine was assumed to be around 0.53. Tanuma et al. [69] presents flow conditions in a full-scale low pressure turbine. The conditions from measurement of the exhaust diffuser in a full scale development turbine shown in Table 3.3 from Tanuma et al. [69] shows that the Mach number at the diffuser inlet is 0.54 which

is consistent with the test rig Mach number of 0.5 at diffuser inlet shown in Table 3.1 at design load.

Table 3.3 – Flow conditions measured in a full-scale low pressure turbine by Tanuma et al. [69]

Flow condition parameters	**Measured data**
Inlet total pressure (kPa)	4.40
Outlet static pressure (kPa)	4.05
Inlet wetness (%)	3.5
Inlet Mach Number	0.54
Inlet Reynolds Number	530000

The total pressure at diffuser inlet for a real turbine (refer to Table 3.3) and for the test rig (refer to Table 3.1) are both sub-atmospheric but that of a real turbine is way much lower than that measured in the test rig used in this study. The reason for this is because the real turbine uses a condenser that operates under vacuum as it continuously condenses steam. In the test rig, there is no real condenser as it is operated by air. In the test rig, a perforated plate is installed below the condenser inlet plane to mimic the condenser. A way lower static pressure is measured downstream of this plate compared to the upstream due to the pressure drop that occur across this plate. As mentioned earlier, results from the test rig are not transferable one to one from the test rig to a real turbine but generic studies of the effects of different parameters have been found to be reliable from previous studies [3, 19].

3.3.6 Flow field visualization

The goal in this chapter is to identify the main sources of loss in exhaust hoods of low pressure steam turbines. To achieve this, a flow field visualization tool was necessary which allows a detailed examination of the flow phenomena occurring within the flow. Eight sectors, each spanning 45°, are created at the diffuser inlet from which flow streamlines originate. Fig. 3.11 shows the eight sectors created at diffuser inlet. The flows which originate from these sectors are named according to the sector position in relation to each other in the flow direction at diffuser inlet. This approach of generating different flows from different sectors was used by Mizumi et al. [46] and later by Yin et al. [82] and is considered to be a very effective method of looking at the complicated flow field of exhaust hoods in 3D.

3.3.7 CFD data analysis

Flow streamlines originating from different sectors at the diffuser inlet are evaluated at predetermined evaluation surfaces along the flow path. A Matlab program interpolates the values of flow variables for individual streamlines at the evaluation surfaces and then performs respective averaging of variables of interest for all streamlines originating from

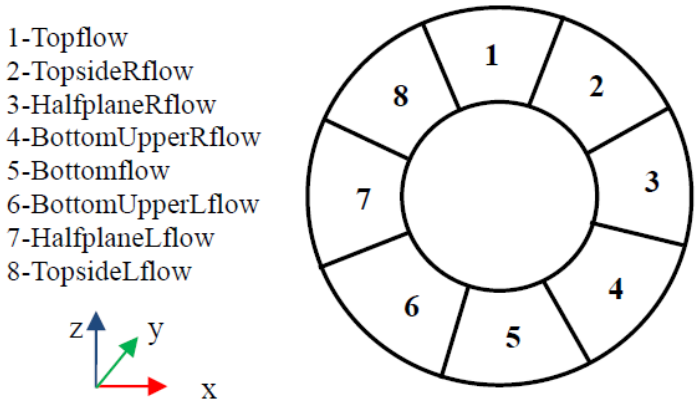

Figure 3.11 – Sectors at diffuser inlet where different flows originate. Direction of view is forward facing aft. Flow in +ve y-direction at diffuser inlet.

one sector at each surface. Fig. 3.12 shows some of the predetermined surfaces of evaluation. The calculated average pressure values for each individual flow are used to calculate three coefficients at each evaluation surface, i.e.

- Pressure recovery coefficient
- Dissipation coefficient
- Residual kinetic energy coefficient (corresponding to leaving loss coefficient at model outlet).

A study was performed to determine the optimum number of streamlines for each flow which gives an independent result. It was found that 500 streamlines are adequate for each flow for the evaluation of the coefficients.

The following equations are used to calculate the three coefficients at the evaluation surfaces:

- Mass flow average of total pressure at a given evaluation surface for a given flow;

$$Pt = \frac{\sum_{i=1}^{n} p_{ti}\rho_i v_i}{\sum_{i=1}^{n} \rho_i v_i} \tag{3.1}$$

- Average static pressure at a given evaluation surface for a given flow;

$$Ps = \frac{1}{n}\sum_{i=1}^{n} p_{si} \tag{3.2}$$

- The mass flow average of total pressure and the average value of static pressure at the diffuser inlet for each flow is calculated using equations 3.1 and 3.2, using variables from the streamlines' origin since the streamlines start at the diffuser inlet.

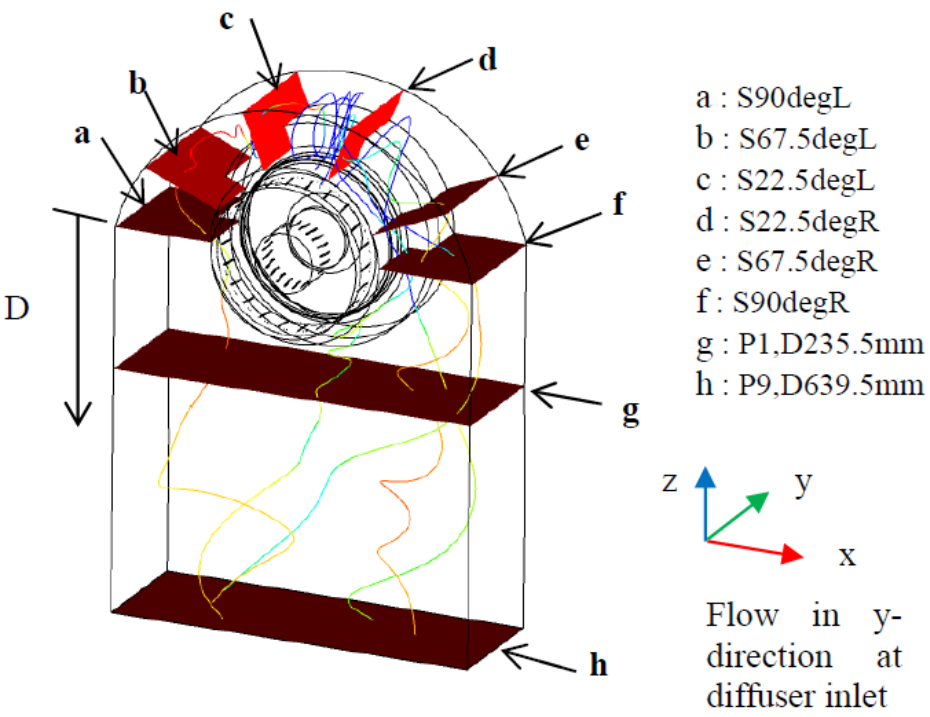

Figure 3.12 – Evaluation surfaces. Direction of view is forward facing aft

The mass flow average of total pressure and average value of static pressure at the diffuser inlet are designated as Pt_{in} and Ps_{in} respectively.

- The pressure recovery coefficient (C_p), the pressure loss (or dissipation) coefficient (ζ) and the residual kinetic energy coefficient (ξ) at each evaluation surface for each flow are calculated using equations 3.3, 3.4 and 3.5 respectively;

$$C_p = \frac{Ps - Ps_{in}}{Pt_{in} - Ps_{in}} \tag{3.3}$$

$$\zeta = \frac{Pt_{in} - Pt}{Pt_{in} - Ps_{in}} \tag{3.4}$$

$$\xi = \frac{Pt - Ps}{Pt_{in} - Ps_{in}} \tag{3.5}$$

- The sum of the pressure recovery, the dissipation and the residual kinetic energy coefficients is equal to unity;

$$C_p + \zeta + \xi = 1 \tag{3.6}$$

The relationship given by equation 3.6 is checked by the Matlab code for quality assurance.

Plotting the coefficient values at the surfaces of evaluation within the exhaust hood presents an opportunity of understanding the flow better and identifying the possible causes of losses within the exhaust hood. To further understand the mechanism of losses within the exhaust hood, values of shear strain rate are exported from ANSYS CFX Post from the evaluation surfaces. A Matlab code reads these values and plots them together with the velocity vectors u and v at the given evaluation surface for each flow. The velocity vectors u and v are calculated at the point of intersection between a streamline and an evaluation surface through interpolation. Since the evaluation surfaces at the upper hood are inclined, the x-coordinates and velocity vector in the x-direction (u) are transposed to lie along the inclined surface for these surfaces. This allows the shear strain rate values obtained from an inclined surface within the hood to be plotted in a horizontal plane together with u and v velocity vectors.

As illustrated in Fig. 3.13, the angle θ is defined in such a way that it is 0° at the topmost point of the exhaust hood and increases in both directions so that it is 90° on both the left-hand side (LHS) and the right-hand side (RHS) of the hood at the half-joint plane.

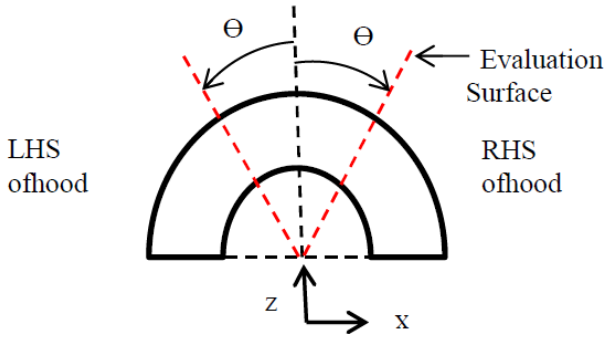

Figure 3.13 – Definition of angle θ for the positioning of the inclined evaluation surfaces. Direction of view is forward facing aft

Therefore;

$$x' = \frac{x}{\sin\theta} \tag{3.7}$$

$$u' = \frac{u}{\sin\theta} \tag{3.8}$$

Equations 3.7 and 3.8 give the x coordinate and the velocity vector in the x direction (u) transposed to lie along an inclined evaluation surface of the upper hood.

3.4 Validation of the numerical results

To validate the numerical results, experiments were carried out on the test rig on which the numerical models are based. Experimental results allow for the calculation of the pressure recovery coefficient of the exhaust hood. Good agreement between the numerical and experimental values of the pressure recovery coefficient would mean that the

flow behavior observed in simulation is close to the behavior of the real flow during experiment. The axial-radial diffuser test rig operated by ITSM is described in detail in section 3.2 and also by Finzel et al. [19] and Becker et al. [3]. It is used to model steam flow in exhaust system, representing a scaled exhaust of a LP steam turbine with an exhaust area of $10m^2$ corresponding to a scaling factor of approximately 1:15. The rig is operated with air from two separate compressors which operate under suction for the main flow and pressure for the tip jet. Sufficient capacity is available to operate at the same Mach number levels as found at the outlet of low pressure steam turbines. The rig is designed for investigations of various effects on the performance of axial-radial diffusers and some earlier results from this rig have been reported [3, 19].

Fig. 3.14a shows the exhaust hood test rig with swirl body and the diffuser inlet and outlet measurement planes. The axial-radial diffuser has two parts; the diffuser inner shell and the outer shell. The inner shell has 8 static pressure taps as can be seen in Fig. 3.14b which constitute the provision for inner wall static pressure measurements after each 22.5° of rotation hence summing up to 128 discrete static pressure measurements at the diffuser inner wall. The diffuser outer shell is fixed and has 8 rows of 8 static pressure taps summing up to 64 discrete static pressure measurement locations at the diffuser outer wall.

There are two measurement planes for probe traverses at the diffuser inlet and the diffuser outlet plane. In both measurement planes, conical five-hole pneumatic probes are used to determine total pressure, static pressure and flow vector. The diffuser inlet probe, installed at the diffuser inner shell, traverses six radial positions. At the diffuser exit plane (plane E3), a second five-hole probe is installed at the diffuser inner shell, which similarly traverses six measurement points in the axial direction. As both probe traverses are repeated after each 22.5° of rotation of the diffuser inner shell, a total of 96 discrete measurement points are obtained at each location. The static pressure (Pk) at the condenser plane (plane c) is measured with eight pressure taps around the casing which are connected to each other (pneumatically averaged) so that the static pressure is measured by only one pressure channel. A measurement tool based on LabVIEW is used to control the measurement process and store all data of interest.

Equation 3.9 is used to calculate the pressure recovery coefficient (Cpk) values for comparison between simulation and experiments. The pressure values used are based on the diffuser inlet (plane E2) and the condenser plane (plane c) values. At the diffuser inlet, the total pressure is mass flow averaged while the static pressure is area averaged.

$$Cpk = \frac{Pk - P_{sin}}{P_{tin} - P_{sin}} \tag{3.9}$$

3.4.1 Comparison of experimental and simulated flow variables at diffuser inlet (Plane E2)

Fig. 3.15a represents the diffuser inlet plane with the points of intersection between the radial lines (span) and the circles representing the 96 measurement points at the dif-

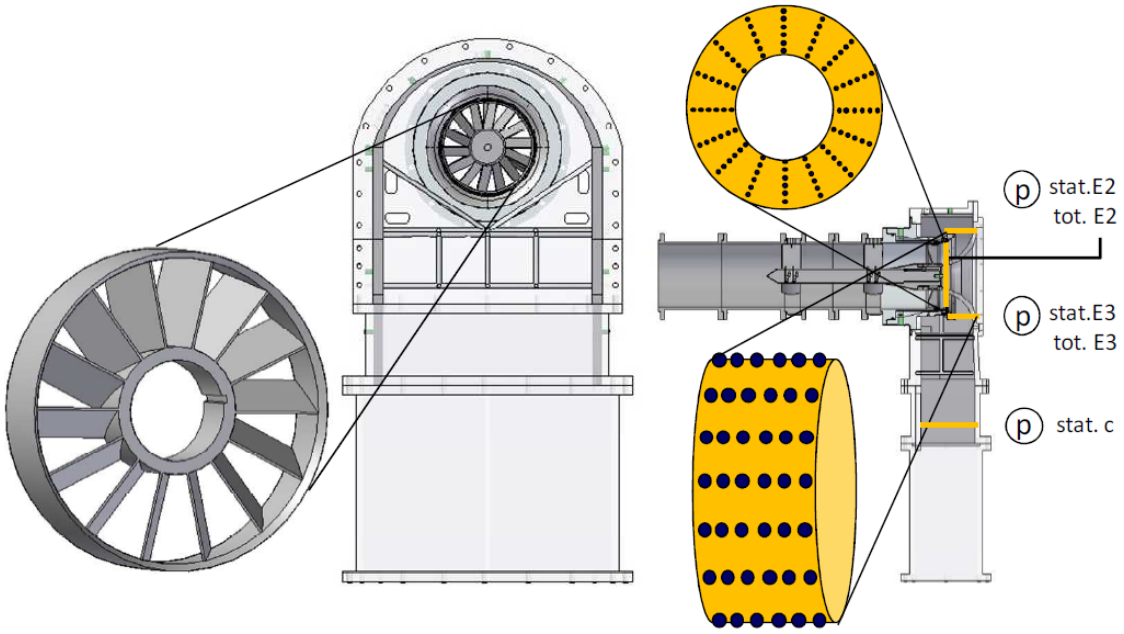

a) Axial-radial diffuser test rig. A swirl body and measurement planes are highlighted [19]

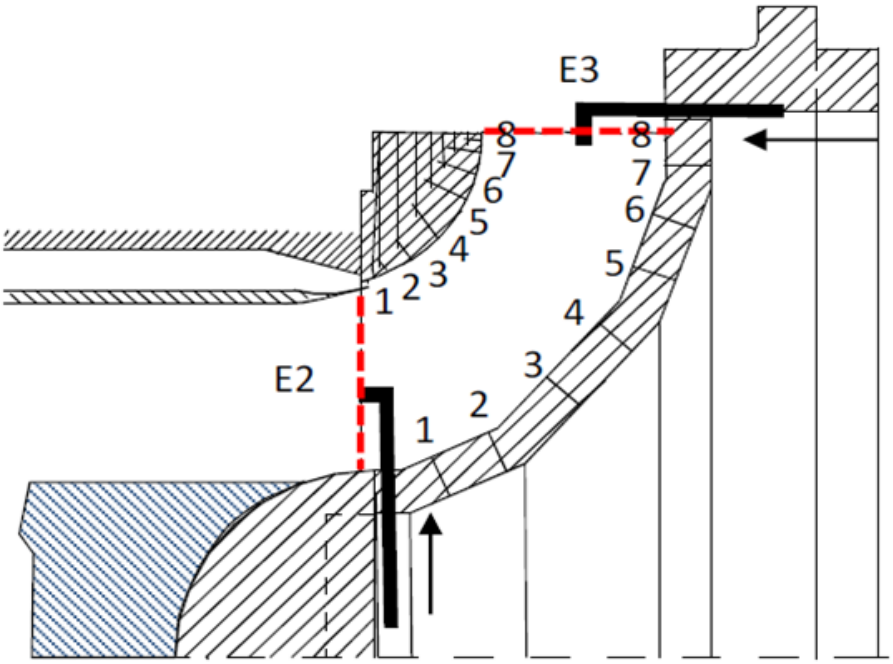

b) A section view of the diffuser showing different measurement locations. The diffuser inlet and outlet planes are represented by red broken lines with pneumatic probes installed at diffuser inner shell

Figure 3.14 – Exhaust hood test rig operated by ITSM with swirl body and measurement planes

fuser inlet. Fig. 3.15b shows a comparison of total and static pressure along span at 45° and 225° (see Fig. 3.15a for span location) at the diffuser inlet between experiment and simulation at design load operating point and at a tip jet Mach number of 0.4. Similarly, Fig. 3.16 shows a comparison between experimental and simulated Mach numbers along span at 45° and 225°.

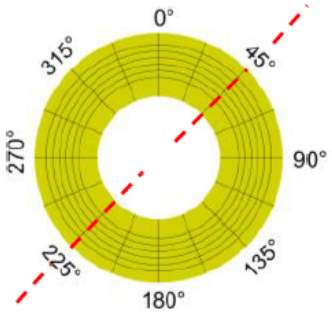

a) Orientation of 16 spans at the diffuser inlet with points of intersection representing measurement points

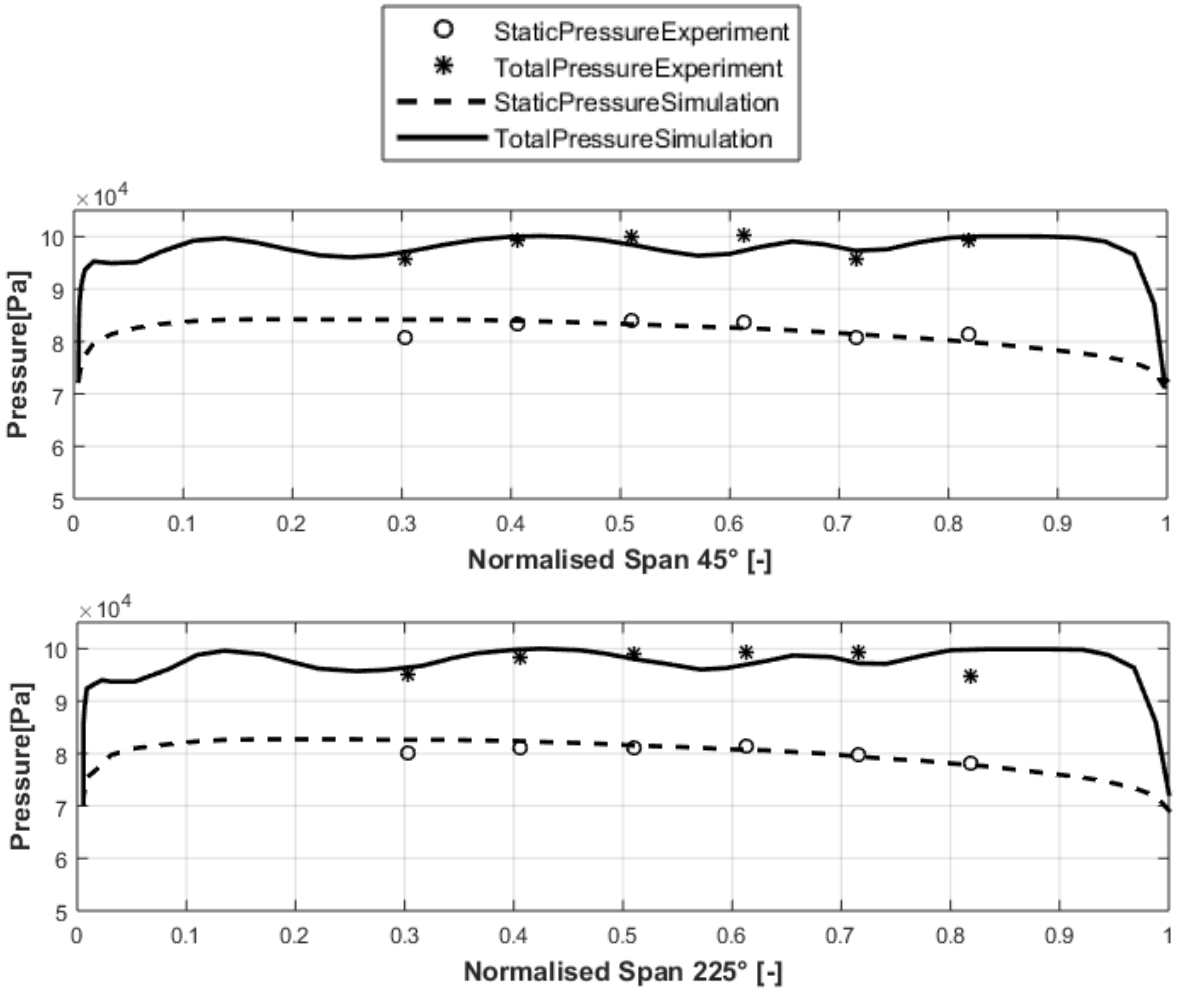

b) Comparison of total and static pressure along span at 45° and 225° at the diffuser inlet. The operating point is design load at tip jet Mach number of 0.4

Figure 3.15 – Total and static pressure validation at the diffuser inlet

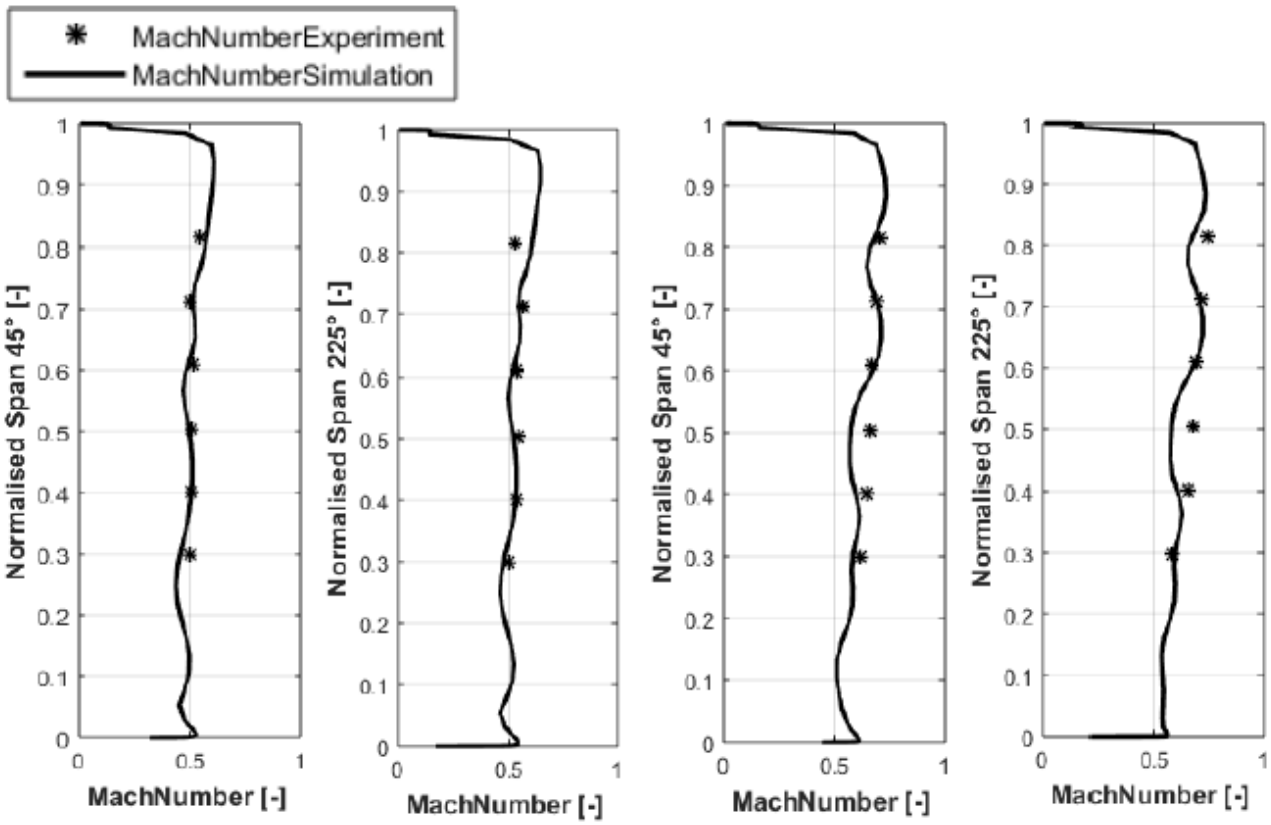

a) Design Load (DL) and tipjet Mach number of 0.4 b) Overload (OL) and and tipjet Mach number of 0.4

Figure 3.16 – Comparison of Mach number along span at 45° and 225° at the diffuser inlet between experiment and simulation.

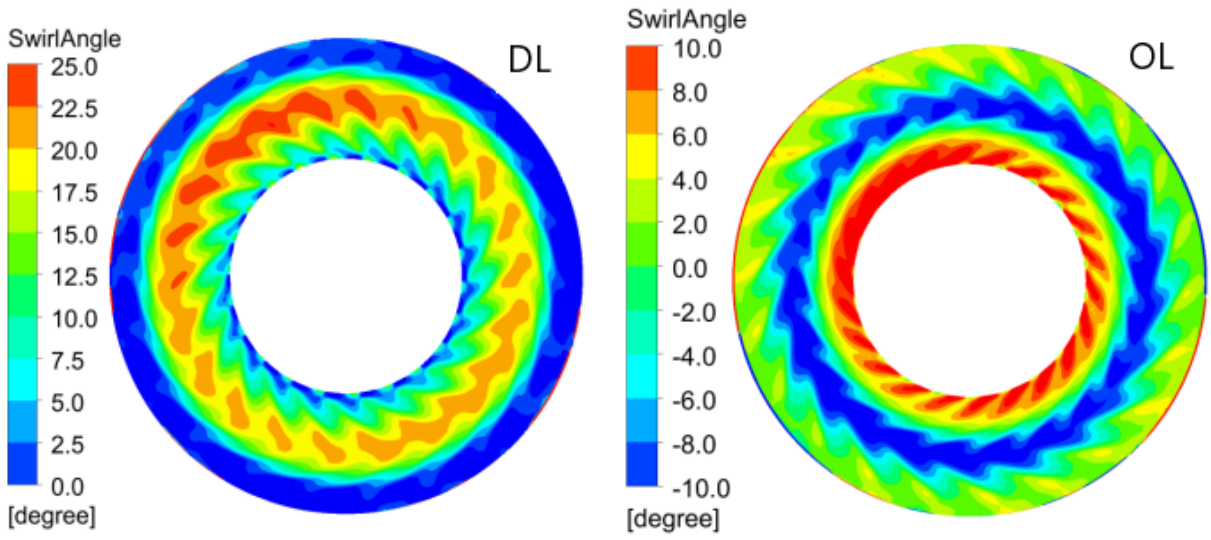

Figure 3.17 – Computed swirl angle distribution at the diffuser inlet for design load (DL) and overload (OL) operating condition. The tip jet Mach number is 0.4 for both cases.

Although the experimental and simulated values of total pressure, static pressure and the Mach number at diffuser inlet are not an exact match, the agreement is considered sufficient for the current study. Fig. 3.17 shows the swirl angle distribution at the diffuser inlet for the design and overload operating condition both at tip jet Mach number of 0.4. These simulation results show more swirl at the diffuser inlet for the design case compared to the overload case. This is the reason for higher flow asymmetry at design case compared to overload case later seen in the comparison of topflow streamlines in Figures 3.19a and 3.23a for design and overload operating conditions respectively.

3.4.2 Comparison of Cpk values from experiment and simulation

Fig. 3.18a shows a comparison between experimental and numerical pressure recovery coefficients (Cpk) values for different operating points. The numerical results using the Shear Stress Transport (SST) turbulence model are validated using experimental data for the design and overload operating points at three tip jet Mach numbers of 0, 0.4 and 1.2. Although these results do not show an exact match between experimental and simulation results, the agreement is very good and is considered sufficient to warrant use of the numerical flow field as a representation of the real flow field for the current study. Both experimental and numerical static pressure recovery coefficient values show similar and expected trends:

- The pressure recovery coefficient (Cpk) is lowest at the tip jet Mach number of 0.4 for the three tip jet cases presented. This is because the Mach number of the main flow is higher than the tip jet Mach number for both design and overload cases (> 0.5) hence the tip jet at this low intensity introduces mixing losses rather than minimizing separation at the diffuser outer shell.

- The pressure recovery coefficient (Cpk) is highest at the tip jet Mach number of 1.2 for both design and overload conditions. It is known from literature that a high tip jet intensity minimizes diffuser separation and hence improves the static pressure recovery. This is made possible by the so called 'Coanda effect' which is a phenomena in which a jet flow attaches itself to a nearby surface and remains attached even when the surface curves away from the initial jet direction. This effect is responsible for energizing the boundary layer along the curved diffuser surface and hence suppressing flow separation. This results in a high static pressure recovery coefficients at tip jet Mach number of 1.2 compared to those at low tip jet intensity.

- The pressure recovery coefficient (Cpk) values are lower at overload compared to design load for all the three different tip jet Mach numbers.

Fig. 3.18b shows a comparison of numerical results using the Shear Stress Transport (SST) and k-ϵ turbulence models at design load and at three different tip jet Mach numbers (0, 0.4 and 1.2). It can be seen that the static pressure recovery (Cpk) values obtained using the k-ϵ turbulence model are very high compared to experimental results.

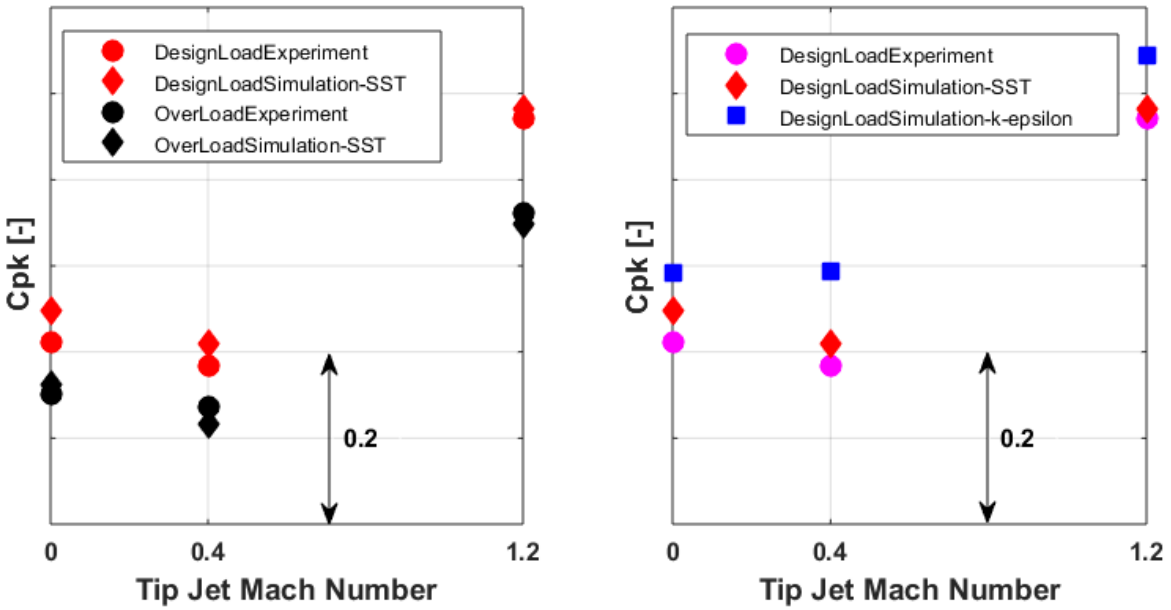

a) Comparison of experimental and numerical Cpk values

b) Comparison of the SST and k-ϵ turbulence models

Figure 3.18 – Validation of numerical results using experimental data

This model also fails to predict the decrease of the pressure recovery coefficient at tip jet Mach number of 0.4 compared to that at no tip jet. It is known from literature that the k-ϵ turbulence model under-predicts boundary layer separation in curved surface flows [7] which is the reason why the model over-predicts the static pressure recovery coefficient (Cpk). Although a number of researchers in diffuser flows have used the k-ϵ turbulence model, they appreciate its shortcomings. Zoe Burton, a researcher who did a thorough literature survey on low pressure steam turbine exhaust hoods [10] writes the following in her PhD thesis [7], *'By far, the most widely adopted turbulence model for exhaust hood simulations is the k-ϵ turbulence model, despite its poor performance in predicting highly separated flows. Both SST and k-ω models are used, although infrequently'*. It should be noted however that the k-ϵ model is still able to predict the trend of the static pressure recovery coefficient between tip jet Mach number of 0.4 and 1.2 as can be seen in Fig. 3.18b . In this PhD thesis, all numerical simulation results reported are done using the Shear Stress Transport (SST) turbulence model which showed a good agreement with experimental results.

3.5 Results and discussion

The numerical results reported in this section are based on the axial-radial diffuser test rig already discussed operated at design and overload operating points. The tip jet Mach number for these two load cases is set to 0.4.

3.5.1 Design load

The different flows named after their relative originating sector at diffuser inlet (see Fig. 3.11) are displayed in Fig. 3.19 for this operating point. These flows depict a very complex 3D flow which would be very hard to visualize without application of the approach presented in section 3.2.4. The streamline color represents static entropy. A close examination shows that the flows originating from the upper sectors, namely the Topflow, TopsideRflow and TopsideLflow are generating higher entropy compared to the rest of the flows. Comparison of the pressure recovery, dissipation and residual kinetic energy coefficients at the evaluation surfaces within the exhaust hood offers a further insight on the approximate position where most of the losses occur and the flows which are involved. Fig. 3.20 shows a comparison of these coefficients at different evaluation surfaces (see Fig. 3.12 for the various evaluation surfaces within the flow domain). From the dissipation coefficient plot, it can be seen that the dissipation coefficient at the diffuser outlet (circular symbols) is very low. By the time the Topflow crosses the S22.5deg surface, considerable dissipation has already occurred to it. The Topflow dissipation coefficient profile shows a large gradient between the S22.5deg surface and the P1,D235.5mm plane. Its value remains relatively constant after this plane for the Topflow, indicating that no appreciable further losses in this flow are incurred. Similar behavior is seen for the other two top flows, i.e. TopsideRflow and TopsideLflow. By the time these two flows cross the S67.5deg surfaces, considerable dissipation has already taken place. The loss is higher for the TopsideLflow compared to the topsideRflow because the overall flow is highly asymmetrical. The flow asymmetry at this operating point is caused by the swirl profile (see Fig. 3.17) at the diffuser inlet generated by the stationary swirl generator upstream of the diffuser inlet which simulates the inlet swirl generated by last stage turbine blades in large scale LP steam turbines. The flow asymmetry can be seen from the behavior of streamlines of the Topflow-sector in Fig. 3.19a. The streamlines are shifted more to the hood RHS as they emerge from the diffuser into the exhaust hood outer casing. As can be seen in Fig. 3.19c, some streamlines of the TopsideLflow are forced to move backwards and flow through the RHS of the hood. This reverse flow in the upper part of the hood causes this flow to have a higher dissipation compared to TopsideRflow.

All the LHS flows have a higher dissipation compared to their respective RHS flows.This is because the inlet swirl directs the flow towards the RHS of the hood and therefore flow going through the LHS of hood must turn first to take this 'not preferred' path hence more dissipation occurs.

The gradients for the dissipation coefficient for TopsideRflow and TopsideLflow are relatively similar to that of the Topflow at the upper hood and after crossing the P1,D235.5mm plane, their profiles remain relatively constant. The three topflows (Topflow, TopsideRflow and TopsideLflow) dominate in terms of losses in the upper hood (hood volume above plane P1, D235.5mm). As can be seen in Fig. 3.19, all the eight flows tend to flow in swirling motion. Streamlines with the smallest radius of curvature belong to Topflow while streamlines with the largest radius of curvature belong to the Bottomflow. This phenomenon was explained by Yin et al. [82]. Because of this, flows originating from a upper sector tend to be entangled by those originating from a lower sector. This phenomenon holds true as long as a difference in kinetic energy exists be-

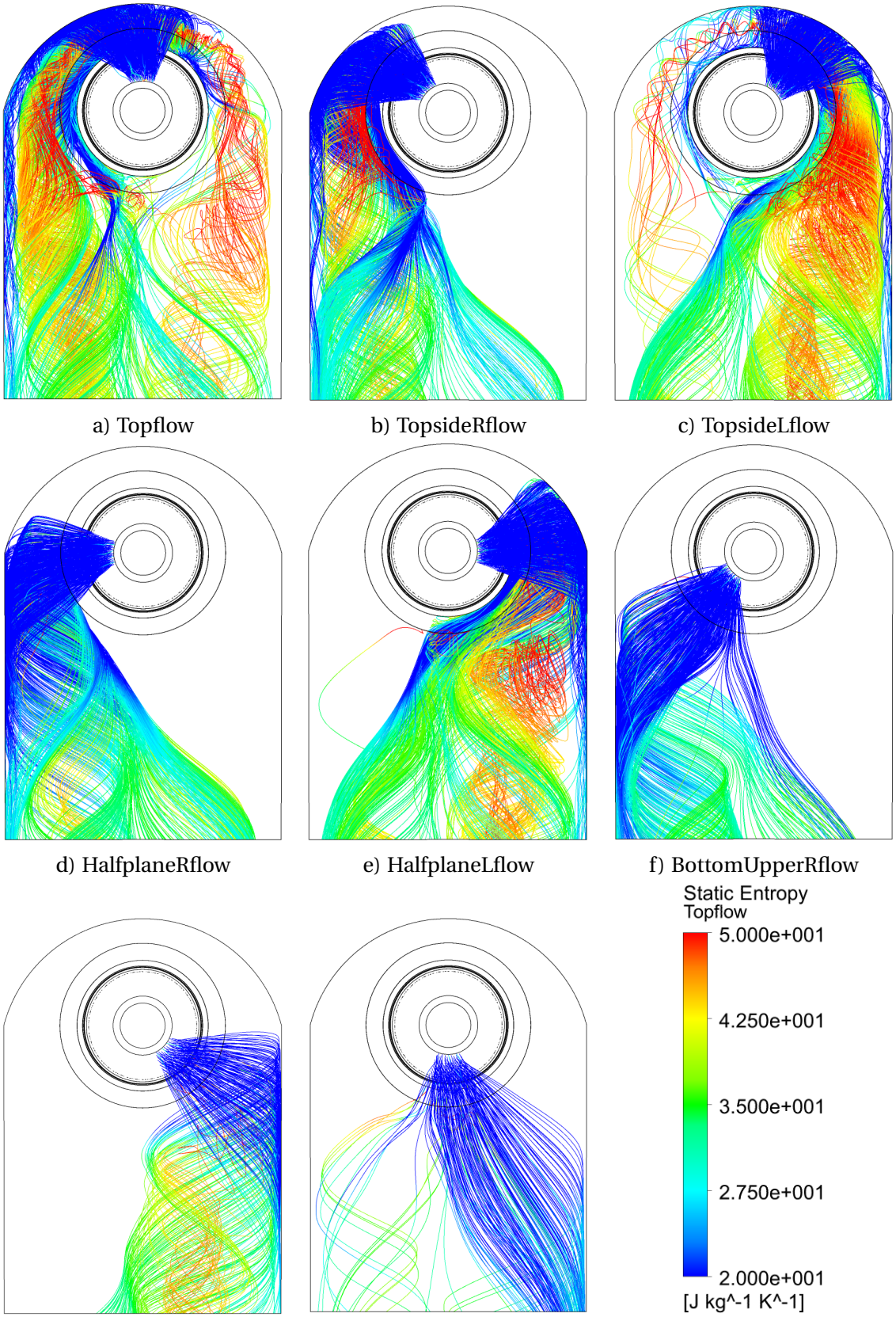

a) Topflow b) TopsideRflow c) TopsideLflow

d) HalfplaneRflow e) HalfplaneLflow f) BottomUpperRflow

g) BottomUpperLflow h) Bottomflow

Figure 3.19 – Flow field at design load. Direction of view is aft facing forward

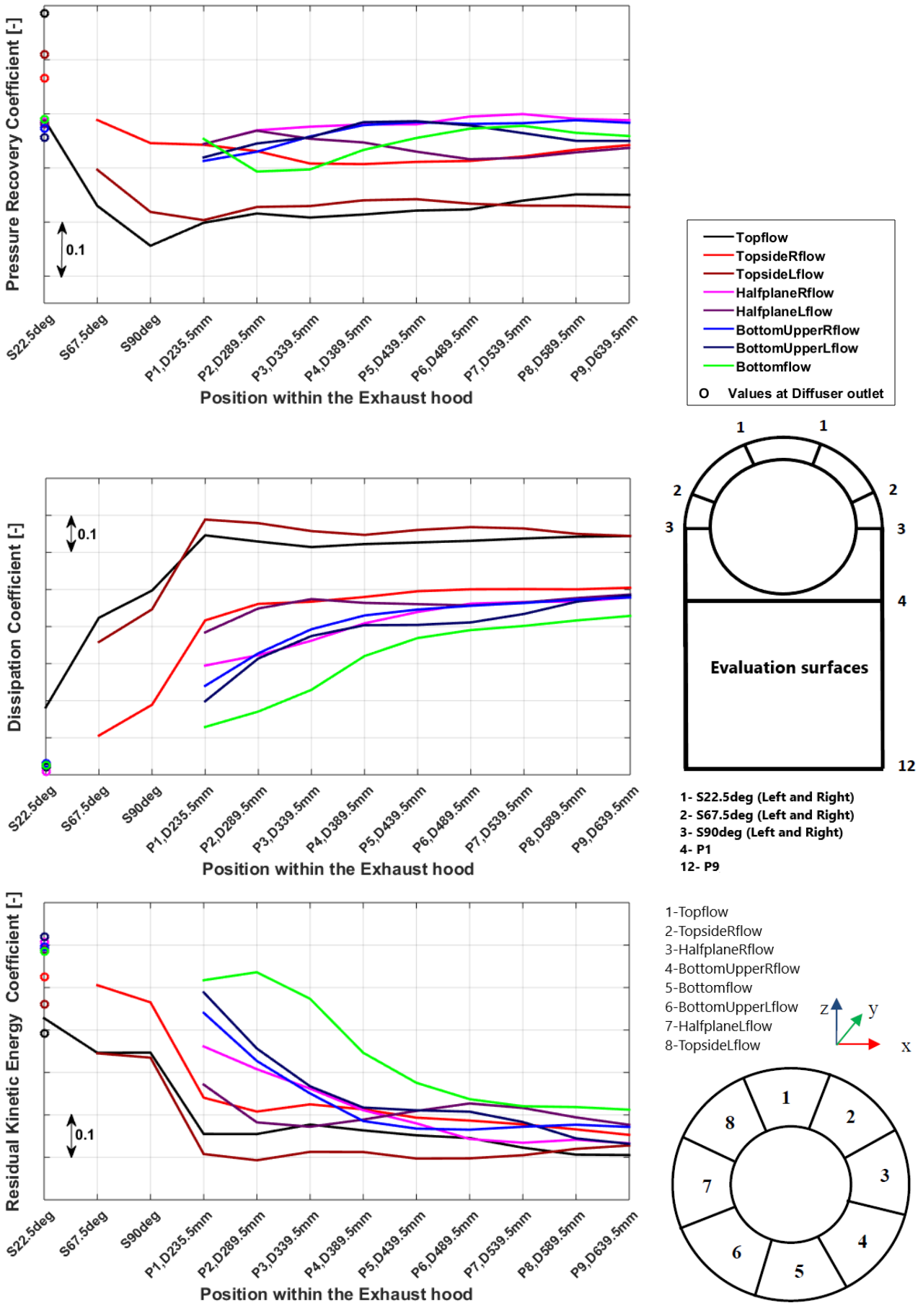

Figure 3.20 – Comparison of coefficients at design load (See Fig. 3.12 for the different positions within the exhaust hood)

tween the flows. As the more energetic flow continues to lose its kinetic energy through dissipation facilitated by the velocity gradients between the flows, a kinetic energy level is reached where the flows in question can mix. From Fig. 3.20, the pressure recovery coefficients for the individual flows do not vary significantly after the flow passes plane P1,D235.5mm. Conversely, the residual kinetic energy coefficient decreases rapidly past this plane for the bottom flows (Bottomflow, BottomUpperRflow, BottomUpperLflow, HalfplaneRflow and HalfplaneLflow) with a differing intensity for individual flows until they reach a relatively constant value. As the residual kinetic energy coefficient decreases, the dissipation coefficient increases for these flows indicating losses. These losses in bottom flows are associated with the shearing forces created when the low-momentum top flows (Topflow, TopsideRflow and TopsideLflow) which have already lost most of their kinetic energy through dissipation are entangled by the faster bottom flows, thus creating high velocity gradients. As the faster moving flows exchange their momentum with the slower flows through the fluid viscosity, viscous forces become significant in relation to the inertia forces. Apart from creating the necessary condition for high shear within the flow, the vortex cores of the swirling flows reduce the available area of flow by acting as aerodynamic blockages.

Figures 3.21 and 3.22 show grey scale plots for shear strain rate including u and v velocity vectors at design load at selected evaluation surfaces. High loss regions are represented by darker areas. In Fig. 3.21a, the high shear strain rate region 'a' is caused by the interaction between a separation at the the diffuser outer shell and the main flow in the diffuser. The low velocity of the separated flow and the high velocity of the diffuser main flow create the velocity gradients which lead to these shear regions. High shear strain rate region 'b' is caused by high velocity gradients created by the counter rotating swirl flows on both the RHS and the LHS of the hood. The magnitude of the loss appears to be more on the RHS of the hood because the flow is asymmetrical with more flow flowing through the RHS. Regions 'c' and 'd' are caused by the interaction between the flow re-circulation in the corner and the high kinetic energy flow deflected by the hood casing. Similar loss regions seen in Fig. 3.21a are observed in Fig. 3.21b and Fig. 3.21c. The magnitude of dissipation appears to decrease as the flow progresses downwards but the mechanism of loss is similar at the six evaluation surfaces at the upper hood (see the location of the six evaluation surfaces at the upper hood in Fig. 3.12).

As can be seen in Fig. 3.22, the main loss mechanism at the lower hood is different from that of the upper hood. Fig. 3.22a show that the top flows (Topflow, TopsideRflow and TopsideLflow) are entangled by the faster moving bottom flows at this evaluation surface. The entire flow forms two huge counter rotating vortices and smaller circulating flows at the four corners. A high shear strain rate region labeled 'e' is attributed to the interaction between the two counter rotating vortices as the flow from the LHS appear to meet the one from the RHS head on. The other major loss region labeled 'f' can be attributed to the angle at which the flows with higher residual kinetic energy (HalfplaneLflow and Bottomflow) collide with each other. This loss region is extended by existence of a small re-circulation region to the right and the interaction between faster flows (Bottomflow and BottomUpperLflow) with slower top flows (Topflow and TopsideLflow) to the left. Further down the flow path, flow mixing occurs as the flows with higher residual kinetic energy lose their energy through dissipation within the shear regions created by the ve-

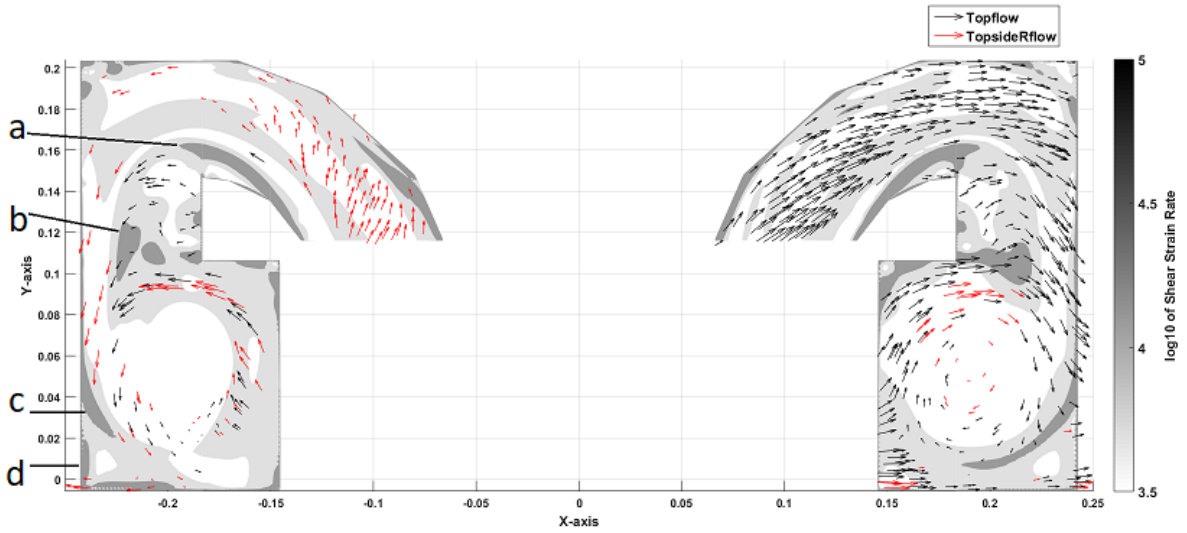

a)Shear strain rate and velocity vectors at evaluation surface *S*22.5°

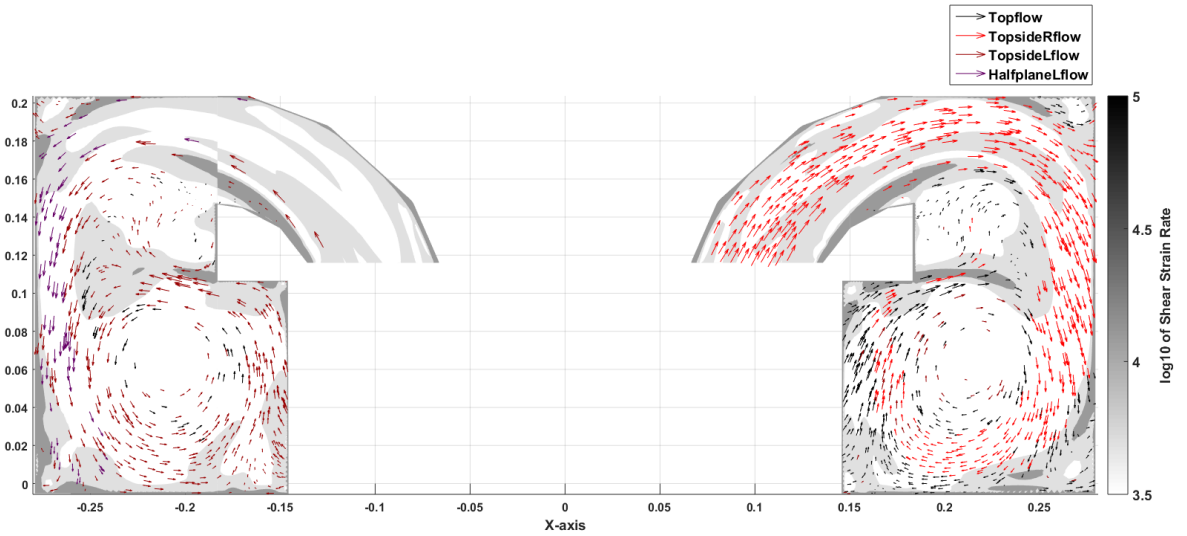

b) Shear strain rate and velocity vectors at evaluation surface *S*67.5°

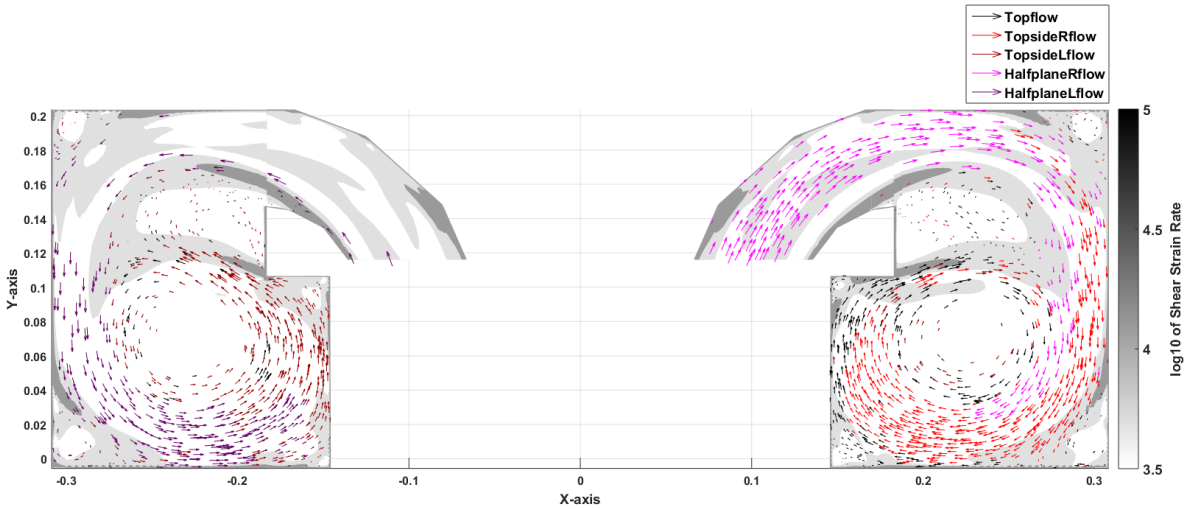

c) Shear strain rate and velocity vectors at evaluation surface *S*90° (Half-joint plane)

Figure 3.21 – Regions of high shear at upper hood at design Load. View from the top (See Fig. 3.12 for the different evaluation surfaces)

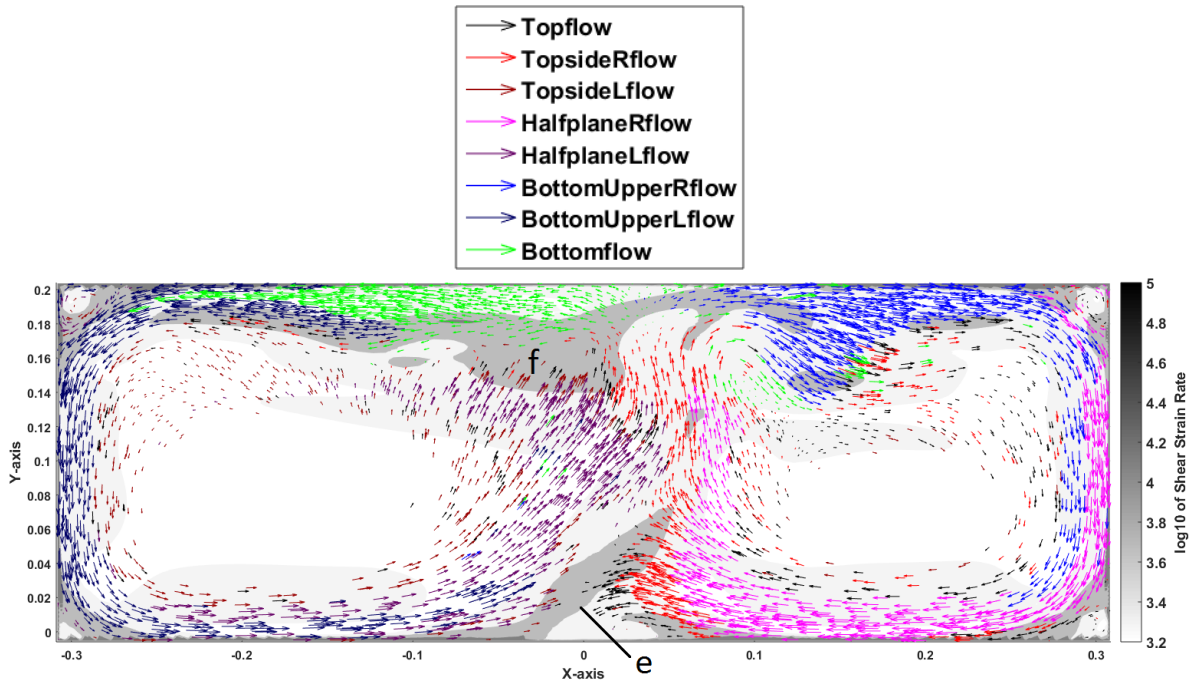

a)Shear strain rate and velocity vectors at evaluation surface P1,D235.5mm

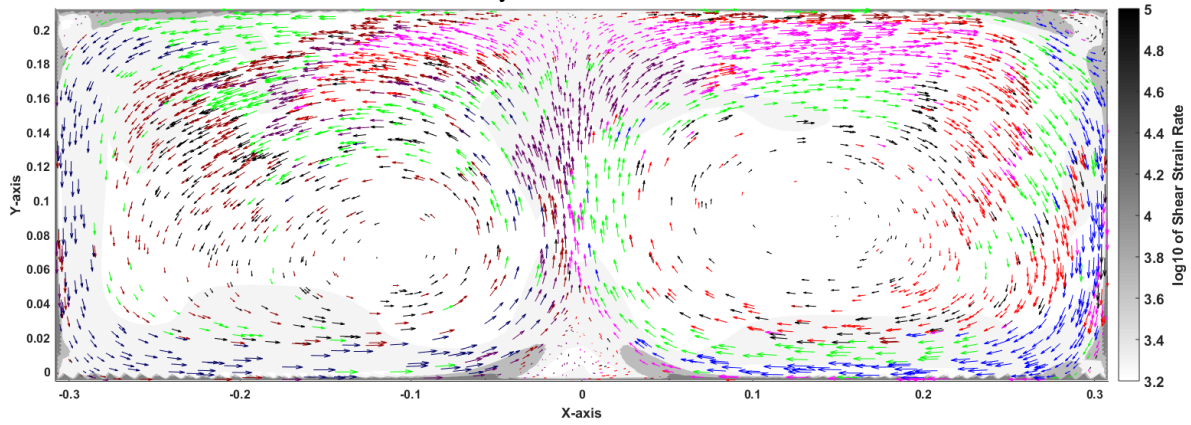

b) Shear strain rate and velocity vectors at evaluation surface P6,D489.5mm

Figure 3.22 – Regions of high shear at lower hood at design load. View from the top (See Fig. 3.12 for the different evaluation surfaces)

locity gradients between the vortex cores, the casing walls and the main flow regions. Some degree of flow mixing is seen in Fig. 3.22b. Lower magnitude of loss can be seen at surface P6,D489.5mm (Fig. 3.22b) compared to that at P1,D235.5mm (Fig. 3.22a) as expected, since the flows have lost most of their residual kinetic energy to dissipation as can be seen in Fig. 3.20 in the residual kinetic energy coefficient plot.

The major dissipation regions in Fig. 3.22b can be attributed to the two main counter rotating vortices, the corner flow re-circulation regions and wall shear. Note that the sequential order in which the flow from the different sectors enters the exhaust hood is still visible in Fig. Fig. 3.22a and Fig. 3.22b.

3.5.2 Overload

The flow field for this operating point is shown in Fig. 3.23. Again, the streamline color represent static entropy. As is the case at design load, the top flows (Topflow, TopsideRflow and TopsideLflow) generate higher entropy at overload compared to the bottom flows as can be seen in Fig. 3.23.

Fig. 3.24 shows values of the different coefficients at the various evaluation surfaces at overload operating condition. In general, the profiles of the different coefficient values at different evaluation surfaces for the overload case are approximately similar to those at design load operating condition.

As can be seen in Fig. 3.23a, for the Topflow case, the flow asymmetry at overload is less compared to that at design load (Fig. 3.19a, Topflow case), yet still more flow goes through the RHS of the hood compared to that which flows through the LHS. This explains the higher dissipation for TopsideRflow compared to the TopsideLflow. There is no reverse flow at the hood top from the TopsideLflow as was the case for the design load. As expected, at overload condition the values of the dissipation coefficients are higher at the various evaluation surfaces compared to the design load case, indicating higher losses. This translates to a lower pressure recovery coefficient at overload compared to those at design load condition as is seen in Fig. 3.18a.

The mechanisms of loss for the overload case are similar to that of design load operating condition. The top flows (Topflow, TopsideRflow and TopsideLflow) contribute the most in terms of dissipation as can be seen in Fig. 3.24 on the dissipation coefficient plot. Fig. 3.25 shows the shear strain rate including u and v velocity vectors for the evaluation surfaces at the upper hood for the overload case. High shear strain rate regions are observed on similar locations as in the design load case. These features are more pronounced at overload as expected signifying more losses at this operating point.

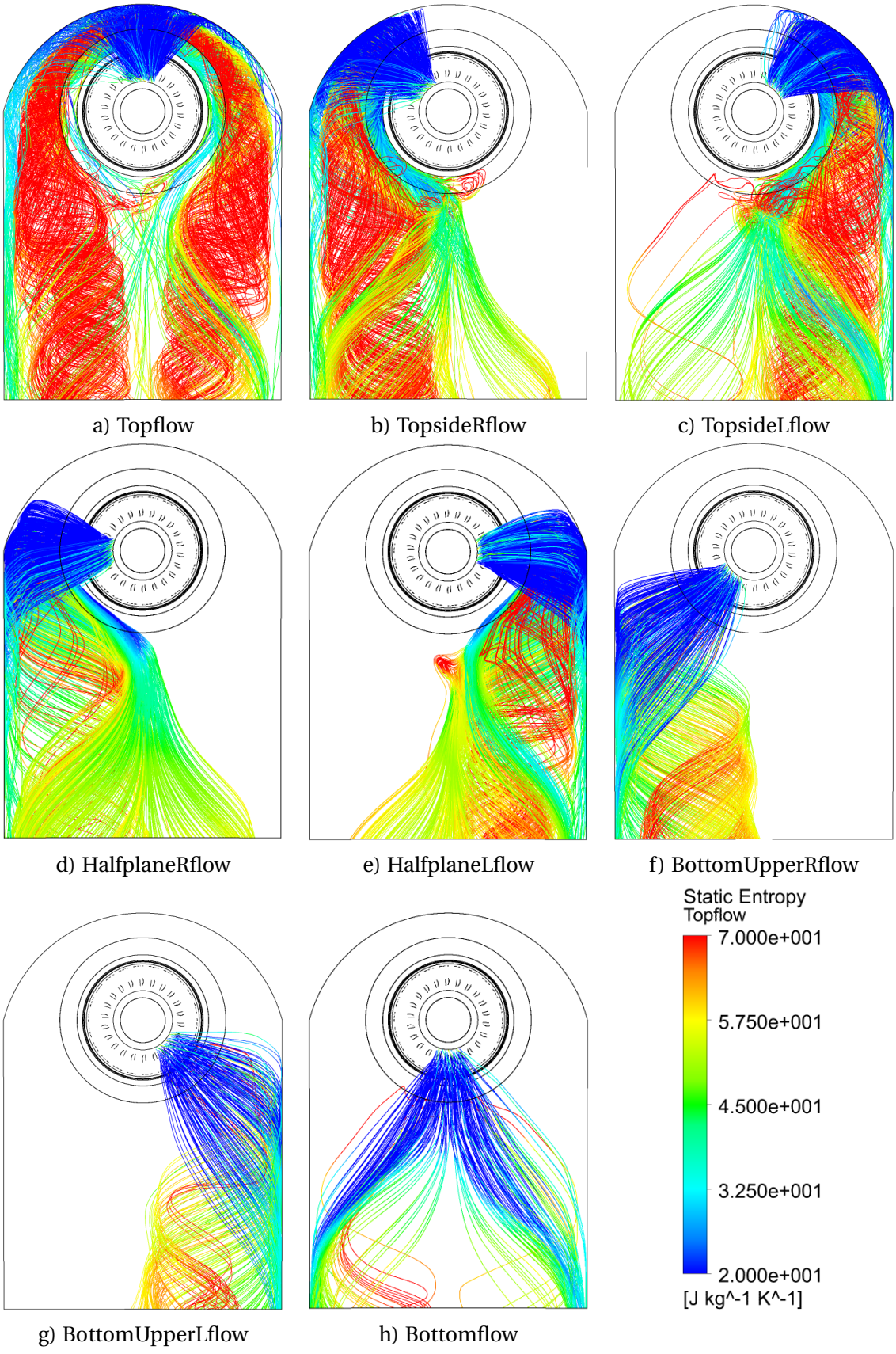

a) Topflow b) TopsideRflow c) TopsideLflow

d) HalfplaneRflow e) HalfplaneLflow f) BottomUpperRflow

g) BottomUpperLflow h) Bottomflow

Figure 3.23 – Flow field at overload. Direction of view is aft facing forward

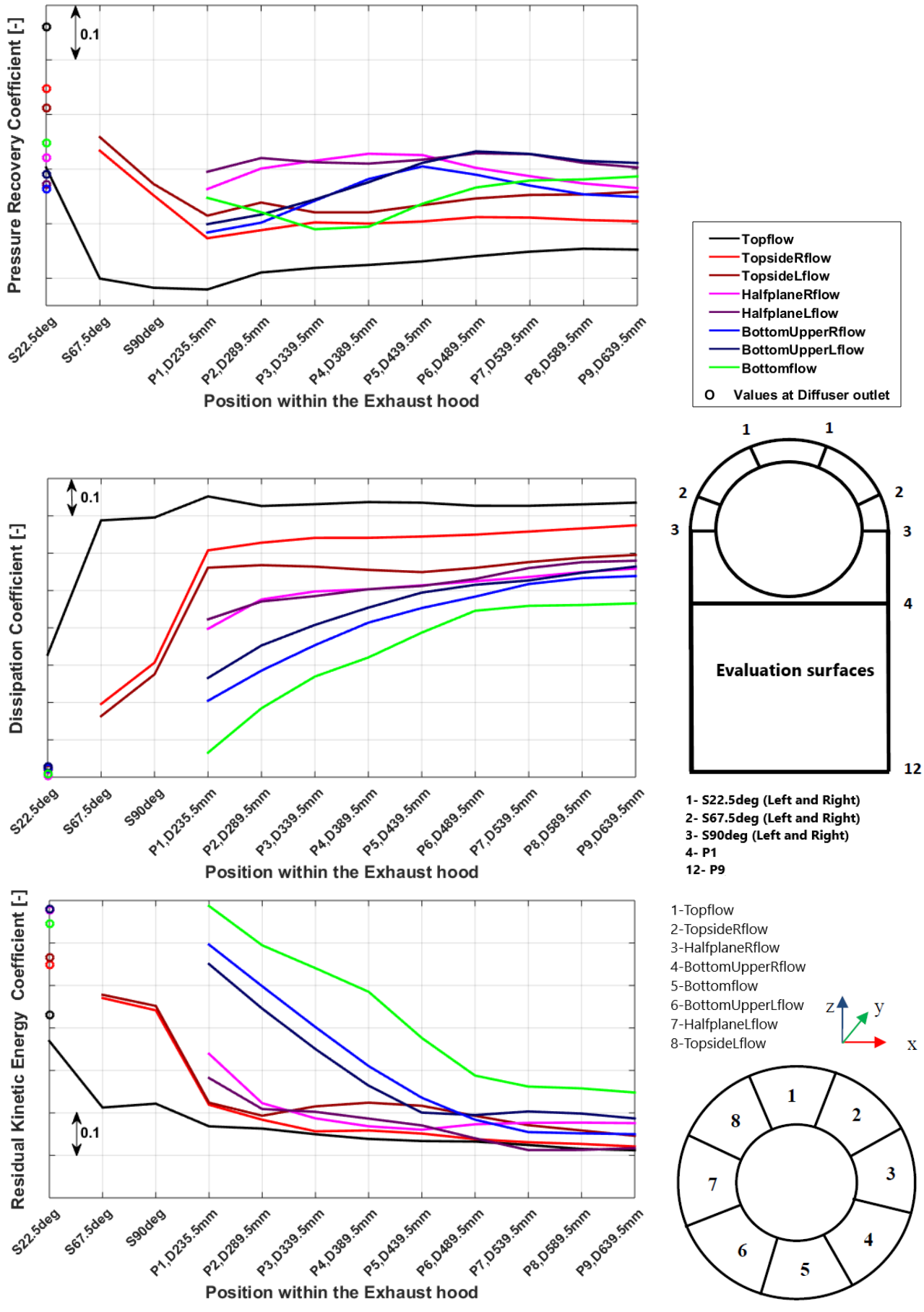

Figure 3.24 – Comparison of coefficients at overload (See Fig. 3.12 for the different positions within the exhaust hood)

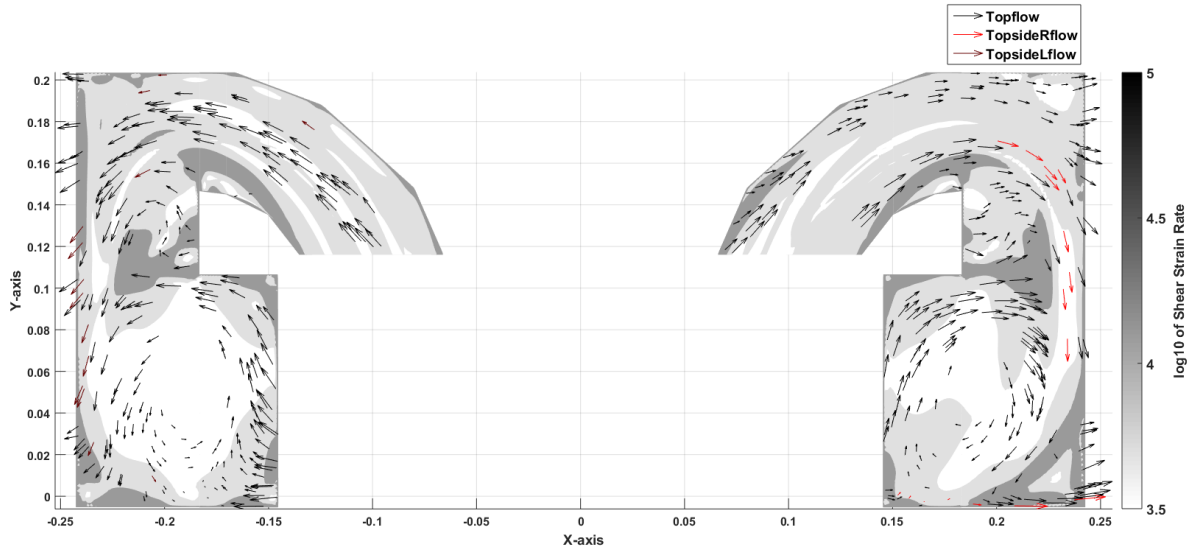

a)Shear strain rate and velocity vectors at evaluation surface *S*22.5°

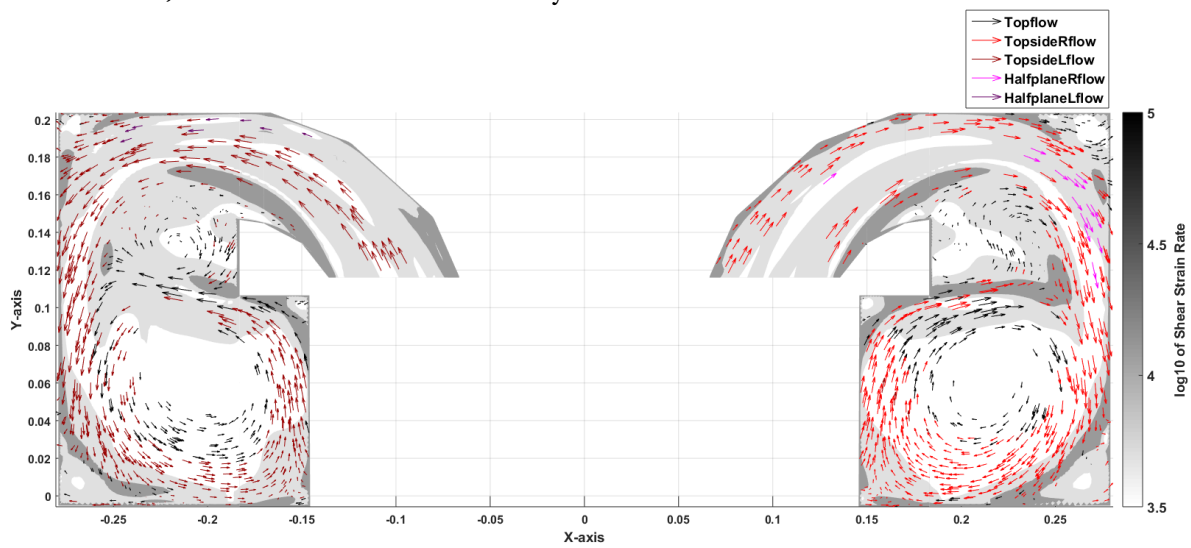

b) Shear strain rate and velocity vectors at evaluation surface *S*67.5°

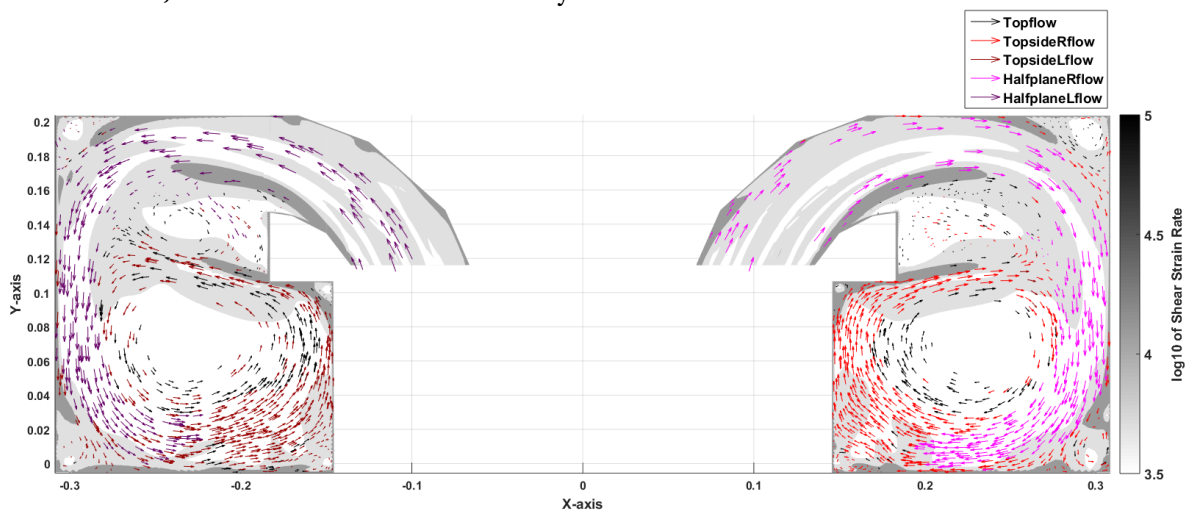

c) Shear strain rate and velocity vectors at evaluation surface *S*90° (Half-joint plane)

Figure 3.25 – Regions of high shear at upper hood at overload. View from the top (See Fig. 3.12 for the different evaluation surfaces).

3.6 Conclusions

The known approach of flow visualization of dividing the diffuser inflow into sectors has been extended considerably by evaluating the streamline properties at the different planes, thus not only a visual impression of the flow can be obtained but rather a quantitative assessment of the flow is now possible. Using this approach, it is shown that the flows originating from the top diffuser sectors (here named Topflow, TopsideRflow and TopsideLflow) contribute the highest in terms of energy dissipation in both the design and overload cases. More losses occur at the upper hood where the flow pattern is complex.

Using plots of shear strain rate including u and v velocity components for different flows, regions of high shear within the flow were identified at different evaluation surfaces along the flow path for both the design and overload case. The high shear regions were shown to appear in the locations where two counter-rotating vortices exist or where a flow circulation occurs either due to diffuser separation or existence of a sharp edge in the hood geometry.

The swirling flows in LP exhaust hoods were shown to be very detrimental to performance. This is because they create high velocity gradients which contribute to entropy generation. Interaction of a number of vortices at any given location along the flow path is undesirable in exhaust hood flows. As the faster flows transfer their momentum to the slower flows through the fluid viscosity, shear forces become important in relation to inertia forces. In addition to creating the conditions necessary for energy dissipation within the flow, their cores act as aerodynamic blockages making a considerable percentage of flow area unavailable for the flow. This makes the pressure recovery coefficient of axial-radial diffuser exhaust hoods worse.

Better optimized exhaust hoods have been designed before by trying to break the swirl profiles. The current study contributes in understanding the loss mechanism and contribution of the swirling flow. This new approach clearly shows where losses occur and therefore illustrates where improvements in design of exhaust hoods should be made.

4 Numerical Investigation of the Influence of Hood Height Variation on Performance of Low Pressure Steam Turbine Exhaust Hoods

4.1 Introduction

Performance optimization of low pressure steam turbine exhaust hoods has been a subject of a number of both numerical and experimental studies. This is driven by the understanding that improving the diffuser and exhaust hood outer casing performance results in a lower turbine back-pressure and hence an increased plant overall output.

The performance of the exhaust hood is greatly influenced by many structural factors such as the size of its outer casing, design of the diffuser parts and the arrangement of the internal supports. A number of studies have shown that a decrease of the hood height is detrimental to the exhaust hood performance [19, 70], however, up to now the impact of increased hood height has not been researched.

In the present study, a scaled axial-radial diffuser test rig operated by ITSM is used as reference configuration for a parameter study. A total of fourteen different configurations with both increased and reduced hood height are investigated numerically. Design load at three different tip jet Mach numbers (0, 0.4 and 1.2) is chosen as operating condition. Numerical and experimental data is available for the reference configuration and the numerical results have already been validated in chapter 3 with published data [48]. While a decrease in hood height shows the expected deterioration of efficiency, an increase of the hood height only initially results in an improved performance. After reaching a maximum efficiency, which is dependent on the tip leakage, the exhaust hood performance decreases noticeably again. Apart from the variation of pressure recovery, the results allow a better understanding of the loss mechanisms and flow phenomena in exhaust hoods.

4.2 Methodology

In order to investigate the influence of hood height variation on performance of exhaust hood, a numerical approach is used. Variation in hood height is studied because sources of loss analysis in chapter 3 revealed that most dissipation occurs at the upper hood. Both the numerical model and the experimental facility for the reference configuration of the exhaust hood are comprehensively described in chapter 3. In this chapter, the swirler model, the tip jet model and the diffuser part of the exhaust hood model are not changed from one configuration to the next; only the height of the outer casing is varied. Hood

height reduction and extension are performed in ICEM CFD and the resultant meshes are used in ANSYS CFX solver Release 17 to calculate the flow field and the static pressure recovery coefficient. The simulations are carried out in the same way as in chapter 3 for the reference configuration. Steady state simulations are performed using the Shear Stress Transport (SST) turbulence model. The y^+ values for the diffuser and exhaust hood walls are less than 1.

4.2.1 Variation of the hood height

Fig. 4.1 shows the upper hood of three different configurations: the shortest hood (case 1), the reference configuration (case 5) and the tallest hood (case 14). All configurations are created from the reference configuration which has been described and analyzed in detail in chapter 3. Points p1, p2 and p3 which define the curved region of the reference hood in ICEM CFD are used to modify the hood to the desired configuration. The three points are translated upwards (+z direction) or downward (-z direction) with a fixed dimension to produce an extended or a reduced hood respectively. The extension dimensions for the various configurations can be seen in Table 4.1 which contains details of all evaluated configurations.

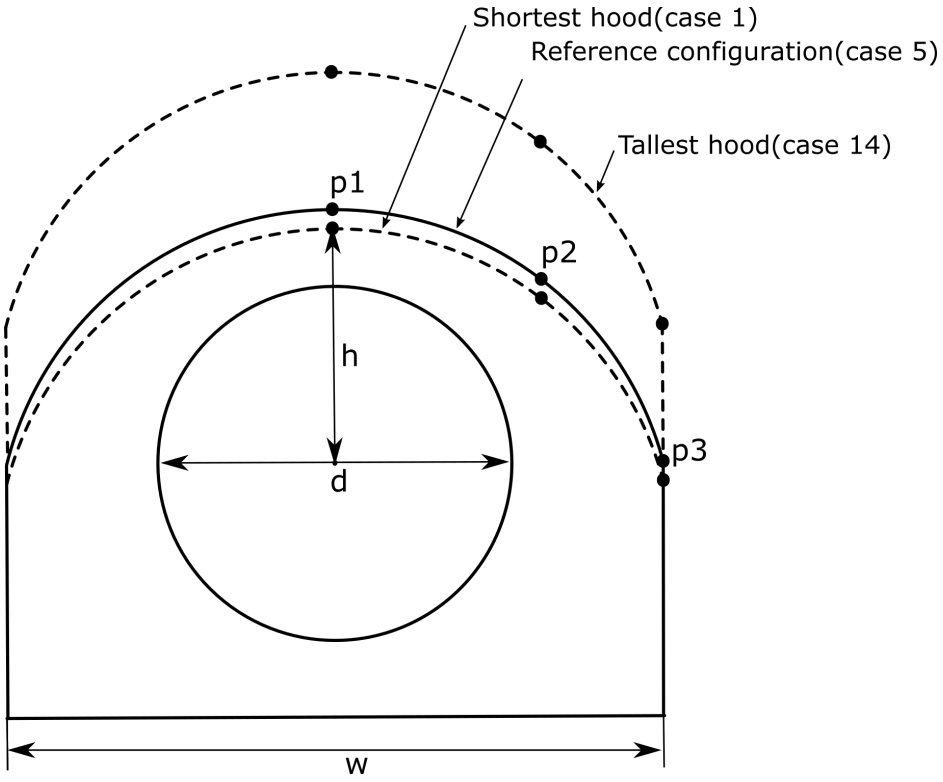

Figure 4.1 – Hood height variation

Table 4.1 – Evaluated configurations. Dimension d is the diffuser outlet diameter.

Case	Height, h(mm)	Extension(mm)	$\frac{h}{d}$ ratio	Normalized $\frac{h}{d}$ ratio
1	219.6	-17.9	0.6	0.92
2	222.5	-15	0.608	0.94
3	227.5	-10	0.622	0.96
4	232.5	-5	0.635	0.98
5(Ref)	237.5	0	0.649	1
6	242.5	5	0.663	1.02
7	249.6	12.1	0.676	1.04
8	261.69	24.2	0.715	1.10
9	274.5	37	0.75	1.16
10	294.5	57	0.805	1.24
11	308.75	71.25	0.844	1.30
12	317.5	80	0.867	1.34
13	325.5	88	0.889	1.37
14	366	128.5	1	1.54

4.2.2 Operating point and boundary conditions

All numerical investigations are done at design load. The axial Mach number at the diffuser inlet is 0.5. Diffuser inlet swirl is generated by a stationary swirler upstream of the diffuser inlet (see the calculated diffuser inlet swirl at design load and Ma_{tip}=0.4 in Fig. 3.17). Three tip jet flow conditions are tested:

- Tip Jet Mach number of 0

  This is a hypothetical case whose results are important because shrouded last stage blades with very good performing seals can result to very low tip jet Mach numbers.

- Tip Jet Mach number of 0.4

  This represents the tip jet Mach number for shrouded last stage blades.

- Tip Jet Mach number of 1.2

  This represents the tip jet Mach number for unshrouded last stage blades.

Since the performance of LP exhaust hood is strongly influenced by its operating point, the inlet and outlet boundary conditions are kept constant from one configuration to the next for a given operating point so that any change in static pressure recovery can be associated to the change in hood height. As was explained in chapter 3, total pressure is used as the inlet boundary condition and mass flow rate is used as the outlet boundary condition (operating conditions at the test rig at different operating points are show in Table 3.1 in Chapter 3 that form the basis of the boundary conditions in the numerical simulation). Table 4.2 shows a summary of the main and the tip jet normalized inlet boundary conditions. The applied total pressures at the design load swirler main inlet

were found to give comparable flow conditions with experimental results at diffuser inlet for the reference configuration. Comparison of total pressure, static pressure and Mach number between experiment and numerical simulation for the reference configuration at design load and tip jet Mach number of 0.4 is shown in figures 3.15 and 3.16 in chapter 3. More information on the boundary condition for the numerical simulation can be read in section 3.3.5 in chapter 3.

Table 4.2 – Inlet boundary condition

Operating point	**Main inlet, normalized total pressure** [-]	**Tip Jet inlet, normalized total pressure** [-]
Design load,tip jet Ma=0	1	inlet as wall
Design load,tip jet Ma=0.4	1	0.843
Design load,tip jet Ma=1.2	0.997	2.510
Total temperature and turbulence intensity at both inlets is set as 296 K and 5% respectively		

4.2.3 Numerical results validation and mesh independency

Steady state simulations are performed using the Shear Stress Transport (SST) turbulence model. Justification for use of steady state simulation and the ideal gas model is given in detail in section 3.3.4 in Chapter 3. The y^+ values for the diffuser and exhaust hood walls are less than 1. Numerical results for the reference configuration (case 5) were already validated both for design- and overload operating point for tip jet Mach numbers of 0, 0.4 and 1.2 in chapter 3 and good agreement was achieved between numerical and experimental results. Fig. 4.2 shows results of the mesh independency study for the tallest hood (case 14) at design load and tip jet Mach number of 0.4. The results confirm mesh independency for 5 million elements.

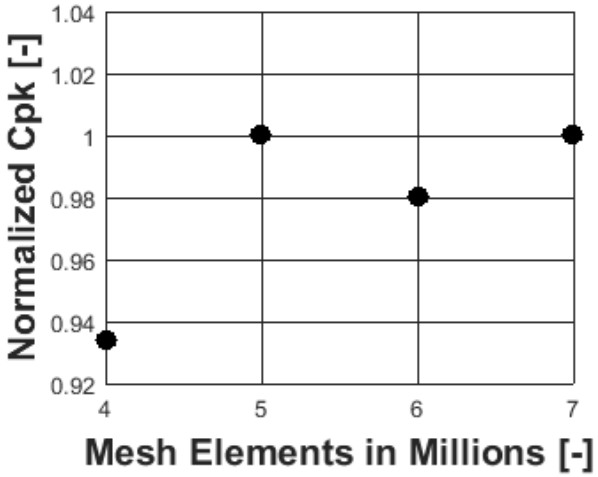

Figure 4.2 – Results of the mesh independency study for the tallest hood (case 14) at design load and $Ma_{tip} = 0.4$

To increase confidence with the calculated results for hood height variation, the quantitative trends obtained are compared with results from literature later on.

4.3 Results and discussion

Fig. 4.3 shows the influence of hood height on the pressure recovery coefficient at design load and at the three investigated tip jet Mach numbers (0, 0.4 and 1.2). Markers represent calculated configurations' percentage change in pressure recovery (ΔCpk) values while continuous curves are fitted to indicate trends. ΔCpk is calculated according to equation 4.1, where Cpk is the static pressure recovery coefficient for a given configuration and Cpk_{ref} is the static pressure recovery coefficient for the reference configuration (case 5) at the same operating point.

$$\Delta Cpk = \frac{(Cpk - Cpk_{ref})}{Cpk_{ref}} \cdot 100\% \tag{4.1}$$

The hood performance improves as the hood height is increased from the shortest hood (case 1) to an optimum value and then deteriorates with further increase in height. This behavior is qualitatively similar for all the three tip jet Mach numbers with each tip jet Mach number depicting a different optimum hood height. The optimum hood for tip jet Mach numbers of 0, 0.4 and 1.2 have a normalized h/d ratio of 0.98, 0.96 and 1.16, respectively, as can be seen from Fig. 4.3. For $Ma_{tip} = 1.2$, the sensitivity to hood height for optimum pressure recovery is not very pronounced.

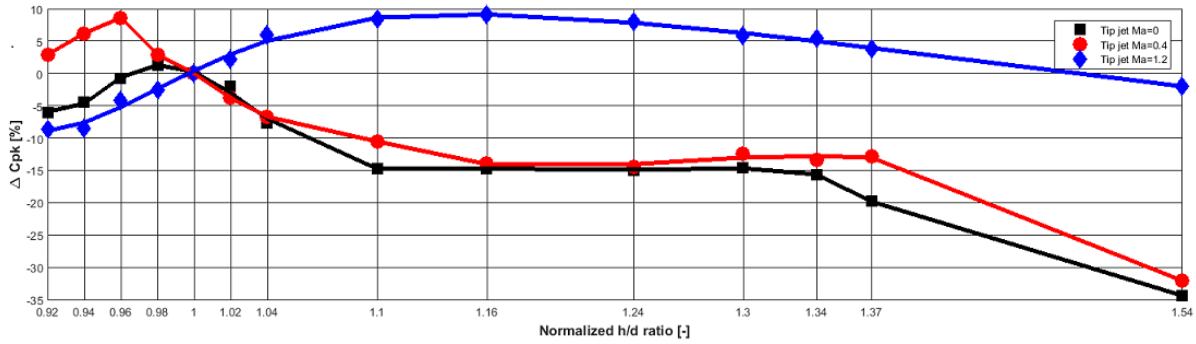

Figure 4.3 – Influence of hood height on the pressure recovery coeffient at design load and different tip jet Mach numbers

Compared to the reference (case 5) these optimum hoods have a performance improvement of 1.2% for a tip jet Mach number of 0, 8.6% for a tip jet Mach number of 0.4 and 9.1% for a tip jet Mach number of 1.2 under the same operating condition. Details about the different cases can be seen in Table 4.1. The course of pressure recovery over hood height is similar for the low tip jet Mach numbers (0 and 0.4), and the optimum hood heights for both configurations are very close, while that of the supersonic tip jet Mach number is completely different. Clearly, from results presented in Fig. 4.3, it is important for an exhaust hood designer to know the expected tip jet Mach number in relation to

the main flow Mach number at the diffuser inlet while optimizing an exhaust hood in consideration of the hood height. Understanding the sensitivity of exhaust hood performance to variation of its key geometrical parameters (e.g. hood height) is very important for the retrofit of steam turbines, where new and more efficient last stage blades and diffuser are fitted into an existing hood.

Four cases are selected for analysis. These are the optimum hood at tip jet Mach number of 0.4 (case 3), reference configuration (case 5), optimum hood at tip jet Mach number of 1.2 (case 9) and a relatively highly extended hood (case 13). These cases are analyzed for design load conditions and tip jet Mach numbers of 0.4 and 1.2, corresponding to shrouded and unshrouded last stage blades of low pressure steam turbines.

4.3.1 Design load, tip jet Mach number of 0.4

At tip jet Mach numbers lower than that of the main flow at the diffuser inlet (main flow Mach number at diffuser inlet is 0.5 for the current study), outer diffuser separation is high and flow blockage is significant for these cases. This can be seen in Fig. 4.4, which shows velocity vector plots in the symmetry plane of the diffuser for selected cases at Ma_{tip} = 0.4. In addition, flow areas at which the total pressure is less or equal to 91% of the massflow averaged total pressure at the diffuser outlet are shaded in grey on the bottom of Fig. 4.4 to visualize outer diffuser separation and blockage due to vortices within the exhaust hood. In the figure, the different flow blockages occurring are illustrated and the blockage parameters whose response to hood height variation is investigated later on are defined. Clearly, two main vortices can be seen at the diffuser symmetry plane for all cases, resulting in respective blockages. Moreover local flow acceleration due to the reduced flow area caused by aerodynamic blockage in regions neighboring the two vortices can be seen. These local flow accelerations are detrimental to exhaust hood performance as they lead to large velocity gradients and thus shear forces in the flow. Increasing the hood height from the reference configuration value at Ma_{tip} = 0.4 does not yield a performance improvement because it results in a further increase of the diffuser separation and hence flow blockage as can be seen for case 9 in Fig. 4.4 . However, when the hood height is decreased from the reference configuration value, the static pressure recovery coefficient initially increases because the diffuser flow separation is reduced. This can be seen for the illustration of case 3 in Fig. 4.4. The reduction of the separation has an impact on the first vortex within the exhaust hood, which is minimized; however, an additional large vortex is formed in the back of the hood. A reduction of the hood height beyond the optimum results in a further increase of flow velocities in the exhaust hood and stronger vortices, thus yielding lower pressure recovery again.

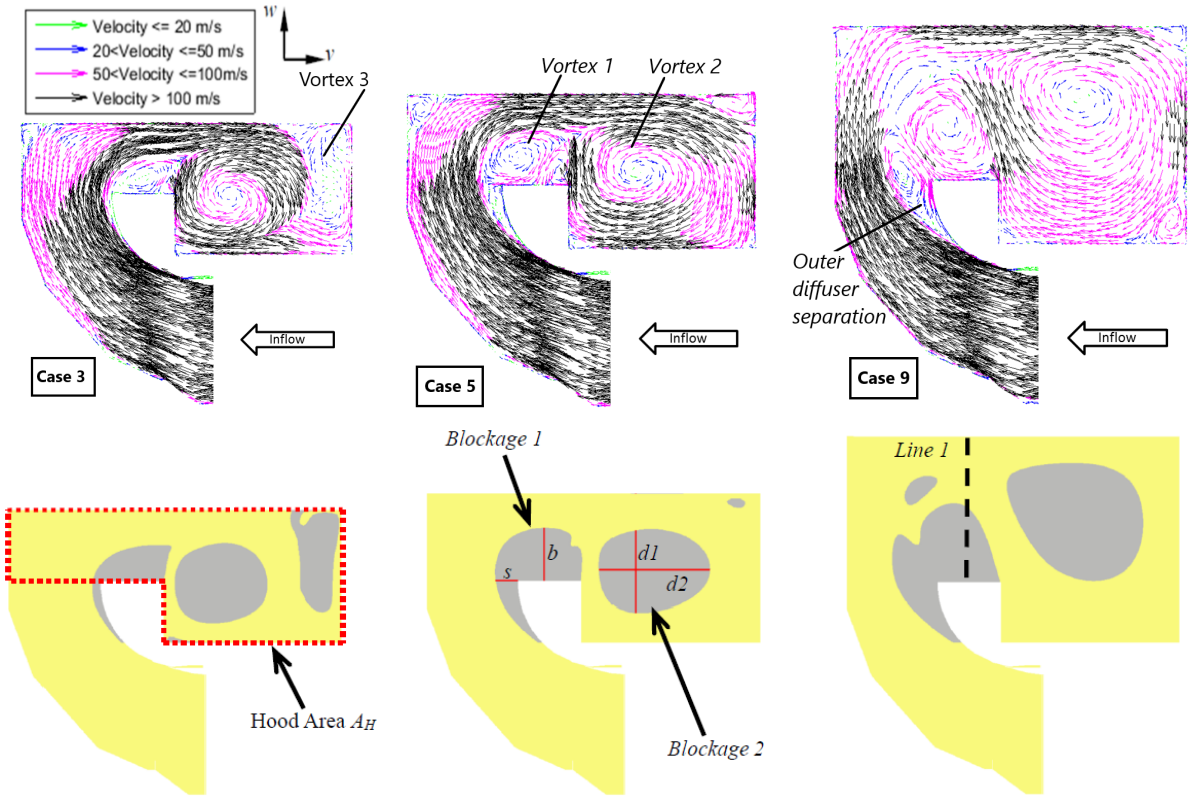

Figure 4.4 – v- and w-velocity vectors and illustration of flow blockage at the diffuser symmetry plane at design load and Ma_{tip} = 0.4. From left to right: case 3 (normalized h/d-ratio 0.96), case 5 (reference case) and case 9 (normalized h/d-ratio 1.16)

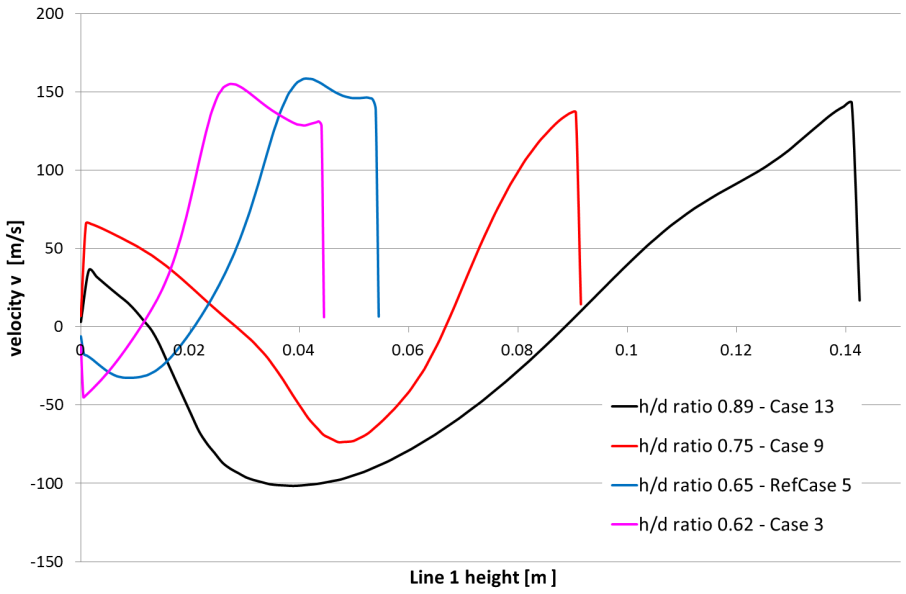

Figure 4.5 – Variation of velocity v along Line 1 (as defined in Fig. 4.4) at design load and Ma_{tip} = 0.4 for selected configurations

The reduction of the outer separation achieved by the smaller hoods (case 3 and 5) directly translates into a reduction of the first vortex and the subsequent aerodynamic blockage (Blockage 1 in Fig. 4.4) located above the diffuser. This can be observed from Fig. 4.5, which shows the v-velocity component along a line above the top part of the diffuser defined in Fig. 4.4 (Line 1). Due to this, the main flow above the vortex has a much more uniform profile compared to the other configurations, yet at relatively high velocities, and covers the majority of the flow path along Line 1.

Fig. 4.6 shows the variation of coefficients used to describe pressure recovery, dissipation and kinetic energy (see equations 3.3-3.5 for calculation of the three coefficients) for Topflow and Bottomflow along the flow path through the exhaust hood, averaged from 500 streamlines originating from the respective sectors (sector 1 and sector 5 in Fig. 3.11). Topflow is represented by continuous lines, Bottomflow by broken lines. The same color is used for a given configuration. The higher kinetic energy for the two smaller hoods (cases 3 and 5) is clearly visible in the upper sections of the exhaust hood in Fig. 4.6c up to about S90deg. At the same time, though, the dissipation coefficient is noticeably smaller (Fig. 4.6b), which results in a higher pressure recovery that prevails for the Topflows of case 3 and case 5 down to the outlet at P9. The lower dissipation is attributed to the more uniform flow profile. Moreover, the flow experiences flow acceleration between S67.5deg and S90deg for the two cases with large hood height, as the joint plane area has not been changed. It has to be mentioned that the reduced hood height (case 3) results in a higher mass flow and hence higher velocities for the Bottomflow. However, the resulting loss is over-compensated by the reduced dissipation occurring for the Topflow of the respective case. For larger hood heights (case 9 and case 13), Vortex 1 spreads out widely as can also be seen from Fig. 4.5 and the main flow is squeezed towards the outer hood. This results in increased dissipation throughout the exhaust hood for the Topflows (see Fig. 4.6b). Interestingly, Fig. 4.6 shows a noticeable impact on the Bottomflow for case 9, which is not present for case 5 and case 13. Generally, Topflows depict substantially higher dissipation compared to Bottomflows for a given configuration. On the other hand, it can be seen that the pressure recovery hardly changes along the flow path through the exhaust hood for the Bottomflows. Basically all residual kinetic energy is dissipated in the exhaust hood. It can be concluded that the state of the flow observed in the symmetry plane at the top of the exhaust hood is also mirrored in the flow behavior through the exhaust hood and the subsequent losses.

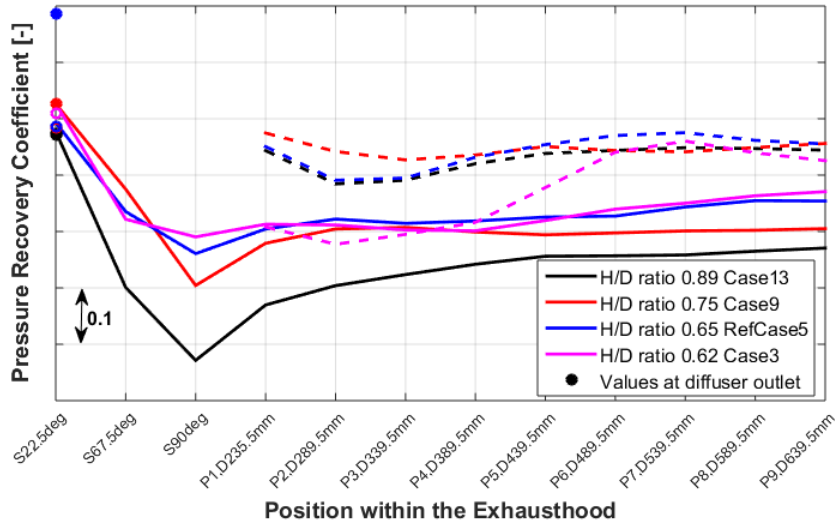

a) Pressure recovery coefficient at different evaluation surfaces

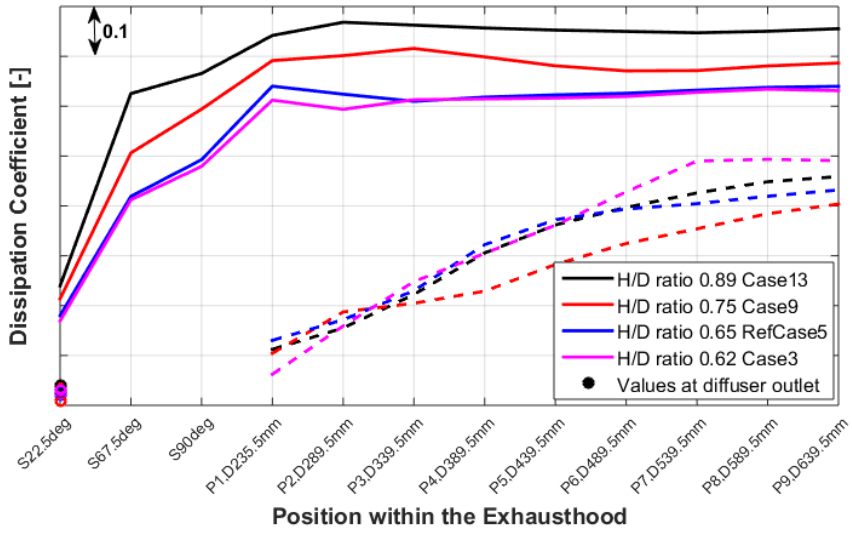

b) Dissipation coefficient at different evaluation surfaces

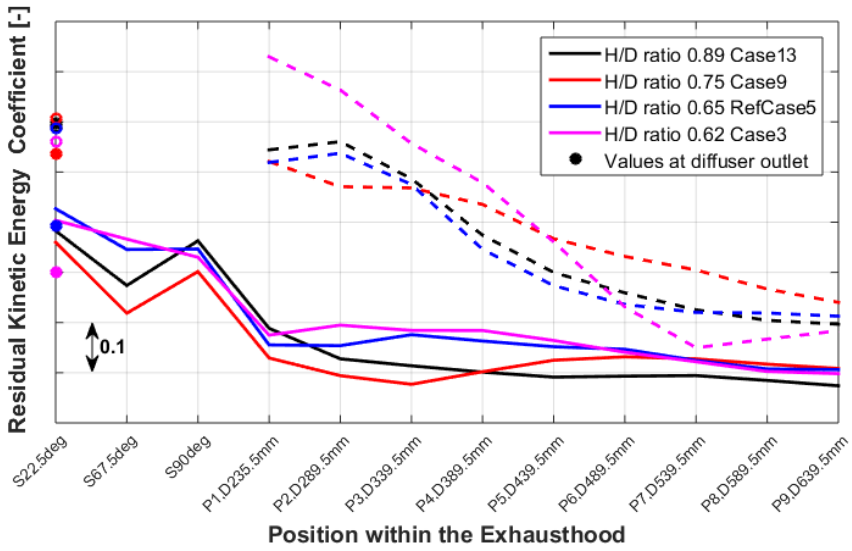

c) Residual kinetic energy coefficient at different evaluation surfaces

Figure 4.6 – Variation of coefficients along the flow path for design load and Ma_{tip}=0.4. Continuous lines represent Topflows while broken lines represent Bottomflows for a given configuration (See Fig. 3.12 for the evaluation surfaces within the exhaust hood)

4.3.2 Design load, tip jet Mach number of 1.2

For tip jet Mach numbers greater than the main flow Mach number at the diffuser inlet, the diffuser flow separation is very low or even completely suppressed as the tip leakage flow energizes the boundary layer. This results in a much better diffusion and correspondingly lower flow velocity at the diffuser outlet and downstream. For Ma_{tip} = 1.2, the v-velocity component at Line 1, plotted in Fig. 4.8, is noticeably smaller for all configurations investigated compared to the respective cases plotted in Fig. 4.5 (for Ma_{tip} = 0.4). At high tip jet Mach number condition, increasing hood height initially improves the performance up to an optimum value as can be seen in Fig. 4.3 for tip jet Mach number of 1.2. Because the width of the flow path is restricted by the width of the diffuser outlet, the quality of the flow within the exhaust hood is hence mainly governed by the flow deflection occurring at the upper hood, which can also be seen in Fig. 4.7. If the hood height is not sufficient, as for case 5, the flow is accelerated again during turning, forming a high-velocity vortex in the back of the hood. At the higher tip jet Mach number, the flow velocities within the vortices are generally lower (compare Fig. 4.4 and Fig. 4.7), hence dissipation is reduced and the overall pressure recovery is better.

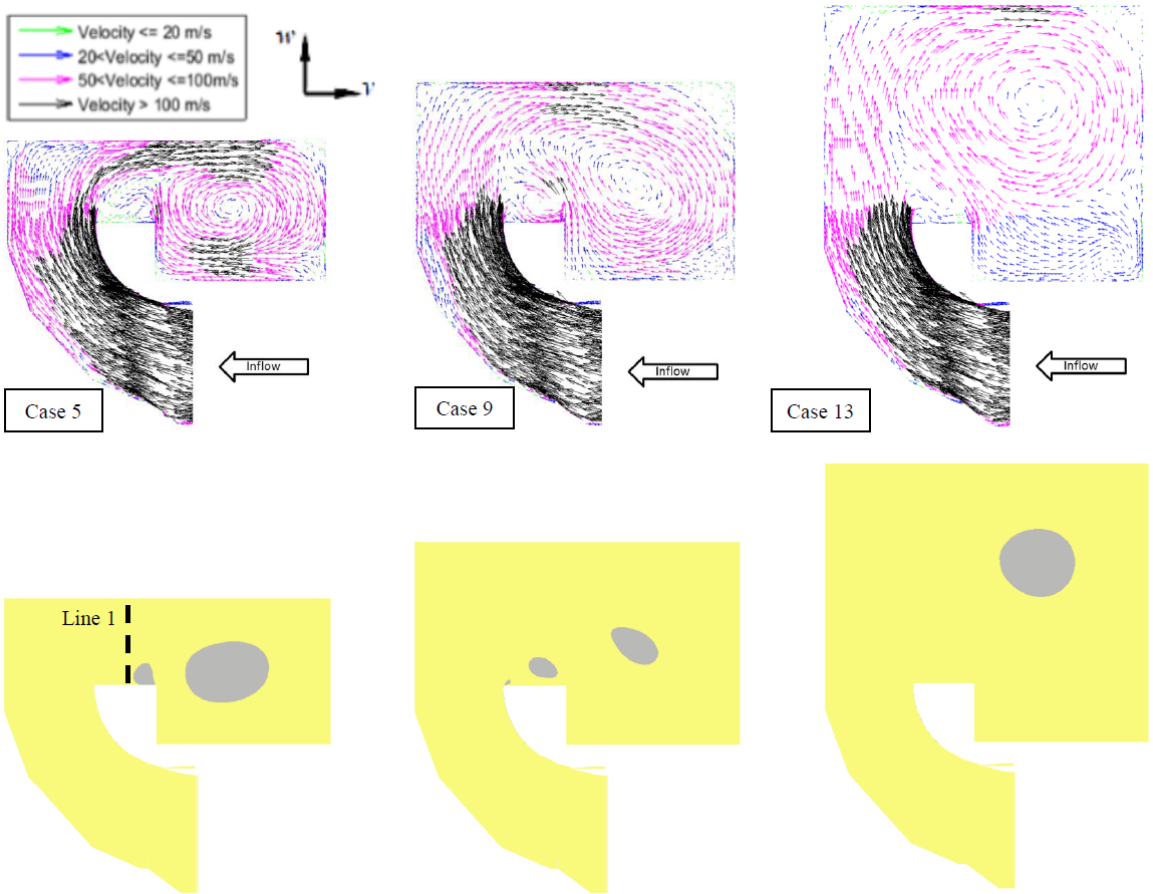

Figure 4.7 – v- and w-velocity vectors and illustration of flow blockage at the diffuser symmetry plane at design load and Ma_{tip} = 1.2. From left to right: case 5 (reference case), case 9 (normalized h/d-ratio 1.16), case 13 (normalized h/d-ratio 1.54)

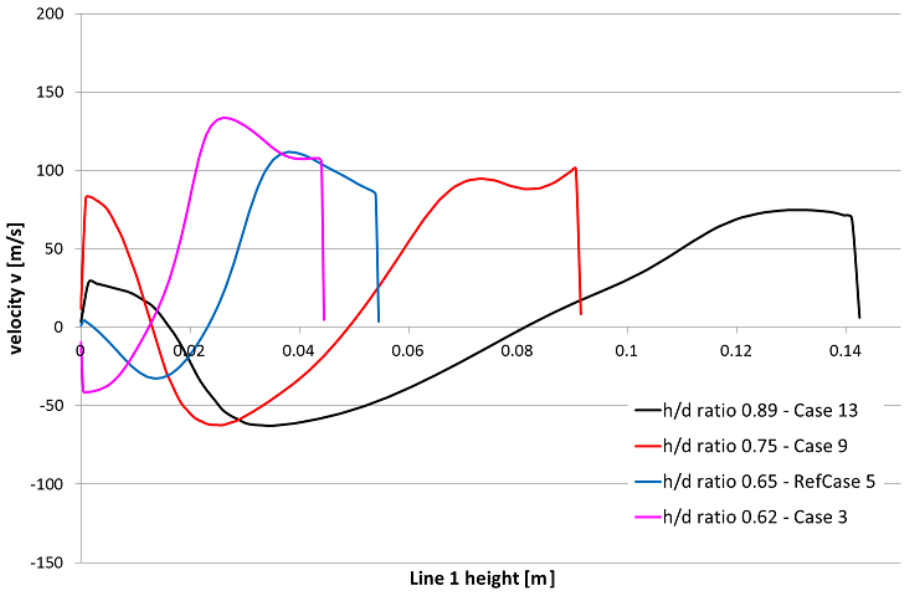

Figure 4.8 – Variation of velocity v along Line 1 (as defined in Fig. 4.7) at design load and Ma_{tip} = 1.2 for selected configurations

This is also evident from Fig. 4.9 which shows the variation of coefficients along the flow path at design load and tip jet Mach number of 1.2. As expected from the vector plots, the lower hood height case Topflows (case 3 and case 5) exhibit a high residual kinetic energy which is mostly dissipated along the flow path. The Topflow of the largest hood case studied here (case 13) has comparable pressure recovery and residual kinetic energy as the optimum case (case 9) in the upper hood at S22.5deg, but suffers from more dissipation along the flow path down to P1, thus having a lower pressure recovery at the outlet. In fact, the course of the dissipation coefficient for case 13 plotted in Fig. 4.9 is comparable to that of cases 3 and 5 along the upper hood. Downstream of the half joint plane, no more substantial dissipation occurs for both larger hood height cases. Again, the flow is accelerated near the half joint plane (S90deg).

The higher dissipation occurring for case 13 results most probably from the larger vortex formed in the back of the exhaust hood and also from the larger wetted surface within the hood. As for the low tip jet Mach number, the kinetic energy of the Bottomflows is mainly dissipated. Only the Bottomflow of case 3 exhibits some pressure recovery because of the higher flow velocities resulting from a massflow redistribution due to the small hood height, while the other cases show no change or even a reduction in Cp along the flow path.

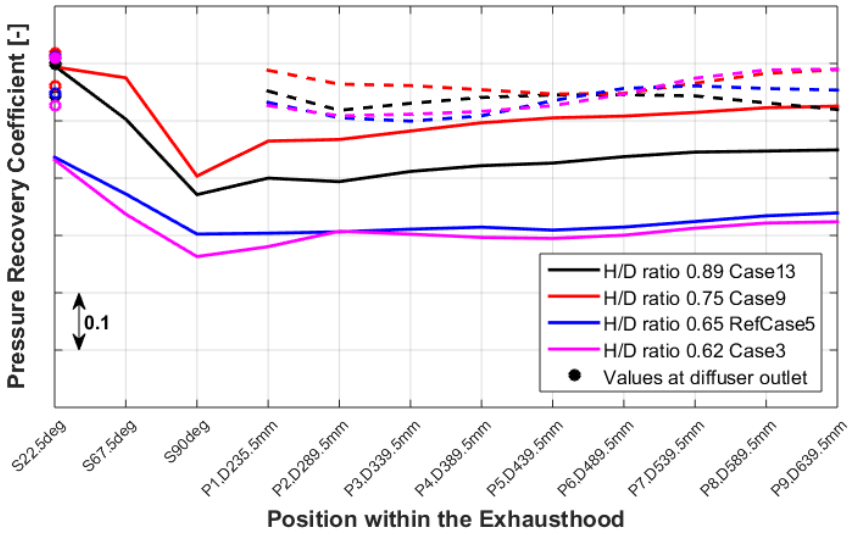

a) Pressure recovery coefficient at different evaluation surfaces

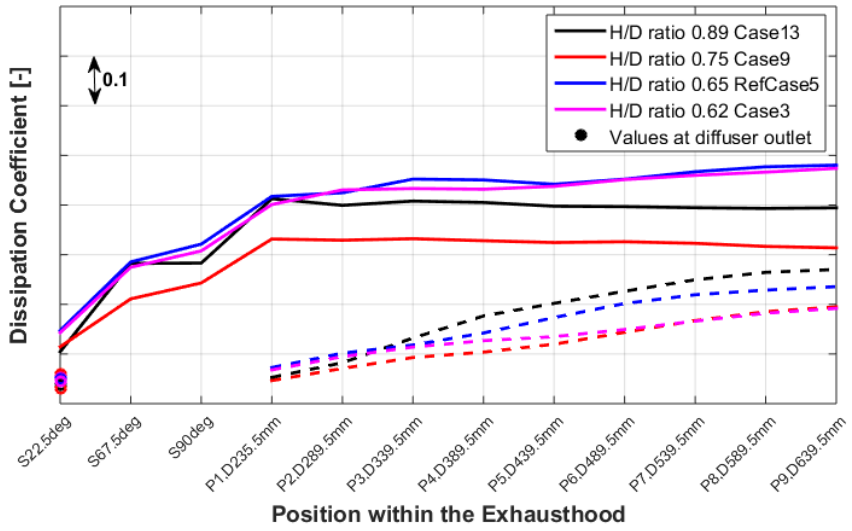

b) Dissipation coefficient at different evaluation surfaces

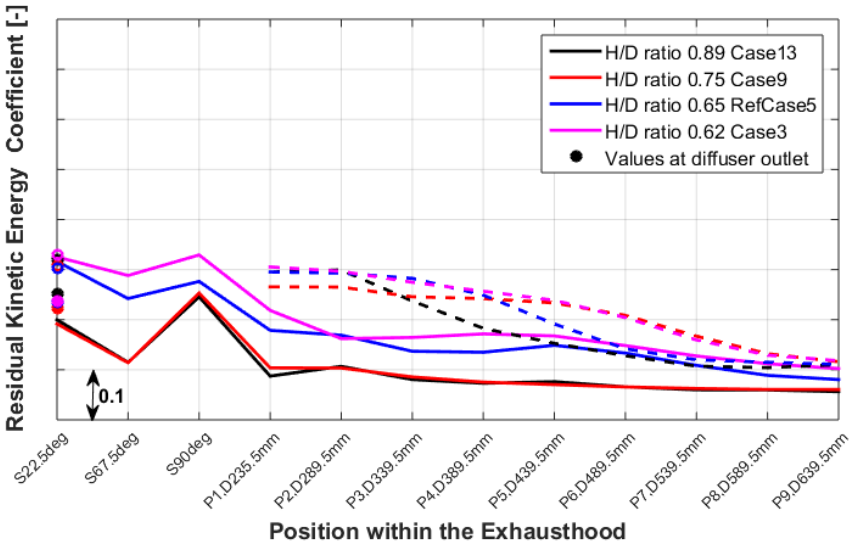

c) Residual kinetic energy coefficient at different evaluation surfaces

Figure 4.9 – Variation of coefficients along the flow path for design load and Ma_{tip}=1.2. Continuous lines represent Topflows while broken lines represent Bottomflows for a given configuration (See Fig. 3.12 for the evaluation surfaces within the exhaust hood)

4.3.3 Comparison of hood height variation results with literature

Finzel et al. [19] performed rigorous experimental investigations of geometrical parameters that are likely to influence significantly the performance of low pressure exhaust hoods. The influence of the exhaust hood area, the flow area in the horizontal joint plane and the location of the steam inlet were experimentally investigated. In their study, these researchers used the same test rig used for the current study and utilized two diffusers already mentioned in Chapter 3 (V3 and KW21) referred to as diffuser A (V3) and diffuser B (KW21) in their published work. For the current comparison with literature, Exhaust hood area, which is related to the exhaust hood height, for it is defined as the flow area above the turbine axis between the outer diffuser shell and the exhaust hood, is considered. Only results for the diffuser A (V3) are shown since the current study used this diffuser throughout the study. Fig. 4.10 shows results obtained by Finzel et al. [19] on the influence of exhaust hood area (which was equivalent to reducing the hood height as can be seen in the figure). Note that a normalized *Cpk* is displayed in the figure. The reference configuration for this experimental study is the same experimental test rig used in the current study to create the numerical models and to obtain experimental data for numerical results validation. Fig. 4.10 shows trends similar to those of the current numerical study for hood height reduction (corresponding to cases with normalized h/d ratio <1 in Fig. 4.3). In both studies, as the reference configuration height is reduced, the exhaust hood performance deteriorates continuously for Ma_{tip} =1.2, while for the case of Ma_{tip} = 0.4, reducing the hood height of the reference configuration initially increases the hood performance and a further decrease in height leads to poor performance. Although the investigated geometries are different, both experimental (Finzel et al. [19]) and numerical (current work) results show similar trends. Finzel et al. [19] used inserts within the upper part of the exhaust box to reduce the exhaust hood area and hence the hood height as can be seen in Fig. 4.10. A0 is the reference configuration with no insert within the upper part of the exhaust box.

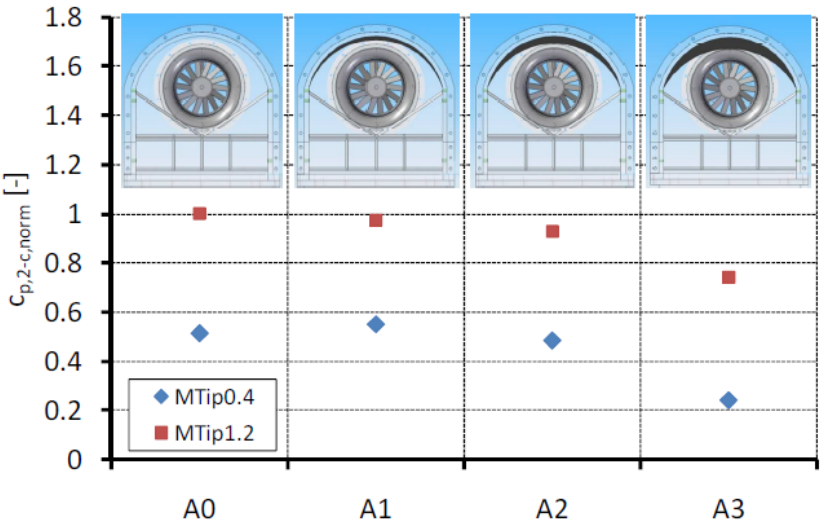

Figure 4.10 – Variation in exhaust hood performance with reduction in flow area (reduction in hood height) [19]

This close correlation of experimental results acquired by Finzel et al. [19] in 2011 with numerical results obtained over 5 years later using completely different methodology for influence of reducing hood height on exhaust hood performance increases the confidence with the numerical results obtained throughout this PhD thesis.

Taylor et al. [70] performed experimental parametric study of diffuser lips and exhaust hood configurations on a model test turbine rig at GE Power to investigate the impact of various geometric parameters on the performance of diffusers. The results from experiments were compared with numerical calculations to confirm the accuracy of GE's standard in-house diffuser design tools popular known as the EDS (Exhaust Design System). The main feature of the model turbine they used is the interchangeable components forming the exhaust hood which allow for a parametric study of the exhaust box geometry to be carried out. They were able to investigate the following parameters:

- W/D ratio - effect of the space between the end of the diffuser lip and the side walls of the exhaust box. W represents the exhaust hood width and D the diameter of the diffuser outlet
- L/H ratio - the impact of the axial length available downstream of the trailing edge where L represents the axial length and H the last stage turbine blade height
- Hub cone angle
- Back wall angle
- Hh/D ratio - influence of the hood height.

In general, these researchers found out that holding other parameters constant and varying one parameter of the exhaust box (Width (W), axial Length (L) and Hood height (Hh)) led to improvement in performance for the exhaust hood if the parameter dimension was increased and a decline in performance if the parameter dimension was decreased reducing the flow area.

For the parameter of interest in the current comparison (hood height variation), these researches compared two exhaust hoods i.e. their reference configuration with a normalized Hh/H ratio of 1 and a second configuration with a reduced hood height with a normalized Hh/H ratio of 0.85. Fig. 4.11 illustrates the two hoods they compared for the influence of exhaust hood height variation.

They found out that reducing hood height results in a decline in exhaust hood performance. Their results show that the performance deterioration occurs across a wide operating range, showing more degradation at high stage pressure ratios (higher pressure ratios result in higher flow velocities within the exhaust hood hence the higher losses). Fig. 4.12 shows the results they obtained on impact of reducing the hood height on performance of exhaust hoods. Since they tested a single variation in height, their research on influence of hood height on performance cannot be regarded as comprehensive but is clearly consistent with the findings of the current study concerning reduction in exhaust hood height, where reduced hood height was shown to lead to reduced performance for tip jet Mach number of 1.2. (refer to Fig. 4.3 for the cases of normalized h/d ratio <1).

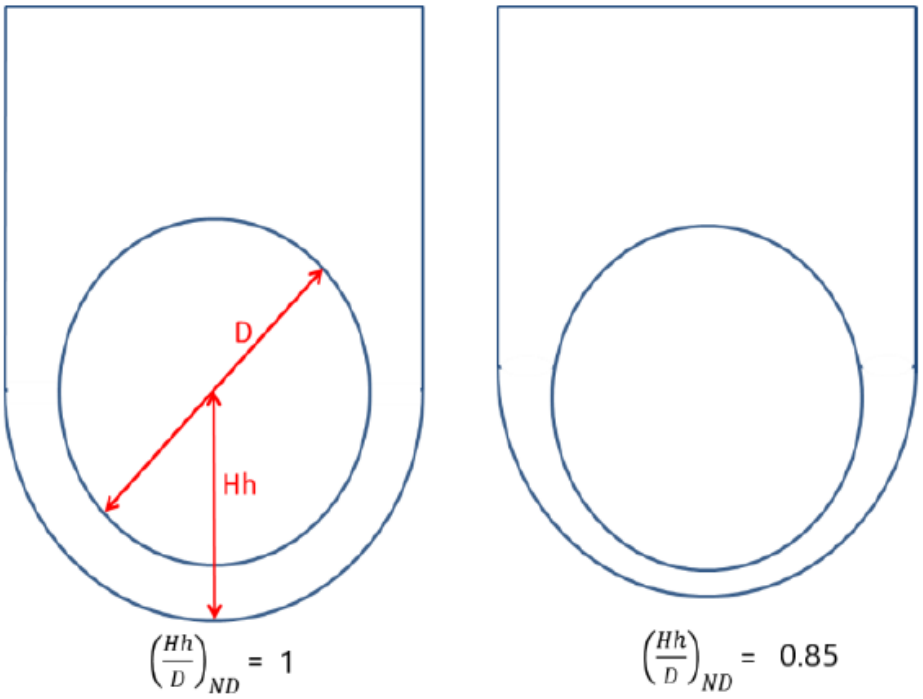

Figure 4.11 – Tested variation in hood height by Taylor et al. [70]

For the subsonic tip jet mach numbers tested (0 and 0.4), there is eventual decline in performance with reduced hood height (refer to Fig. 4.3 for the cases of normalized h/d ratio <1).

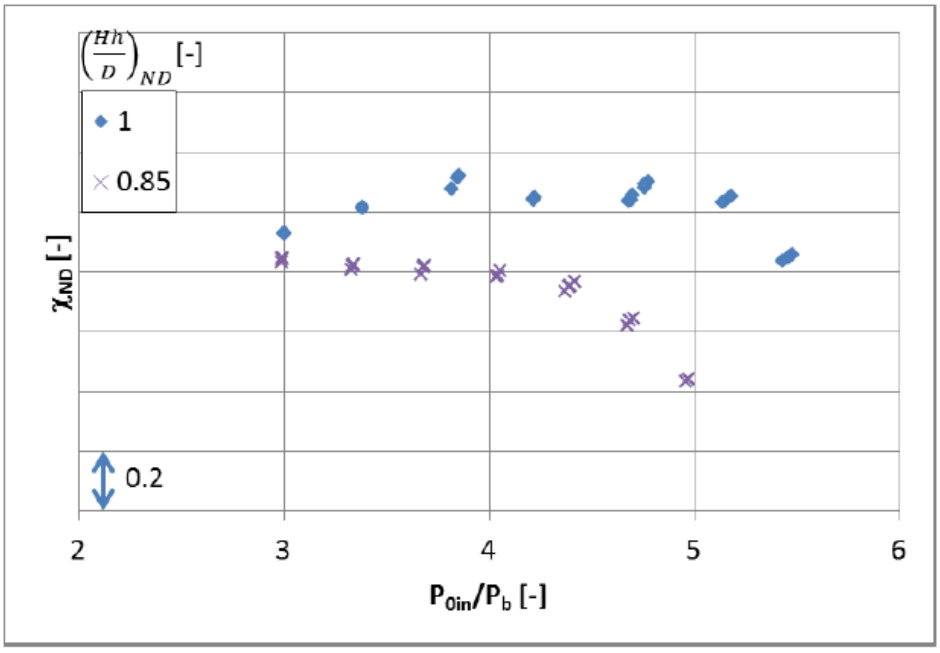

Figure 4.12 – Measured effect on diffuser recovery coefficient due to change in hood height by Taylor et al. [70]

4.3.4 Correlation of flow blockage at upper hood and exhaust hood performance

In chapter 3, it was shown that most losses in exhaust hoods occur within the upper hood. The flows originating from the top diffuser inlet sectors (Topflows) form complex vortices within the exhaust hood. The vortex cores affect the exhaust hood performance by creating velocity gradients which lead to high dissipation. In addition, they act as aerodynamic blockage reducing the available flow area within the exhaust hood, thus preventing proper diffusion. This is also evident from the vector plots in Fig. 4.4 and Fig. 4.7. Especially for the low tip jet Mach number, two main vortices are visible at the diffuser symmetry plane. Blockage 1 and Blockage 2 are surfaces created in ANSYS CFD-Post where the total pressure is less or equal to 91% of the massflow averaged total pressure at the diffuser outlet. Correlations were sought between the exhaust hood performance and the blockage parameters shown in Fig. 4.4. No relationship was found to exist between the parameters s (for diffuser separation thickness), b (for the Blockage 1 height), d1 and d2 (for the Blockage2 diameters) as the hood height is varied. However, Blockage 1 -area (A_1) has been found to correlate with hood performance when an outer diffuser separation is present, i.e. for low tip jet Mach numbers. Apparently, the blockage incurred has a major influence on the flow through the hood. In order to visualize the relationship between Blockage 1-area A_1 and normalized h/d-ratio, Blockage area ratio (α) is calculated by dividing the Blockage 1-area (A_1) for a given configuration to that of the reference configuration (case 5) at the same operating point. Thus,

$$\alpha_1 = \frac{A_1}{A_{1ref}} \tag{4.2}$$

On the other hand total blockage area (A_T) is the main factor that correlates with hood performance for supersonic tip jet Mach numbers, when diffuser outer separation is suppressed. The total blockage area (A_T) is the total area of the entire grey regions of each case. The blockage area ratio (α) is calculated by dividing the total blockage area (A_T) for a given configuration to that of the reference configuration (case 5) at the same operating point. Thus,

$$\alpha_T = \frac{A_T}{A_{Tref}} \tag{4.3}$$

Fig. 4.13 shows the variation of the respective blockage area ratio (α) with hood height. Comparing Fig. 4.13 to Fig. 4.3 reveals a correlation between flow blockage and hood performance. An inverse relationship exists between flow blockage and hood performance as expected. For low tip jet Mach numbers (0 and 0.4), a few data points do not conform to the said correlation between Blockage 1-area (A_1) and performance especially for configurations with highly reduced hood heights. For example, the optimum performing hoods with normalized h/d ratios of 0.96 and 0.98 as seen in Fig. 4.3 cannot be directly inferred from Fig. 4.13. This is because for these cases the diffuser lip separation as well as the subsequent vortex (Vortex 1) is suppressed due to the small hood height and the

exceedingly high velocities in the main flow due to the restriction of the flow path in the upper hood incur additional losses.

Defining the free area ratio γ

$$\gamma = 1 - \frac{A_T}{A_H} \tag{4.4}$$

where A_H is the hood area defined in Fig. 4.4. Plotting it over the normalized h/d-ratio as shown in Fig. 4.14, a correlation between the exhaust hood performance (first shown in Fig. 4.3) and the free area ratio γ can be identified.

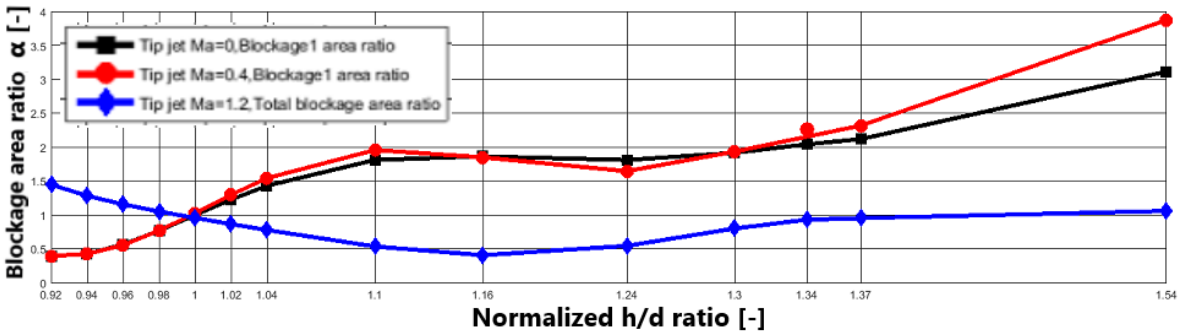

Figure 4.13 – Variation of blockage area ratio (α) with change in hood height. For low tip jet Mach numbers (0 and 0.4), Blockage 1-area (A_1) is used while for the supersonic tip jet Mach number (1.2), total blockage area (A_T) is used

An increase in hood height leads to an increase in the free area ratio (γ) up to an optimum value. Further height increase results in a decline in free area ratio. A noticeable difference between the curves for variation of hood performace and free area ratio (γ) with change in hood height at design load and $Ma_{tip} = 1.2$ can be seen towards the tail end of the profiles. While the free area ratio (γ) remains relatively constant, the hood performance decreases continuously, which is most probably due to increased boundary layer losses along the exhaust hood walls. In general, a correlation exists between flow blockage and hood performance for all data points whether using blockage area ratio (α) or the free area ratio (γ) for the supersonic tip jet Mach number (1.2).

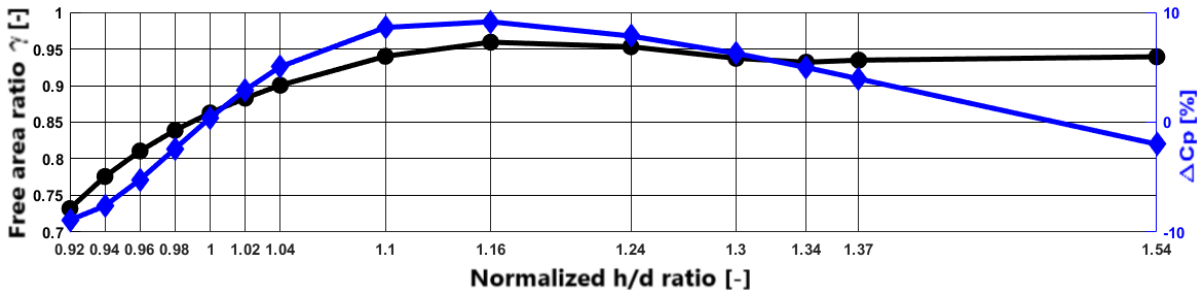

Figure 4.14 – Variation of free area ratio (γ) with hood height for design load and $Ma_{tip} = 1.2$. Percentage ΔCp profile shown in Fig. 4.3 for the same operating point is included

4.4 Conclusions

A detailed analysis of influence of hood height variation on exhaust hood performance at design load has been carried out. For the investigated tip jet Mach numbers of 0, 0.4 and 1.2, it is shown that an optimum hood height exists which is different for each tip jet Mach number and that reducing or increasing the height beyond this point results in performance decline. The current study is consistent with results from literature on hood height reduction which show performance deterioration. Understanding the sensitivity of exhaust hood performance to variation of its key geometrical parameters (e.g. hood height) and the influence of the tip leakage flow is very important for the retrofit of steam turbines, where new and more efficient last stage blades and diffuser are fitted into an existing hood.

The optimum hoods at tip jet Mach numbers of 0, 0.4 and 1.2 recorded a performance improvement of 1.2%, 8.6% and 9.1% respectively compared to the reference configuration at the same operating condition. There is still a considerable potential for LP-turbine efficiency improvements based on exhaust hood optimization. Although such a large improvement has not been achieved in the present study using very simple geometric variations, the results of this study can be used to improve exhaust hood geometries in the future.

It has been shown that an outer diffuser separation does not only affect axial-radial-diffuser performance, but also the performance of the exhaust hood flow. Thus, generating a uniform diffuser outflow profile is an important task for the designer.

A new concept of defining flow aerodynamic blockage within the exhaust hood, using total pressure criteria below a given percentage of massflow averaged value of total pressure at diffuser outlet, is introduced. It gives a good correlation between flow aerodynamic blockage and exhaust hood performance. The blockage areas calculated are directly related to vortex cores of swirl flows in exhaust hood which are the main sources of loss in exhaust hood flows. The findings on hood height variation and how it affects performance is very important to exhaust hood designers. Correlation of blockage area to hood performance shows that key point to improve hood efficiency is a reduction of these blockages. The lessons learnt from hood height variation can be applied to hood modifications.

5 Numerical Investigations of Influence of flow deflection at the upper hood on Performance of Low Pressure Steam Turbine Exhaust Hoods

5.1 Introduction

A detailed analysis of loss generation within the exhaust hood was done in chapter 3 where it was established that most losses occur at the upper hood and is caused by the swirling flows which mostly originate from the top diffuser inlet sectors. Although the flow behaviour of the top diffuser inlet sector flows is to a large extent acceptable within the diffuser, highly dissipative swirling flows develop from the diffuser outlet because of the complicated turning that the flow is required to make in order to propagate towards the condenser. The situation is worsened by diffuser separation which leads to a higher flow blockage as was explained in chapter 4. Problems caused by swirling flow are less severe for the bottom diffuser inlet sector flows as the initial direction of flow at the diffuser outlet permits easier movement of steam to the condenser.

With the loss mechanisms in exhaust hoods reasonably well understood, and with the knowledge that most dissipation occurs at the upper hood, the next step is to investigate simple modifications to the upper hood which could yield better performance. An idea of flow deflection to minimize the intensity of the formed vortices and hence reduce the exhaust loss, is investigated. The deflector configurations analyzed are modifications of the walls of the reference configuration's outer casing to include deflector portions. The numerical models of the reference configuration which are based on a scaled axial-radial diffuser test rig operated by the Institute of Thermal Turbomachinery and Machinery Laboratory (ITSM) of the University of Stuttgart have been validated in chapter 3.

5.2 Methodology

Deflector configurations are developed in ICEM CFD by modifying the reference configuration at the upper hood. In this chapter, as was the case in Chapter 4, the swirler model, the tip jet model and the diffuser part of the exhaust hood model are not changed from one configuration to the next; only the upper part of the outer casing is modified to include a deflector portion as an integral part of the outer casing. Steady state simulations are performed using ANSYS CFX Solver Release 17. The Shear Stress Transport (SST) turbulence model is used. Justification for use of steady state simulation and the ideal gas model is given in detail in section 3.3.4 in Chapter 3. All deflector configurations are run at design load and at three tip jet Mach numbers (0, 0.4 and 1.2). The boundary condi-

tions used are as detailed in chapter 4 for design load and different tip jet Mach numbers (0, 0.4 and 1.2). The applied boundary conditions for a given operating point are maintained from one configuration to the next so that any variation in performance can be attributed to the included deflector portion on the outer casing. The best performing hood configuration is further investigated at overload operating point. Its results are further analysed using methods developed in chapter 3 in comparison with the reference configuration to ascertain the source of its benefit in performance.

5.2.1 Deflector configuration conceptualization and testing

In chapter 3, a detailed numerical analysis of the sources of loss in low pressure steam turbine exhaust hoods was undertaken. It was found out that most losses occur at the upper hood and is mainly due to the complicated flow path that the flow originating from the upper diffuser sectors has to take. This flow has to move from an axial direction to a radial direction through the diffuser and finally has to change direction within the exhaust box to downwards towards the condenser. The diffuser inlet swirl generated by the last stage turbine blades makes the flow even more complicated. The complex flow path is bound to enhance generation of losses. The losses were found to be enhanced by presence of diffuser separations as was seen at design load and at tip jet Mach number of 0.4. At overload condition and tipjet Mach number of 0.4, the losses generated were the highest for the investigated operating conditions for the reference configuration. The investigated operating conditions in chapter 3 were the design load and overload at three tipjet Mach numbers of 0, 0.4 and 1.2.

In chapter 4, while numerically investigating the influence of hood height on the performance of low pressure steam turbine exhaust hoods, the performance of the exhaust hood was shown to correlate well with flow blockage area that is created by vortices formed within the upper hood. This blockage area was only shown at the diffuser symmetry plane (see Fig. 4.4 in Chapter 4). The vortices which form at the upper hood region are 3D features that stretch all the way to condenser plane as was shown by flow streamlines in chapter 3. These 3D vortex structures are the main causes of loss and a number of researchers have indicated this [7, 46, 82]. Some researchers including Zoe Burton [7] have indicated that the flow into the condenser is characterized by two counter-rotating vortices which push the main flow towards the walls since nearly no flow goes through the vortex structures with even reverse flow having been observed by some researchers in this region. Burton et al. [9] explains that the counter rotating vortices at the condenser plane are detrimental to condenser performance as a uniform distribution of pressure at the condenser plane is more preferable for better performance.

With the flow structure and the main sources of loss in low pressure exhaust hood well understood, the next step was to propose modification on the upper hood that could lead to improved performance. The goal is to introduce flow deflection at the upper hood in order to interfere with formation of vortices or reduce their intensity by guiding the flow better towards the condenser. Fig. 5.1 shows the reference exhaust hood and velocity vectors at the diffuser symmetry plane at design load and tipjet Mach number of 0.4 with velocity vectors color coded in order to reflect relative velocity at the diffuser symmetry

plane. The reference exhaust box has flat front and back walls curved at the top as shown in Fig. 5.1. This figure further shows two vortices in 2D as formed at the upper hood at the diffuser symmetry plane. The velocity vectors also show regions of flow acceration as the flow area is reduced due to the existence of the two vortices. Whenever two flows with different velocities interact, shear losses are bound to occur hence the existence of these vortices makes occurence of losses within the exhaust hood inevitable.

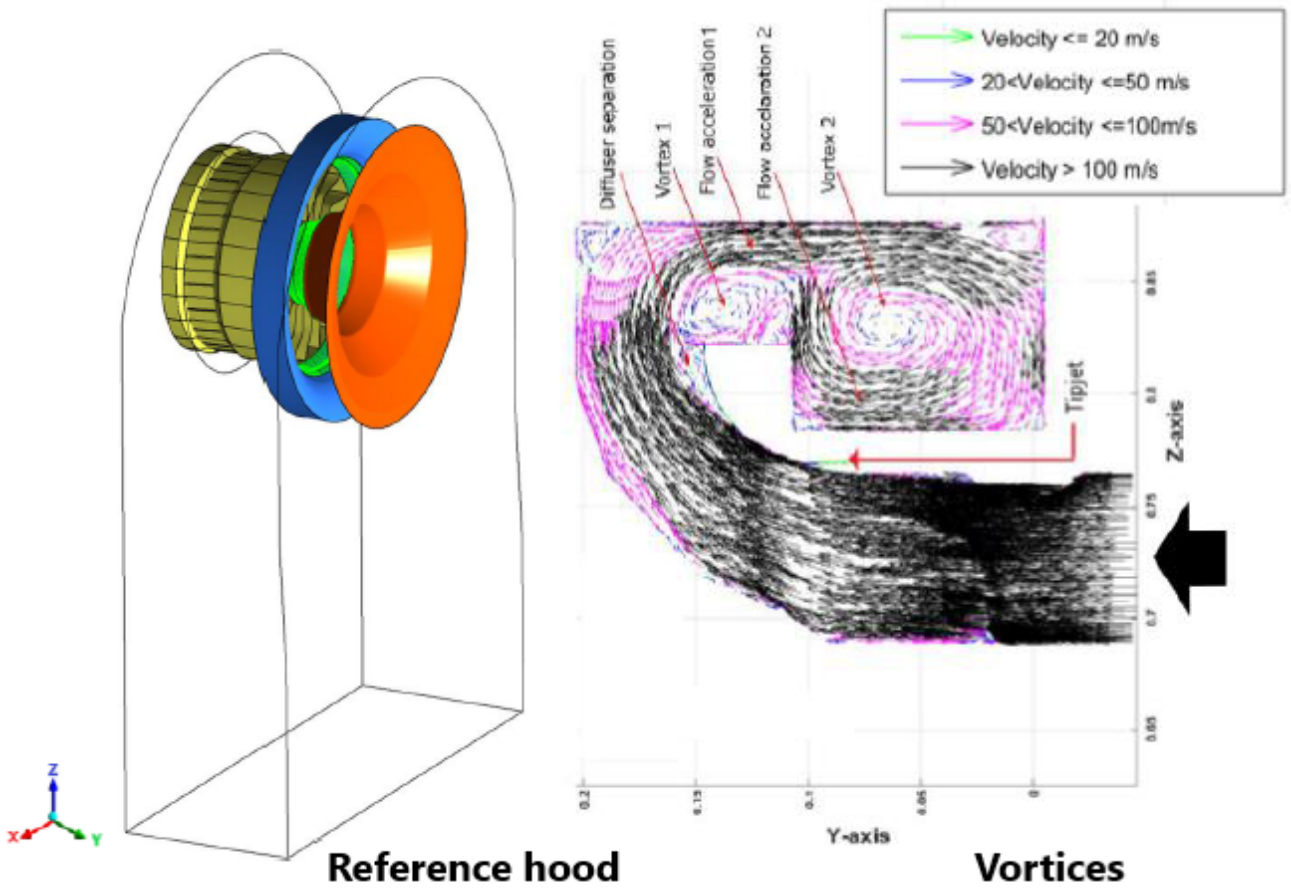

Figure 5.1 – Reference exhaust hood with diffuser and Swirl generator model visible. Included is velocity vectors at the diffuser symmetry plane at design load and tipjet Mach number of 0.4. Velocity vectors are color coded to reflect relative velocity at the diffuser symmetry plane

Since the problem region was found to be at the upper hood, modification of this region was considered to be necessary to test if a better performing exhaust hood could be proposed. It was considered that the vortices form due to lack of proper guidance of the flow towards the condenser at the upper hood and hence flow deflection was thought to be the most likely effective way of doing this. Flow deflectors were hence introduced as part of the out casing to create new configurations from the reference configuration for investigation. Because of the many possibilities of deflector configurations that could be created, the work presented here is not considered to be fully comprehensive but the few cases presented are thoroughly done and the results obtained are quite encouraging. Further work in this area is recommended. As an example for better understanding

by the reader, Fig. 5.2 is included which shows the reference configuration in comparison with the best performing configuration (a double wall deflector configuration with the angle between the deflectors being 135°). The two configurations are presented without the side walls for ease of visual comparison. It must be mentioned that this is the best performing configuration based on the cases investigated in this study i.e. it is not the optimal deflector configuration. As earlier stated, further work is required in order to make a more comprehensive conclusion on performance of exhaust hood with deflectors at the upper hood as part of the outer casing. Experimental work and numerical studies carried out by Taylor et al. [70] where they investigated the impact of varying key dimensions of the exhaust box (width, axial length and height) clearly showed that reducing the exhaust box size by variation of either of these parameters lead to a decline in performance of the exhaust hood. This double wall deflector configuration was found to result in significant performance improvement although it actually reduces the exhaust box volume at the upper hood.

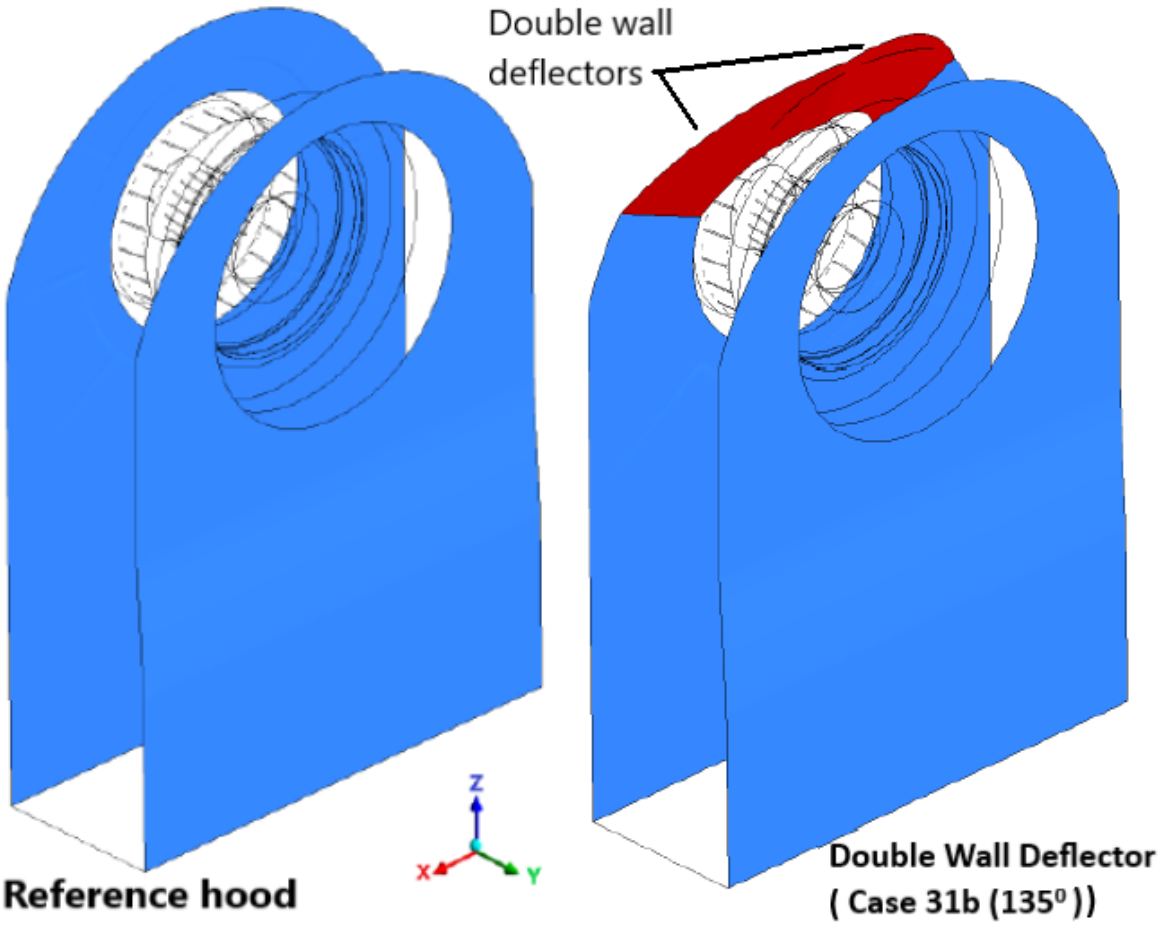

Figure 5.2 – Reference exhaust hood referred to as case 0 in this Chapter and best performing configuration referred to as case 31b whose angle between the double wall deflectors is 135° . The double wall deflectors shown in red are part of the outer casing. Both hoods are presented without the side walls for ease of visual comparison

Fig. 5.3 shows three deflector ideas (Front wall, Back wall and the Double wall) illustrated at the diffuser symmetry plane. These deflectors are included as part of the outer casing. As this is a simple illustration in 2D at the diffuser symmetry plane, the figure is to be viewed together with the 3D models of the same deflectors shown in Fig. 5.4 which shows the perspective views of the reference and the deflector configurations.

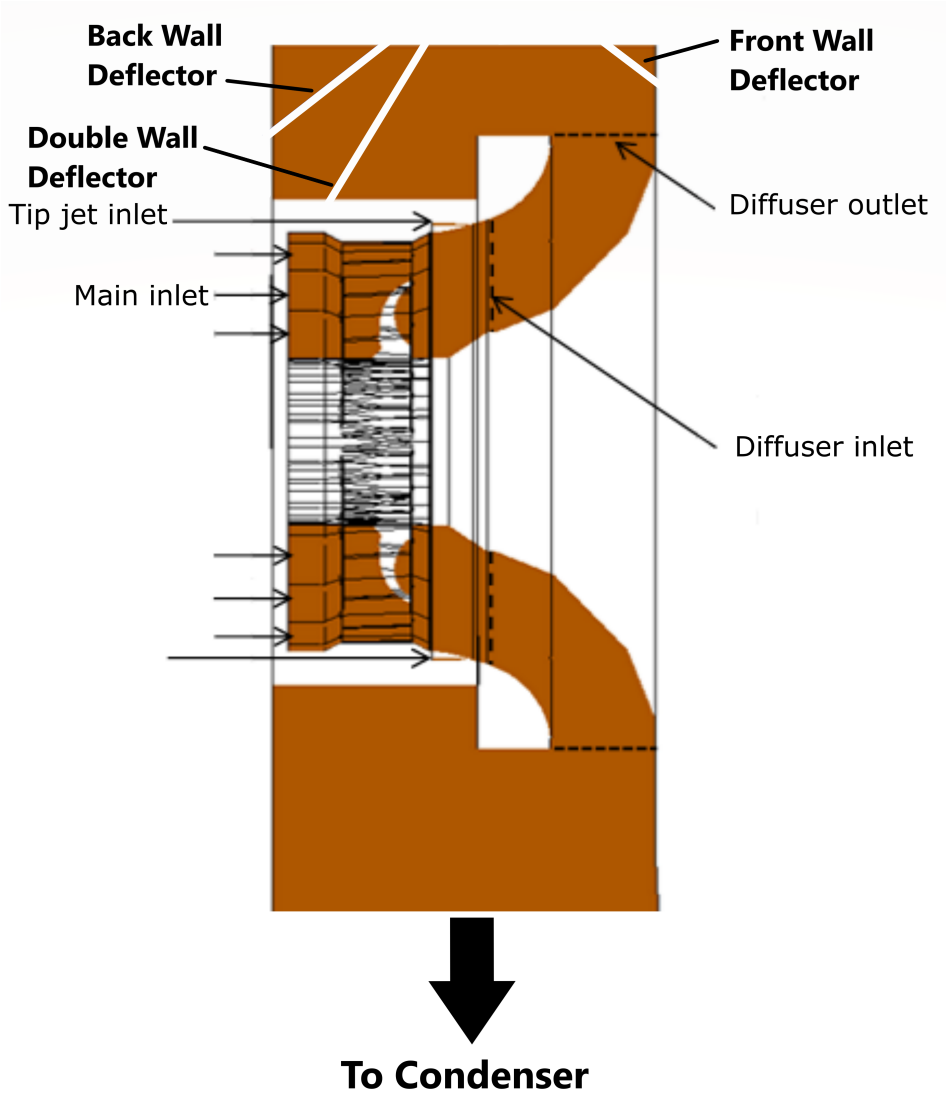

Figure 5.3 – Illustration of the deflector configuration ideas at the diffuser symmetry plane. Main color represent the diffuser symmetry plane for the reference configuration while the 3 white lines are included to illustrate the 3 deflector ideas

The three deflector ideas are described as follows:

- Case 1 (Front wall deflector)

  The initial configuration from front wall deflector idea is illustrated in Fig. 5.4b. The front wall deflector is expected to reduce the diffuser lip separation and vortex 1 shown in Fig. 5.1. Reducing the magnitude of vortex 1 would lead to reduction of

the blockage effect caused by this vortex and hence lead to improvement in performance. Similarly, a reduction in diffuser lip separation would lead to improved performance.

- Case 2 (Back wall deflector)

  The initial configuration from back wall deflector idea is illustrated in Fig. 5.4c. The back wall deflector is expected to gradually change the flow direction to a predominantly downward direction hence reduce the swirling intensity of vortex 2 shown in Fig. 5.1. In this case, the flow at the upper hood is better guided towards the condenser compared to the reference configuration. This is expected to lead to improved performance.

- Case 3 (Double wall deflector)

  The initial configuration of the double wall deflector idea is illustrated in Fig. 5.4d. The angle between the two deflector walls is 90°. This configuration is expected to improve performance since the flow at the topmost part of the upper hood meets a deflector surface at an angle hence giving it a favourable direction of flow to predominantly towards the condenser. This is expected to minimize the intensity of vortex 2 show in Fig. 5.1, which would lead to better performance.

Although the two vortices shown in Fig. 5.1 are shown in 2D at the diffuser symmetry plane, these vortices are 3D features that extend all the way to the condenser plane with some mixing at lower hood as is seen in Fig. 3.19a in chapter 3. Therefore, reducing the intensity of these vortices at the upper hood would result in minimized dissipation throughout the flow domain.

5.2.2 Numerical results validation and mesh independency

Steady state simulations are performed using ANSYS CFX Solver Release 17 using the Shear Stress Transport (SST) turbulence model. Justification for use of steady state simulation and the ideal gas model is given in detail in section 3.3.4 in Chapter 3. The y^+ values for the diffuser and exhaust hood walls are less than 1. Numerical results for the reference configuration (case 0) were already validated in chapter 3 both for design- and overload operating point for three tip jet Mach numbers of 0, 0.4 and 1.2 and good agreement was achieved between numerical and experimental results. 5 million elements are used for the diffuser and exhaust hood of the reference configuration. Since the domain volume for deflector configurations is reduced compared to the reference configuration (case 0), the deflector configuration meshes are expected to produce mesh independent results as well. Nevertheless, a mesh independency study was carried out for the best performing configuration (case 31b) at design load and tip jet Mach number of 0.4. Fig. 5.5 shows the result obtained from this mesh independency study, confirming mesh independency for the selected mesh size of 5 million elements.

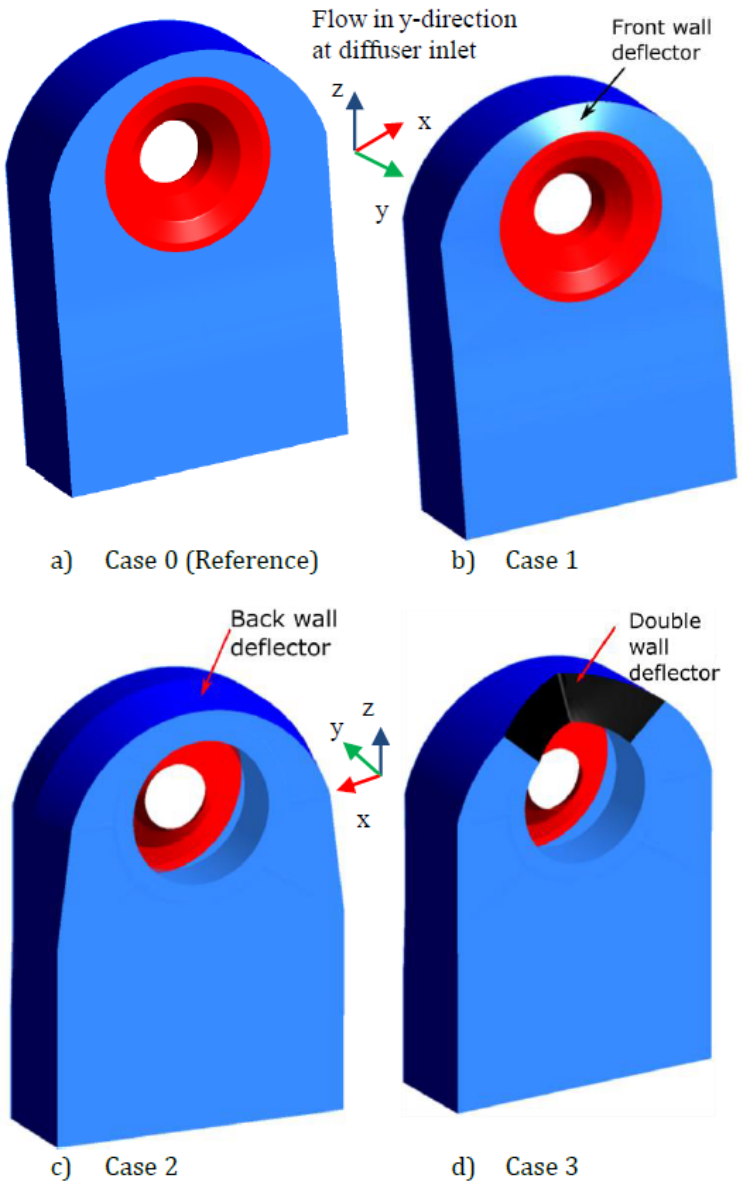

Figure 5.4 – Perspective views of the reference and deflector configurations

5.3 Results and discussion

The performance of the initial geometries of the three deflector configurations (shown in Fig. 5.4) relative to the reference configuration (case 0) is presented in Fig. 5.6. All the three deflector configurations indicate an improvement in performance at design load, at three tip jet Mach numbers (0, 0.4 and 1.2) except for case 1 (front wall deflector) at tip jet Mach number of 1.2 which records a slightly lower performance compared to the reference configuration. The front wall deflector is expected to improve performance by minimising the flow separation at the diffuser lip. At tip jet Mach number of 1.2, the diffuser lip separation is very low for the reference configuration, hence the poorer performance of the front wall deflector is not surprising at this operating point. The double wall

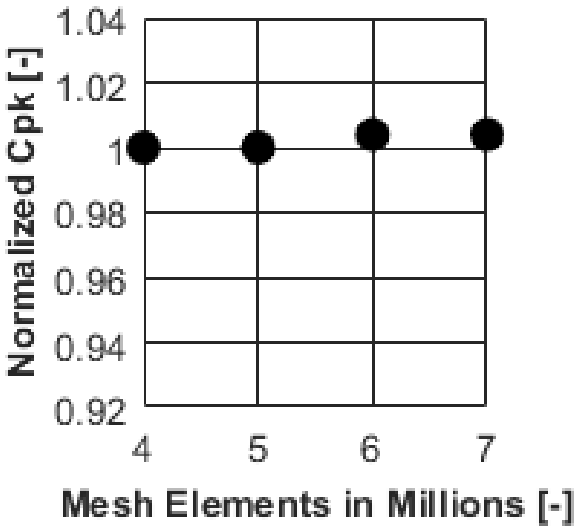

Figure 5.5 – Results of the mesh independency study for the best performing double wall deflector configuration (case 31b) at design load and Ma_{tip}=0.4.

deflector configuration (case 3) shows the highest performance improvement of 11% (at tip jet Ma=0), 19% (at tip jet Ma=0.4) and 6.3% (at tip jet Ma=1.2). Because of this higher performance compared to the front and the back wall deflectors for the initially tested cases, further modifications and simulations are based on case 3. The time required to modify the hood geometry and perform the simulations led to the decision to narrow the investigation to this higher performing configuration. It is possible that other variations of the front and the back wall deflectors could yield better performance compared to their initial results.

5.3.1 Modification of the double wall deflector (case 3)

Having shown the highest performance improvement compared to the other two deflector (front wall and back wall) configurations, the double wall deflector configuration was chosen for further investigation. A better approach would have been to investigate several configurations for each deflector type but due to the time required to create the new modifications and run the simulations, a decision was made to narrow down the investigation to this high performing double wall deflector configuration.

Two approaches are used to modify the double wall deflector configuration (case 3) which result into two groups of modifications:

- Group 1- configurations in this group are created by changing the angle between the walls of the double wall deflector (case 3) while maintaining symmetry. The position of the front edge remains unchanged while the two back edges are either moved closer or further from each other. Two additional cases are tested in this

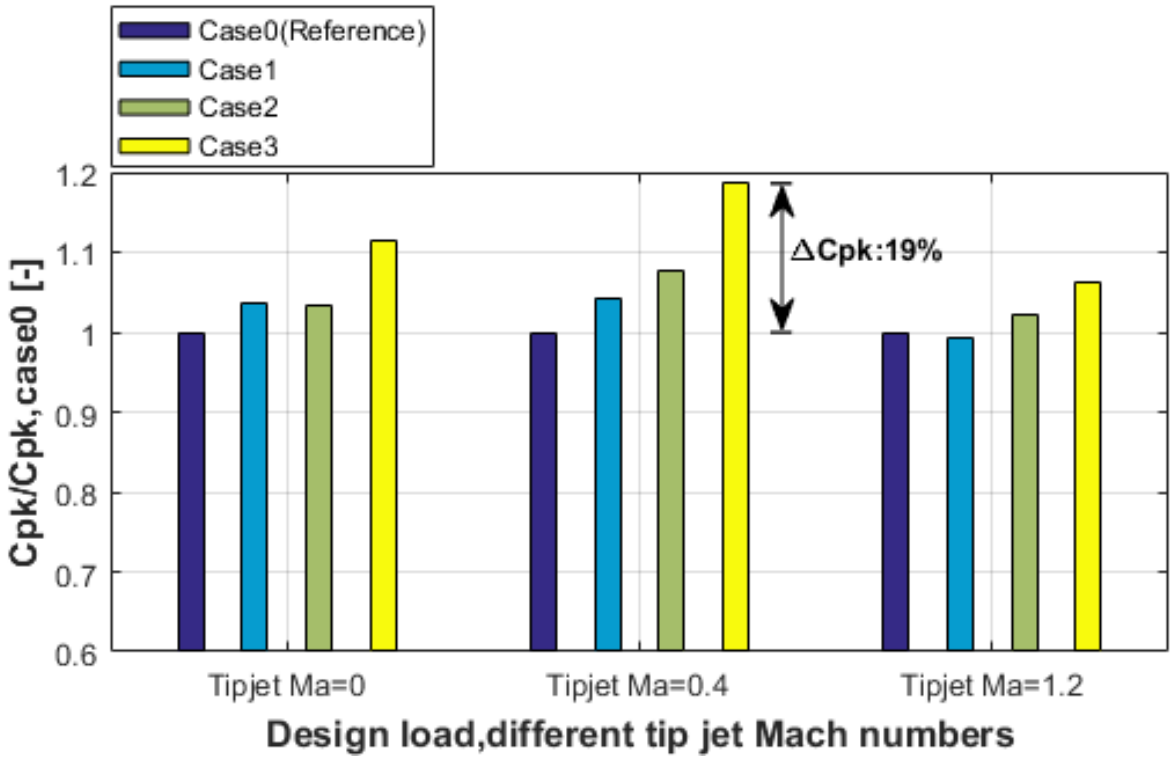

Figure 5.6 – Relative performance of initial deflector configurations as shown in Fig. 5.4.

group. The angle between the deflectors are 45° (case 31a), 90° (case 3) and 135° (case 31b). Fig. 5.7 shows perspective views of these three configurations.

- Group 2- configurations in this group are created by changing the position of the front edge of the double wall deflector (case 3) while maintaining symmetry. The position of the two back edges remain unchanged. In so doing, the angle between the deflector and the flow will change and the distance the flow has to travel before encountering the deflector also changes. Two additonal deflector configurations are created based on this modification of case 3 namely case 32a and case 32b.

Fig. 5.8 shows perspective and top views of the three configurations in group 2. A dimension labelled t (defined here as the length between the front wall of the hood and the front edge of the double wall deflector) on the top views is included to demonstrate that the configurations are significantly different from each other.

Case 3, which is the base configuration for the two groups of configurations shown in figures 5.7 and 5.8, is purposely repeated and placed accordingly to show a given sequence of modification. Figures 5.9 and 5.10 shows the performance of group 1 and group 2 configurations respectively relative to the reference configuration (case 0). As can be seen in Fig. 5.9, the double wall deflector performs poorly when the angle between the deflectors is low and at low tip jet Mach numbers. Although only three configurations with different angles between the deflectors (45°, 90° and 135°) are compared here, a trend is seen where the performance increases with increase in angle for tip jet Mach numbers of 0.4

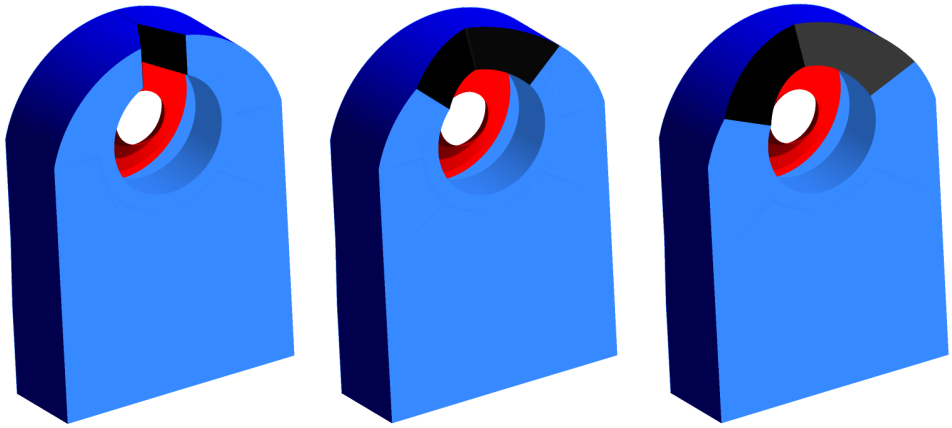

a) Case 31a (45°) b) Case 3 (90°) c) Case 31b (135°)

Figure 5.7 – Perspective views of group 1 modifications

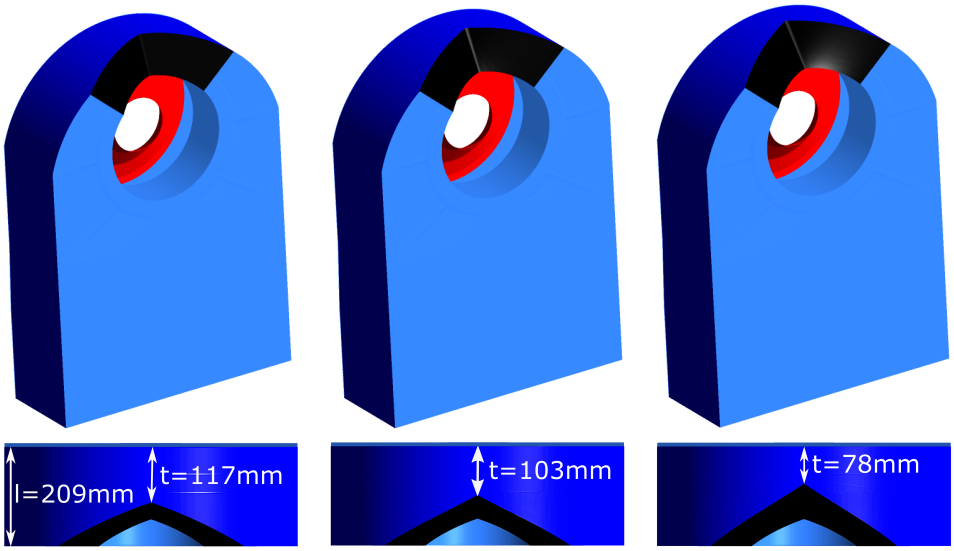

a) Case 3 b) Case 32a c) Case 32b

Figure 5.8 – Perspective and top views of group 2 modifications

and 1.2. The highest recorded performance improvement is 20% for case 31b with the highest angle between deflectors (135°) at tip jet Mach number of 0.4. Case 31b (with an angle of 135° between the deflector walls) and case 3 (with an angle of 90° between the deflector walls) though significantly different in geometry, record almost the same performance improvement suggesting that the performace is not so sensitive to the angle between the deflectors as long as the angle is above a certain value (low angle was found to cause performance deterioration like in case 31a whose angle between deflectors is 45°). However, more variations are required to make a more comprehensive conclusion.

Fig. 5.10 shows that cases 32a, 32b and 3, though significantly different in geometry as can be seen in Fig. 5.8, record almost equal performance improvement for all the three tip jet Mach numbers, again indicating some level of insensitivity to certain aspects of the double wall deflector. More modifications and testing are however required to make

a more comprehensive conclusion. As was the case for performance of group 1 modications shown in Fig. 5.9, the highest recorded performance improvement is 20% for case 32a at tip jet Mach number of 0.4.

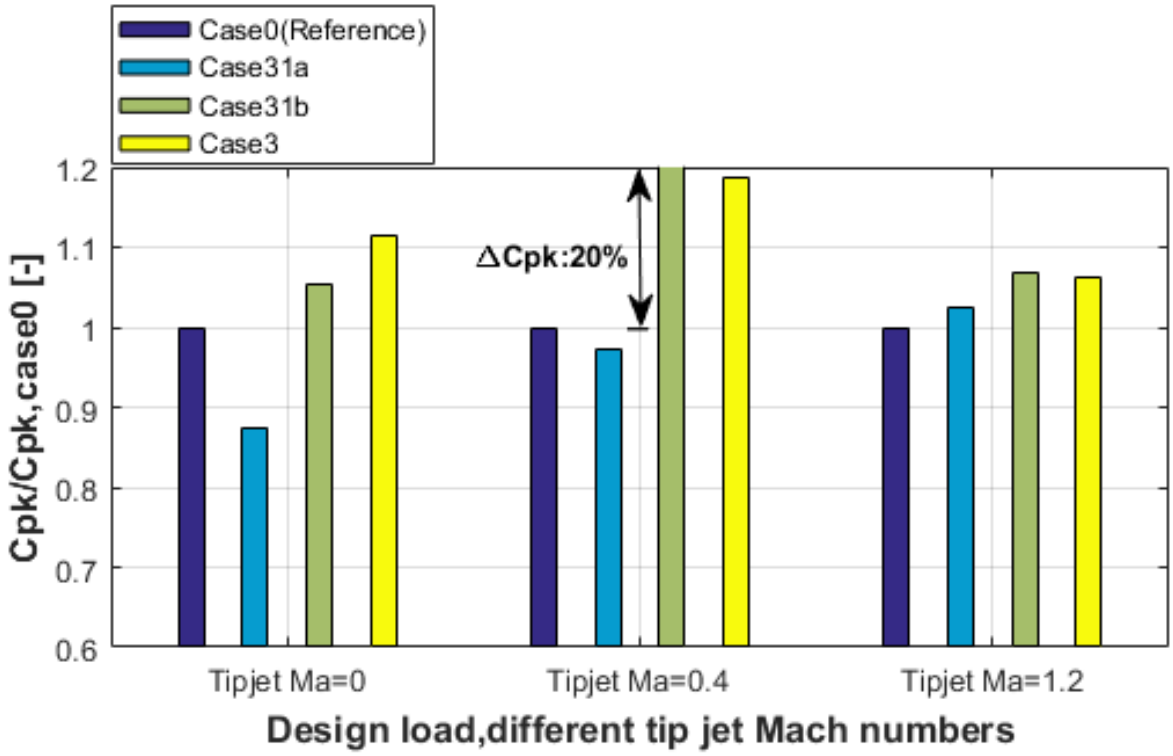

Figure 5.9 – Relative performance of group 1 configurations as shown in Fig. 5.7.

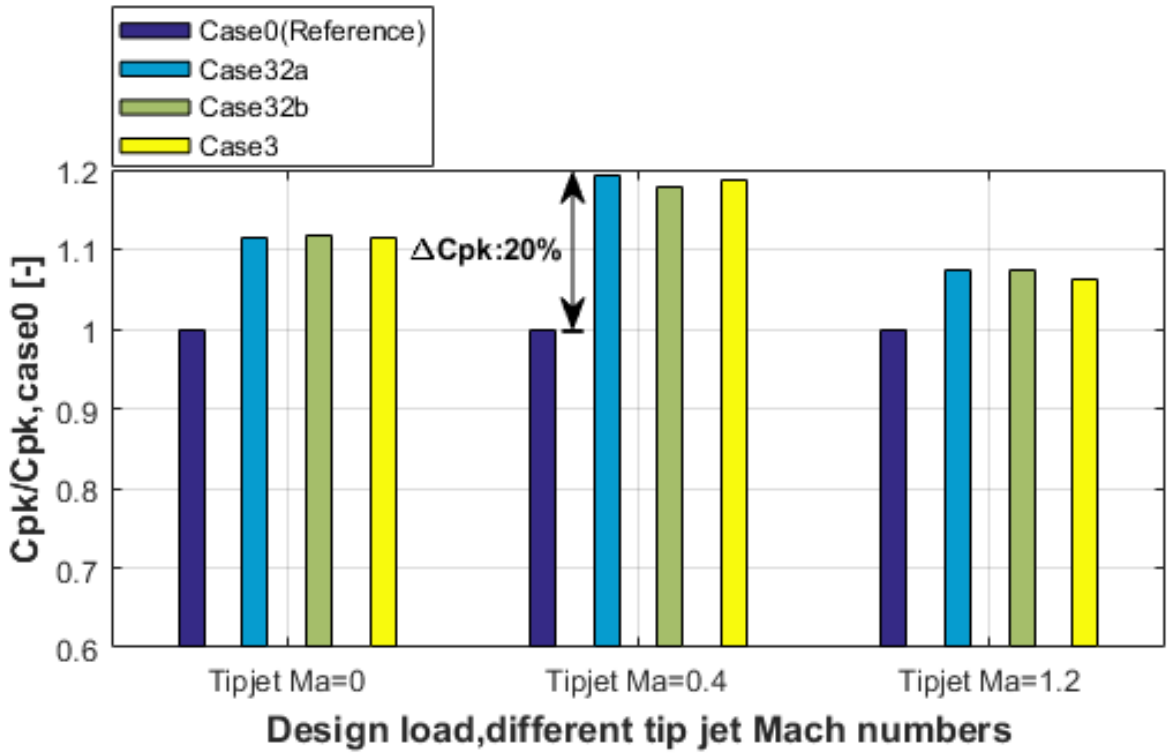

Figure 5.10 – Relative performance of group 2 configurations as shown in Fig. 5.8.

The best performing configuration at tip jet Mach number of 1.2 is case 32b which recorded a performance improvement of 7.5%. The performance improvement for higher tip jet Mach number is lower because at higher tip jet Mach number, the diffuser lip separation is very low, hence the flow exiting from the diffuser outlet is well diffused with lower residual kinetic energy. Because of this, its potential for loss generation along the flow domain is lower and hence a relatively lower improvement in performance is achieved by introducing the double wall deflector. Having recorded the highest performance improvement at tip jet Mach number of 0.4, case 31b is further tested at overload operating point. Fig. 5.11 shows its performance relative to the reference configuration (case 0) at tip jet Mach numbers of 0.4 and 1.2. Case 31b records a high performance improvement of 40% at overload and at tip jet Mach number of 0.4. However, at tip jet Mach number of 1.2, this configuration records a performance decline of 14%. Having registered a performance improvement of 7% at design load and tip jet Mach number of 1.2, this decline in performance at overload and tip jet Mach number of 1.2, further demonstrates the importance of knowing the expected operating point and tip jet Mach number of the turbine last stage as the exhaust hood is being designed. Otherwise, an optimal exhaust hood configuration can lead to massive losses in performance if the turbine is operated outside the design operating condition.

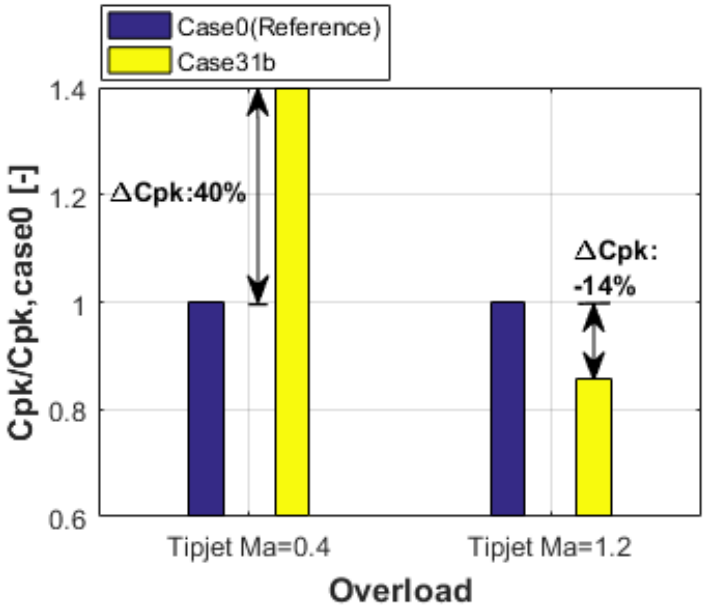

Figure 5.11 – Relative performance for case 31b as shown in Fig. 5.7c at overload.

5.3.2 Analysis of the impact of the double wall deflector on the flow

In order to investigate the underlying mechanisms for the substantial improvement of performance obtained by case 31b compared to the reference case, the methodology developed and presented in detail in chapter 3 is used. At various evaluation surfaces (see Fig. 3.12) the thermodynamic properties of the respective streamlines (originating from different diffuser inlet sectors) are averaged and the pressure recovery coefficient (Cp), the dissipation coefficient (ζ) and the residual kinetic energy coefficient (ξ) are calculated. Comparison of these coefficients along the flow domain for the two configurations reveals both the quantitative and qualitative influence of the double wall deflector. Fig. 5.12 shows the course of the three coefficients for the Topflows (Topflow, TopsideRflow and TopsideLflow) for the double wall deflector (case 31b) and the reference configuration (case 0). This figure clearly shows that the double wall deflector positively influences the behavior of the Topflows leading to improved performance. Compared to the reference configuration (case 0), the dissipation coefficient is significantly reduced along the entire flow domain for the double wall deflector (case 31b). The effectiveness of the geometry modification of case 31b can be deduced from the strongly reduced decrease in pressure recovery coefficient (Cp) of the Topflow towards the half-joint plane (position 3) and the subsequent drastic increase downstream. Instead of being dissipated, a large part of the kinetic energy of the flow is preserved and converted into potential energy below the half-joint plane (position 3). The residual kinetic energy coefficient for the topflow is initially higher for case 31b compared to the reference configuration (case 0). This demonstrates that the deflector walls indeed guide the flow and hence minimize the formation of vortices, which would otherwise reduce the overall flow velocity by dissipation. However, compared to the other two coefficients, the residual kinetic energy coefficient is least affected by the double wall deflector surfaces for the three topflows.

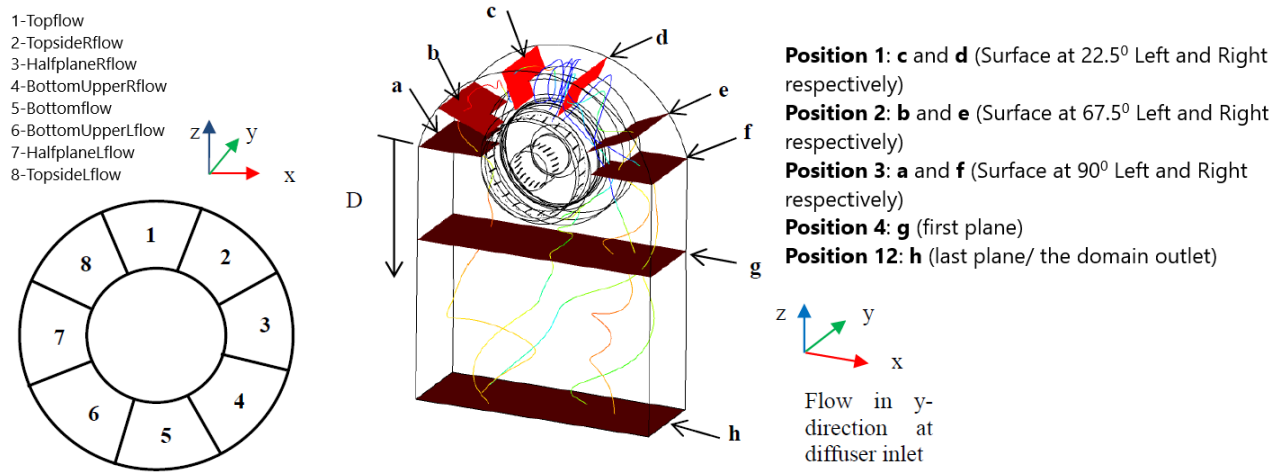

a) Nomenclature of eight diffuser inlet sector flows (Left) and various evaluation surfaces within the flow domain (Right)

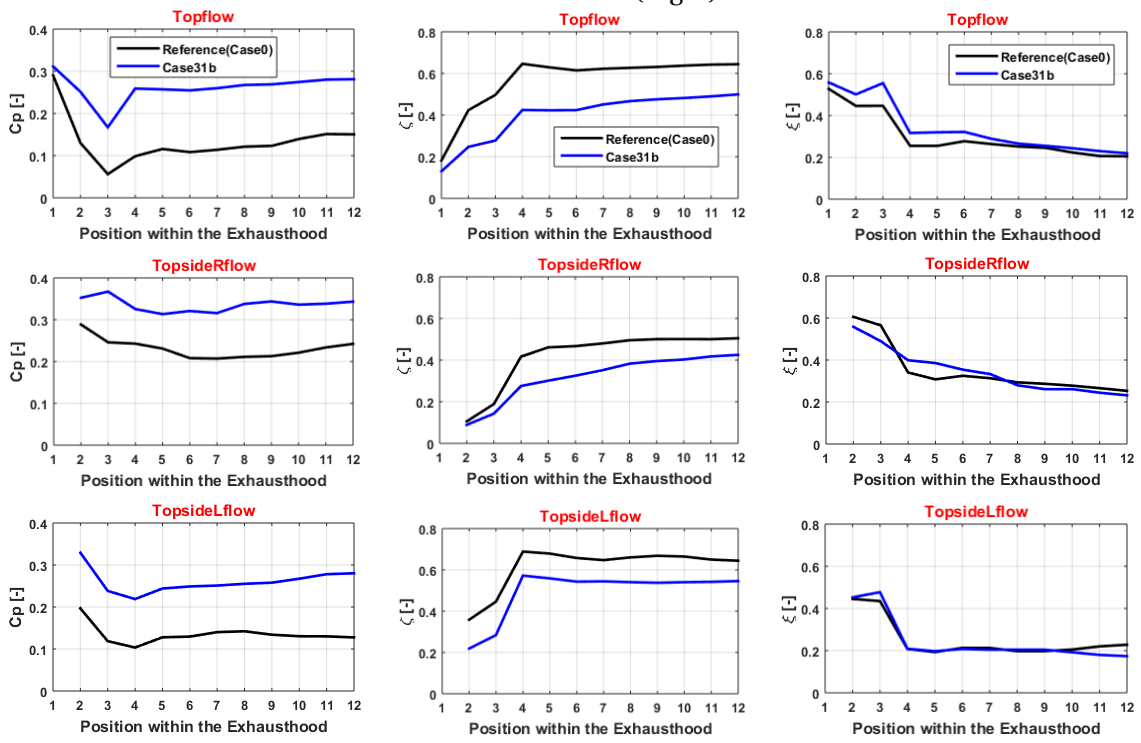

b) Pressure recovery (Cp) c) Dissipation (ζ) d) Residual kinetic energy (ξ)

Figure 5.12 – Coefficients comparison along the flow domain for topflows (Topflow, TopsideRflow and TopsideLflow) at design load and $Ma_{tip} = 0.4$. Numbers 1 to 12 represent evaluation surfaces along the flow domain.

The reduction in dissipation coefficient means that the deflector walls are able to reduce the intensity of the vortices formed within the exhaust hood as expected during their conceptualization. Considering the high change in dissipation coefficient profiles between case 31b and the reference configuration (case 0), it can be suggested that a proper design of the deflector walls with an optimum angle between them and possibly with varying profile along their length could yield even better results. In the current study, only symmetrical deflector configurations have been investigated because the meshes were generated for one half of the geometry in ICEM CFD for reasons of simplicity and then mirrored to give the full geometry. Considering that the flow is actually asymmetrical as earlier discussed in chapter 3, carefully designed asymmetrical deflector walls might produce even better results. Faster shape optimization approaches could be developed in the future to enable further optimization of the deflector shape at the upper hood for better performance realization.

Fig. 5.13 is a velocity vector plot at the diffuser symmetry plane for the two cases under comparison (case 0 and case 31b) at design load and tip jet Mach number of 0.4. This figure confirms that the double wall deflector (case 31b) minimizes the vortices seen for the reference configuration (case 0). The deflector configuration further eliminates diffuser lip separation.

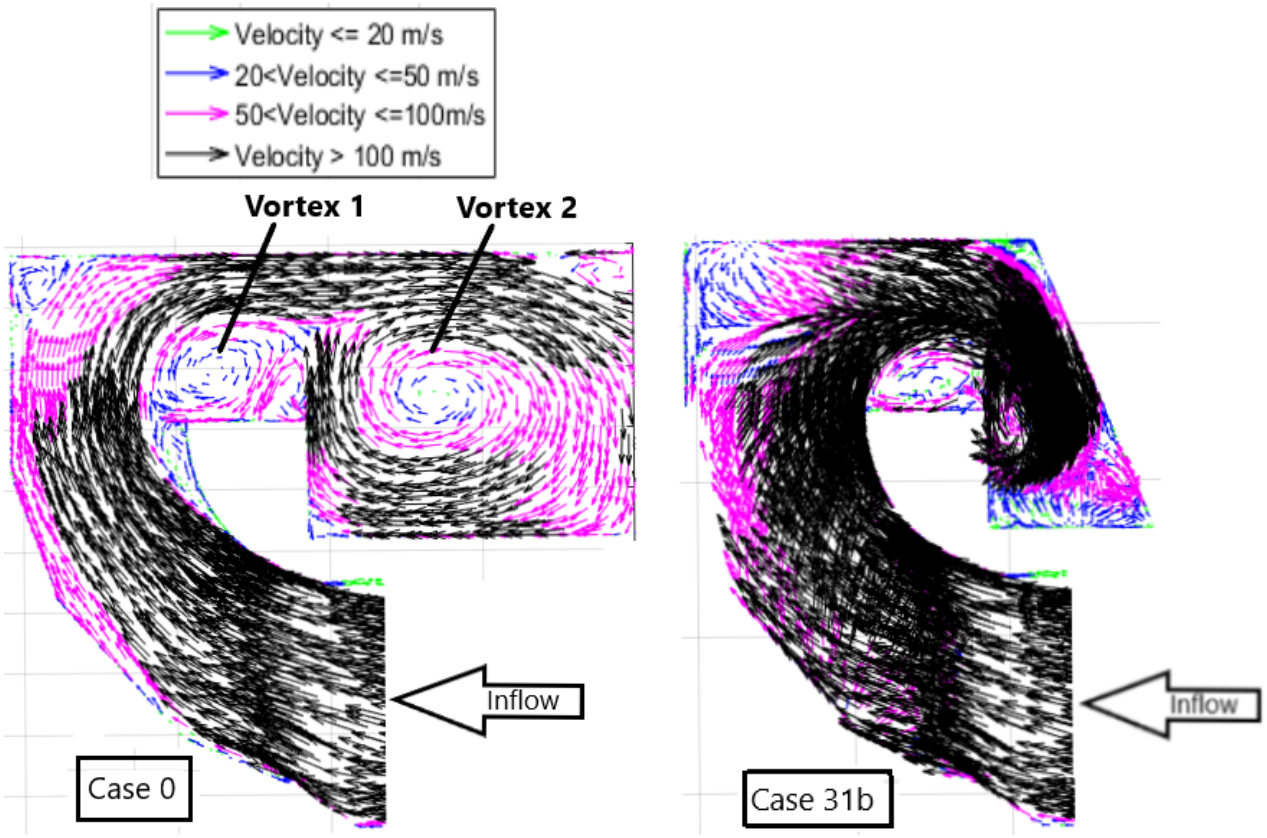

Figure 5.13 – v- and w-velocity vectors at the diffuser symmetry plane for the reference configuration (case 0) and the double wall deflector (case 31b) both at design load and Ma_{tip}=0.4

Fig. 5.14 shows the behavior of Topflows (Topflow, TopsideRflow and TopsideLflow) streamlines for the two configurations at design load and tip jet Mach number of 0.4. The streamlines are colored by static entropy. Comparing the respective Topflows for the reference configuration (case 0) and that of the double wall deflector configuration (case 31b), it can be seen that the deflector configuration lowers the swirling tendency of the streamlines and hence the entropy. This translates to improved performance (see Fig. 5.9).

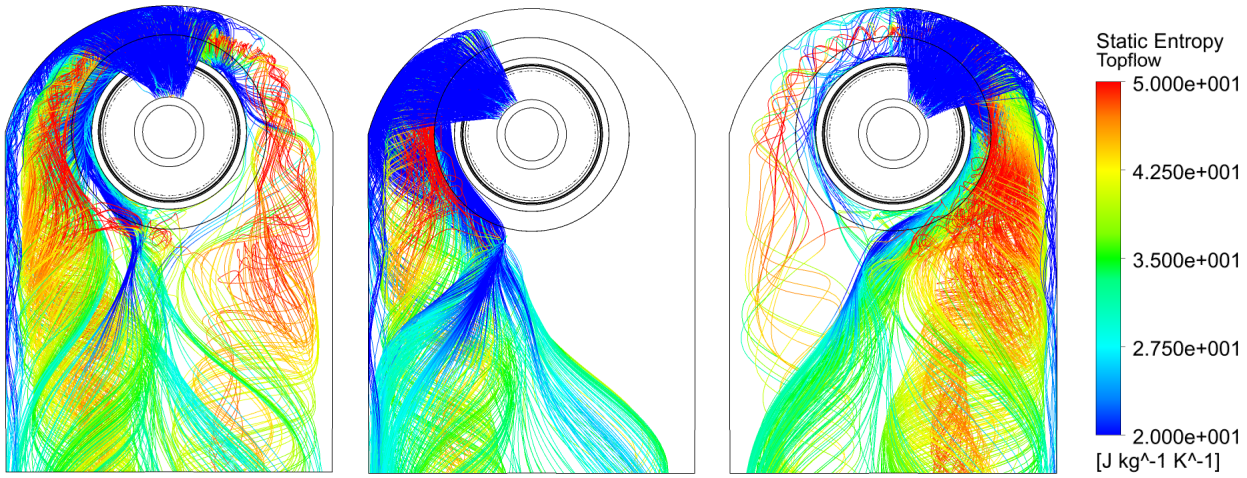

a) Case 0: Topflow (Left), TopsideRflow (Centre) and TopsideLflow (Right).

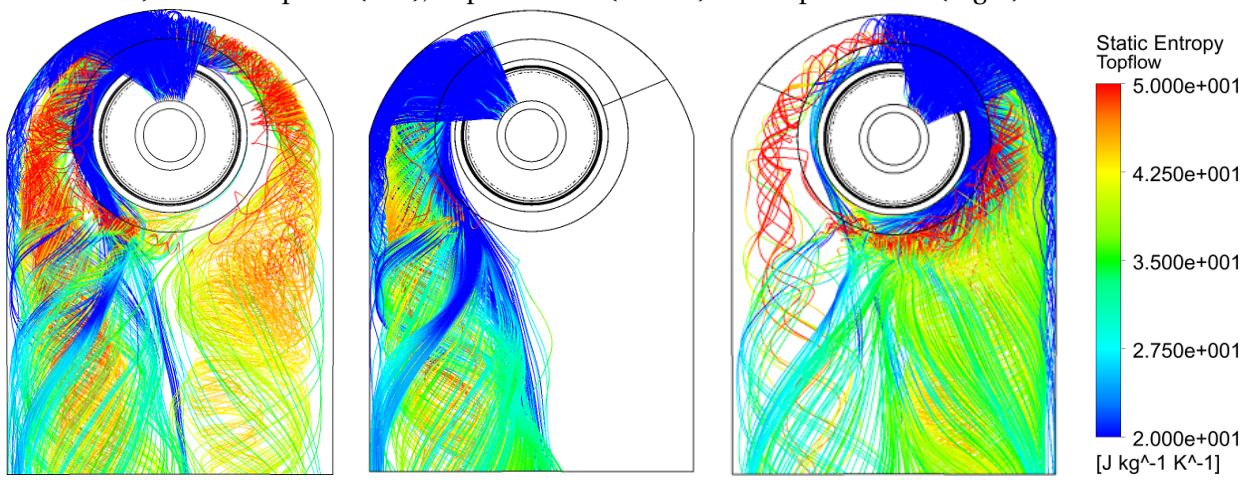

b) Case 31b: Topflow (Left), TopsideRflow (Centre) and TopsideLflow (Right).

Figure 5.14 – Topflows for the reference configuration (case 0) and the double wall deflector (case 31b) at design load and Ma_{tip}=0.4.

Fig. 5.15 shows a comparison of coefficients for the Bottomflows (HalfplaneRflow, HalfplaneLflow, BottomUpperRflow, BottomUpperLflow and Bottomflow) between the double wall deflector (case 31b) and the reference (case 0) configurations along the flow domain. This figure clearly shows that the double wall deflector has minimal influence on the behaviour of the bottomflows. This is expected since the double wall deflector is located at the topmost part of the exhaust hood and is designed to influence the topflows which were identified as the main contributors of loss in chapter 3. Looking at the dissipation coefficients for the bottomflows, the dissipation coefficient for the LHS flows

(HalfplaneLflow and BottomUpperLflow) is higher for case 31b compared to the reference configuration (case 0). This behaviour can be associated with the flow asymmetry since the RHS flows (HalfplaneRflow and BottomUpperRflow) have the dissipation coefficient for case 31b equal or less than that of the reference configuration.

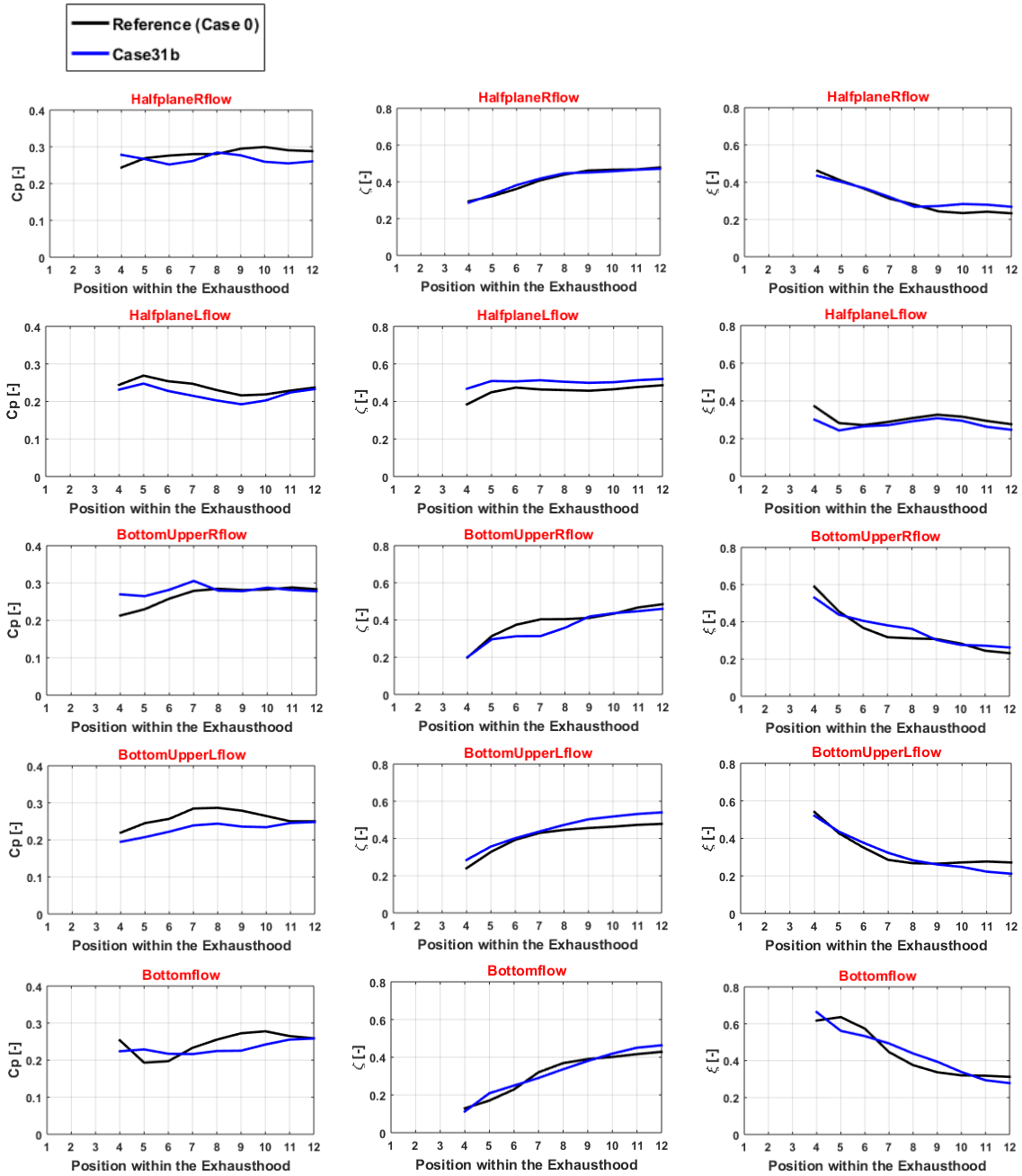

a) Pressure Recovery (Cp) b) Dissipation (ϵ) c) Residual Kinetic Energy (ξ)

Figure 5.15 – Coefficients comparison along the flow domain for bottomflows (HalfplaneRflow, HalfplaneLflow, BottomUpperRflow, BottomUpperLflow and Bottomflow) at design load and $Ma_{tip} = 0.4$. Numbers 1 to 12 represent evaluation surfaces along the flow domain as shown in Fig. 5.12.

The best performing hood configuration at design load (case 31b) numerically tested at overload and tip jet Mach number of 0.4 achieved a high improvement in performance of 40% compared to reference configuration (case 0) as was shown in Fig. 5.11. Fig. 5.16a shows velocity vector plots at the diffuser symmetry plane for these two configurations at overload and tip jet Mach number of 0.4.

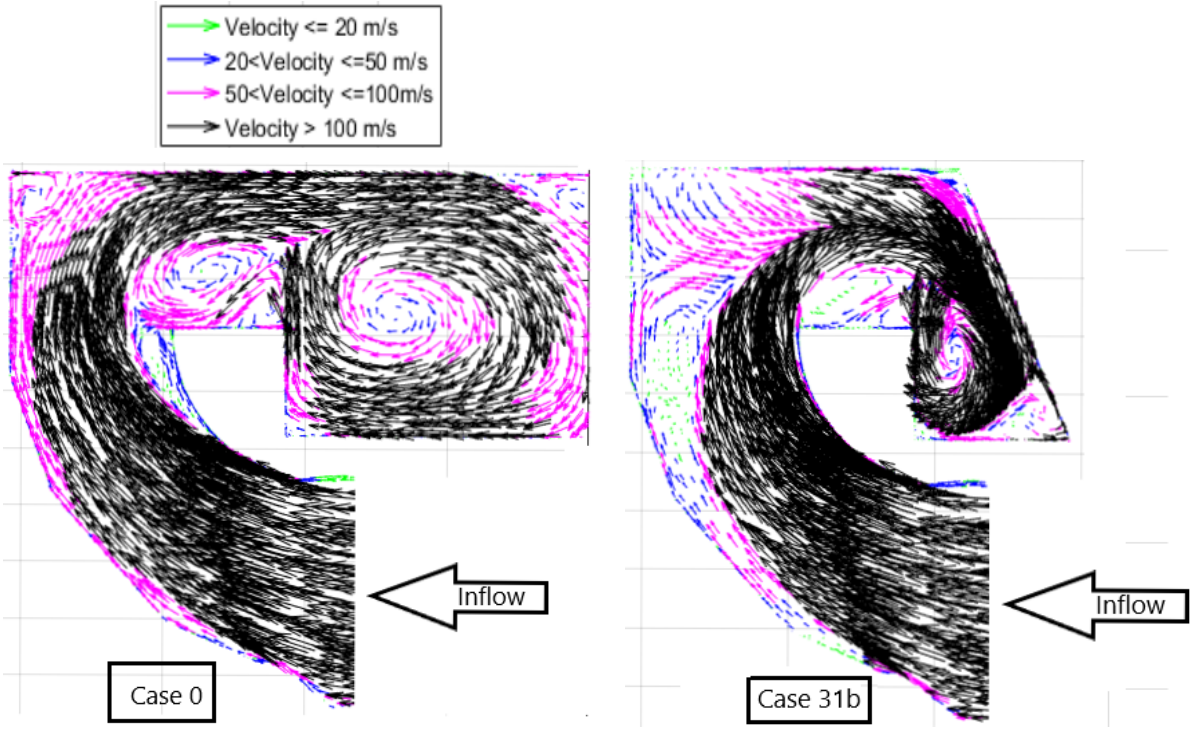

a) velocity vectors at overload and Ma_{tip} = 0.4

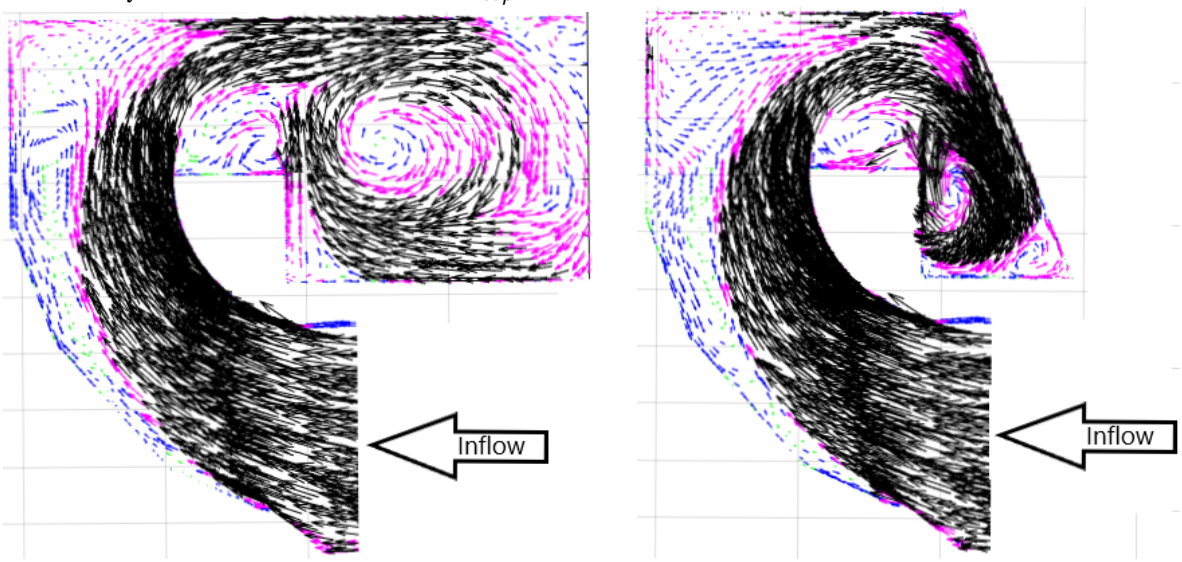

b) velocity vectors at overload and Ma_{tip}= 1.2

Figure 5.16 – v- and w-velocity vectors at the diffuser symmetry plane for the reference configuration (case 0) and the double wall deflector (case 31b) at overload (at Ma_{tip}= 0.4 and Ma_{tip}= 1.2).

Fig. 5.16a shows that at overload and tip jet Mach number of 0.4, the double wall deflector configuration (case 31b) eliminates the diffuser lip separation and also minimizes the intensity of vortex 1. It also prevents formation of vortex 2. This leads to a high improvement in performance for case 31b compared to the reference configuration (case 0) at this operating point. At overload and tip jet Mach number of 1.2, case 31b registers a performance decline of 14% compared to the reference configuration (see Fig. 5.11). Fig. 5.16b shows velocity vector plot at the diffuser symmetry plane for these two configurations at overload and tip jet Mach number of 1.2. This figure shows that the diffuser lip separation is already eliminated by the high intensity tip jet flow for the reference configuration (case 0) meaning that that the advantage associated with case 31b of minimizing the diffuser lip separation at low tip jet intensity is not realized at this operating point. At design load and tip jet Mach number of 1.2, case 31b registers about 7% performance improvement compared to reference configuration (case 0) as can be seen in Fig. 5.9, however at overload due to the higher mass flow and hence a higher residual kinetic energy at the diffuser outlet, the benefit associated with reduction in vortex intensity is overshadowed by the dissipation associated with the deflector walls.

5.4 Conclusions

The results presented in this chapter give some useful insights to exhaust hood designers. A number of deflector configurations have been numerically investigated at design load and at three tip jet Mach numbers (0, 0.4 and 1.2). The results show that deflectors included as part of the outer casing yield better performing exhaust hoods. The deflector surfaces minimize the intensity of vortices formed within the exhaust hood by directing the flow better towards the condenser and especially at the upper hood where the initial flow direction at the diffuser outlet is opposite the desired direction. A double wall deflector configuration (case 31b) recorded a high performance improvement of 20% and 40% at design- and overload for a tip jet Mach number of 0.4 (corresponding to shrouded last stage blades). It was shown that the deflectors for this case significantly lower the dissipation within the topflows (Topflow, TopsideRflow and TopsideLflow) by directing the flows and minimizing the intensity of the vortices formed. Performance improvement at tip jet Mach number of 1.2 (corresponding to unshrouded last stage blades) was moderate, the highest achieved improvement by the double wall deflector being around 7.5%. Apart from this, the main impact of the deflectors seems to be a reduction of outer diffuser lip separation, which leads to an improved pressure recovery towards the outlet of the axial-radial diffuser in the upper hood. For flows without pronounced diffuser separations, e.g. flow with high tip leakage flows, the deflectors only result in a minor improvement or partly even in a deterioration of exhaust hood performance as was seen for overload condition and tip jet Mach number of 1.2.

It is important to note that because of the many possibilities of the deflector configurations, they were not exhaustively investigated in this study. Therefore, future deflector investigations utilizing well designed shape optimization approaches may prove better performance improvement.

6 Conclusions, Recommendations and Future work

6.1 Conclusions

One important output of this thesis is its contribution to understanding the loss mechanism and effects of the swirling flow in LP turbine exhaust hoods. The known approach of flow visualization of dividing the diffuser inflow into sectors, used by Mizumi [46] and later by Yin [82], has been extended considerably by evaluating streamline properties at different planes, thus not only a visual impression of the flow can be obtained but rather a quantitative assessment of the flow is now possible. This new approach clearly shows where losses occur and therefore illustrates where improvements in design of LP turbine exhaust hoods should be made.

Having identified that most losses occur at the upper hood, it was important to investigate the influence of hood height variation on performance of LP turbine exhaust hoods. Increasing or decreasing the hood height especially above the diffuser is expected to have a significant impact on exhaust hood performance since this region of the exhaust hood is found to contribute significantly to the loss generation due to the complicated turning the flow is expected to make in order to move towards the condenser. Two groups of researchers, Finzel et al. and Taylor et al. [19, 70] have already shown that reduction in hood height leads to deterioration of LP turbine exhaust hood performance but no research has been done on the influence of hood height increase on performance. Using three tip jet Mach numbers (0, 0.4 and 1.2) and design load operating point for the main flow, fourteen different configurations with different heights have been calculated and analysed. The numerical results show that an increase in hood height results in an increase in exhaust hood performance up to an optimum height. Further increase in hood height beyond this optimum value results in performance decline. The optimum hood height was found to be different for each tip jet Mach number. This means that an optimized hood could perform poorly if the tip jet Mach number varied significantly (during operation) from that expected during design. This could occur either due to different ambient conditions under which the condenser is operating or after a retrofit project if optimized shrouded last stage blades are used to replace unshrouded last stage blades (the tip jet Mach number for unshrouded blades is supersonic while that of a shrouded blade could be as low as 0.4). In retrofit steam turbines projects, new last stage blades and diffuser are fitted into an existing exhaust hood [70]. The reduction in hood height in the current study was found to lead to decline in performance for the supersonic tip Mach number of 1.2. For the subsonic tip jet Mach numbers tested (0 and 0.4), reduction in hood height initially leads to improvement in performance but further decrease results in decline in performance. These trends for the various tip jet Mach numbers (0, 0.4 and

1.2) were consistent with experimental results obtained by Finzel et al. [19] though these researchers used different geometries and methodology to reduce the height. This striking resemblance of the Finzel et al. experimental results with numerical results obtained in this study for influence of hood height on performance of LP exhaust hoods proves the reliability of the numerical results obtained throughout this thesis. The Finzel et al. results were obtained over 5 years earlier using the same test rig used in the current study. Their goal was to reduce the exhaust hood area above the turbine axis which had the same effect as reducing hood by use of inserts within the upper hood.

Using the flow regime of the reference configuration and the loss mechanism knowledge acquired, an improved exhaust hood design with deflector surfaces incorporated at the upper hood as integral parts of the outer casing was investigated. The deflector surfaces are numerically shown to guide the flow and reduce the intensity of the resultant vortices which have been shown in this study as the main sources of loss in LP turbine exhaust hood flows. The blockage area of the vortex cores and diffuser separations have been shown to fairly correlate with the exhaust hood performance with an inverse relationship as expected. The improvement in performance of the exhaust hood due to the inclusion of a double wall deflector at the upper hood as part of the outer casing was seen to be highest the worse the performance of the reference hood under a given operating point, with the double wall deflector (case 31b) configuration registering a 40% improvement in performance for the overload operating point at tip jet Mach number of 0.4 (this operating point recorded the lowest Cp for the reference configuration for both the experiment and numerical simulation). The main impact of the deflector configuration seems to be a reduction of outer diffuser lip separation, which leads to an improved pressure recovery towards the outlet of the axial-radial diffuser in the upper hood. For flows without pronounced separation, e.g. flow with high leakage flows, the deflectors only result in a minor improvement or partly even in a deterioration of exhaust hood performance. This was an important observation since it might mean that the double wall deflector configuration could improve the performance of a number of poor performing (some real LP exhaust hoods record negative pressure recovery coefficient values) large scale LP steam turbine exhaust hoods in operation today regardless of the cause of their poor performance (in real LP steam turbine exhaust hoods, other than unfavorable diffuser inlet conditions, poor performance of exhaust hoods could be due to an axial-radial diffuser which is not optimally designed, influence of exhaust hood internal furniture and off-design condenser operating point). Another reason why this finding is important is that future demands on efficiency and operational diversity of steam turbines, call for usage of shrouded last stage blades in the LP turbines. This is aimed at minimizing tip leakage losses (hence increasing stage efficiency) and positively modifying blade oscillations and therefore increase operational availability [51]. For tip jet Mach number of 0.4 (corresponding to shrouded last stage blades), the double wall deflector configuration demonstrated a higher performance improvement of the LP turbine exhaust hood compared to the case of tip jet Mach number of 1.2 (corresponding to unshrouded last stage blades) both at design- and overload operating conditions. According to Stein et al. [64], a 10%-points improvement in pressure recovery roughly translates into a 1% improvement in last stage efficiency. This suggests that the improvement in performance of LP turbine exhaust hood of 20% and 40% at design- and overload respectively for a tur-

bine with shrounded last stage blades achieved by inclusion of a double wall deflector configuration at the upper hood is significant.

The experimental data for the reference configuration of the scaled LP turbine exhaust hood showed a good agreement with the numerical data obtained using the Shear Stress Transport (SST) turbulence model for both the design- and overload operating conditions. The few simulations performed for the reference configuration using the k-ϵ turbulence model confirmed the assertions from literature [7] that this turbulence model is not suited for flows where serious flow separation is expected, e.g. flow over curved surfaces, despite being used frequently in diffuser studies. The numerical results using the k-ϵ turbulence model showed over-predicted pressure recovery values compared to the experimental data. It should however be mentioned that the k-ϵ turbulence model was able to predict relatively well the general trend of the pressure recovery values between a low tip jet Mach number to a supersonic tip jet Mach number for the design load case (the only operating point tested with this turbulence model).

6.2 Recommendations and future work

Computational Fluid Dynamics (CFD) is used extensively in LP turbine exhaust hood design process. Compared to experimental testing, it is easier and cheaper to modify a configuration and simulate its performance. Therefore, an iterative approach could be employed by exhaust hood designers whereby after validating the numerical results of the reference configuration, modifications are carried out on the reference configuration based on an analysis of loss according to the proposed methodology in this thesis and then the process of modification and analysis is repeated until an optimum hood is obtained. The already reported double wall deflector configuration of the exhaust hood could act as the base configuration for future work or designers could try different configurations depending on their results of analysis of the reference configuration of the exhaust hood to be optimized.

It is important to note that because of the many possibilities of the deflector configurations, they were not exhaustively investigated in this study. Therefore, future deflector investigations utilizing well designed shape optimization approaches are necessary to prove better deflector performance. A more detailed numerical investigation on influence of deflector walls as part of the outer casing at the upper hood is recommended. The few deflector configurations investigated in the current study indicated considerable improvement in performance especially for the double wall deflector configuration (case 31b). Although the numerical results obtained throughout this thesis using steady state simulations and utilizing the Shear Stress Transport (SST) turbulence model proved to be reliable based on experimental results obtained in this study for the reference configuration and experimental results obtained in 2011 by Finzel et al. [19] for hood height variation, unsteady simulations can also be performed by researchers with enough computing resources to see how they compare with steady state simulations and experimental results.

The different optimum hood heights for different tip jet Mach numbers demonstrated in the current study underscores the importance of taking into consideration the expected operating tip jet Mach number for the installed turbine during the LP turbine exhaust hood optimization efforts. This is also important in retrofit projects where an existing exhaust hood is used with new optimized diffuser and last stage turbine blades. If the new turbine last stage has a different tip leakage flow regime (this is highly likely), this will result in serious exhaust hood losses since the exhaust box is not optimized to correspond to the new tip jet Mach number. Because of the new optimized diffuser, turbine blades and/or the reduced tip jet leakage, the stage efficiency is improved hence justifying the retrofit project, yet the performance improvement could probably be higher if the optimum hood design for the new tip jet was also introduced as part of the retrofit project.

It is expected that the next project in the axial-radial diffuser test rig at the Institute of Thermal Turbomachinery and Machinery Laboratory (ITSM) of the University of Stuttgart will validate through experiments a number of CFD simulation results obtained in this study on influence of hood height and deflector configurations. The experimental work to validate these numerical results is expected to be expensive in terms of materials for the test rig modifications and time requirement and are likely to be performed only if an industrial partner expressed interest in these results and provided funding. Although the reference scaled LP turbine exhaust hood was validated in the current work, it is important to demonstrate the performance improvement recorded by the double wall deflector configuration experimentally.

References

[1] Angel, F.; Kubiak, J.; Marino, C.; Marcinkowski, S.; Gardzilewics,A.: Experimental Investigation of Exhaust Losses of a Low Pressure Steam Turbine., : *Joint Power Generation Conference,volume 32, Pages 367-372, New York, USA*, June 2011

[2] ANSYS, Inc.: *ANSYS CFX, Solver Theory Guide, Release 15.0*, Nov. 2013

[3] Becker, S.; Gretschel, E.C.; Casey, M.: Influence of a Tip Clearance Jet on a Swirling Flow in an Axial-Radial Diffuser, in: *6th European Conference on Turbomachinery - Fluid Dynamics and Thermodynamics*, Lille, France, 07–11 March 2005

[4] Beevers, A.; Congiu, F.; Pengue, F.; Mokulys, T.: An Analysis of the Merits of CFD for the Performance Prediction of a Low Pressure Steam Turbine Radial Diffuser, in: *Proceedings of ASME Turbo Expo 2010: Power for Land, Sea and Air*, June 2010

[5] Benim, A.C; Geiger, M.; Doehler, S.; Schoenenberger, M.; Roemer, H: Modelling the Flow in the Exhaust Hood of Steam Turbines under Consideration of Turbine-Exhaust Hood Interaction, in: *VDI BERICHTE, 1185:343-357*, June 1995

[6] Burton, Z; Ingram, G.; Hogg, S.: A Literature Review of Low Pressure Steam Turbine Exhaust Hood and Diffuser Studies , in: *Journal of Engineering for Gas Turbines and Power, GTP-12-1424*, 2013

[7] Burton, Z.: *Analysis of Low Pressure Steam Turbine Diffuser and Exhaust Hood Systems*, Ph.D. thesis, Durham University, 2014

[8] Burton, Z.; Ingram, D.G.; Hogg, D.S.: A Generic Steam Turbine Exhaust Diffusor with Tip Leakage Modelling and Non-Uniform Hood Outlet., in: *Proc. 10th Europ. Conf. on Turbomachinery, Fluid Dynamics and Thermodynamics*, 2013

[9] Burton, Z.; Ingram, G.; Hogg, S.: The Influence of Condenser Pressure Variation and Tip Leakage on Low Pressure Steam Turbine Exhaust Hood Flows, *Proc. IMechE, Part A: J. Power and Energy*, 2014

[10] Burton, Z.; Ingram, G.L.; Hogg, S.: A Literature Review of Low Pressure Steam Turbine Exhaust Hood and Diffuser Studies, *Trans. ASME, J. Eng. Gas Turb. Power*, 2013

[11] Cerantola, D.J.: *Evaluation of Swirl and Tabs in Short Annular Diffusers*, Ph.D. thesis, Queen's University Kingston, Canada, 2014

[12] Cordova, M.; Stoffel, B.: Comparison of Various Turbulence Models in Respect to their Suitability for CFD Calculations of Diffuser Flows, In: ASME Turbo Expo, Barcelona, Spain. GT2006-90524, 2006

[13] Dejean, F.; Bourdonneau, L.; Duplex, J.: Three-dimensional Coupled Flow Calculations in a Low Pressure Steam Turbine Last Stage and Exhaust Hood, in: 2nd European Conference in Turbomachinery: Fluid Dynamics and Thermodynamics, Antwerpt, Belgium, March 1997

[14] Denton, J.D.: Loss Mechanisms in Turbomachines, *ASME Paper 93-GT-435*, 1993

[15] Denton, J.D.: Some Limitations of Turbomachinery CFD, in: *Proceedings of ASME Turbo Expo 2010: Power for Land, Sea and Air. GT2010-22540*, June Glasgow, UK, 2010

[16] Epiphanov, V.K.; Gaev, V.D.; Lisyanskii, A.S.; Kirillov, A.I.; Nikolaev, M.A.; Smirnov, E.M.; Zajtsev, D.K.: Effect of Deflector Vane Geometry on Performance of Large-Scale Turbine Exhaust Hood at Transonic Flow Conditions: Air-Test Experiments and 3D Numerical Simulation, in: *5th European Conference on Turbomachinery – Fluid Dynamics and Thermodynamics*, pp. 803–812, 2003

[17] Evans, C.: Precision Enineering: *An Evolutionary View, Kluver, Dortrecht, 1989*

[18] Fan, T.; Xie, Y.; Zhang, D.; Sun, B.: A Combined Numerical Model and Optimization for Low Pressure Exhaust System in Steam Turbine. In ASME Power Conference, San Antonio, Texas. POWER2007-22147,2007

[19] Finzel, C.; Schatz, M.; Casey, M.V.; Gloss, D.: Experimental Investigation of Geometrical Parameters on the Pressure Recovery of Low Pressure Steam Turbine Exhaust Hoods, in: *Proceedings of ASME Turbo Expo, Vancouver*, June 2011

[20] Fu, J.; Liu, J.; Zhou, S.: Experimental and Numerical Investigation of Interaction between Turbine Stage and Exhaust Hood, *Proc. IMechE, Part A: J. Power and Energy*, 221:991–999, 2007

[21] Fu, J.; Zhou, S.; Liu, J.: Experimental and Numerical Investigation of Interactions between Axial Turbine and Non-axisymmetric Exhust Hood, in: *Proceedings of ASME Turbo Expo*, 2008

[22] Fu, J.L.; Liu, J.J.: Influences of Inflow Condition on Non-axisymmetric Flows in Turbine Exhaust Hoods, in: *Journal of Thermal Science, 17(4):305-313*, 2008

[23] Fu, J.L.; Liu, J.J.: Investigation of Influential Factors on the Aerodynamic Performance of a Steam Turbine Exhaust System,in: *ASME Turbo Expo, Glasgow, UK. GT2010-22316*, 2010

[24] Fu, J.L.; Liu, J.J.; Zhou, S.J.: Unsteady Interactions Between Axial Turbine and Non-axisymmetric Exhaust Hood under different Operational Conditions, *Trans. ASME, J. Turbomach.*, 134(4):041002-1–041002-11, 2012

[25] GE. Powering industries,: *http://www.ge.com/stories/powering-industries/*, 2014

[26] Gray, L.; Sandhu, S.S.; Davids, J.; Southall, L.R.: Technical Considerations in Optimizing Blade-Exhaust Hood Performance for Low Pressure Steam Turbines, *ASME Joint Power Generation Conference*, pp. 89–97, Oct. 1989

[27] Gudkov, E.I.; Mikhailov, V.E.; Lisyanskii, A.S.; Nazarov, V.V.; Efifanov, V.K.; Baranovskaya, L.V : Comparison between the Results of Calculation and Experimental Aerodynamic Studies of the Exhaust Hoods Used in the Low-Pressure Cylinders of Steam Turbines of Nuclear Power Stations, *Thermal Engineering 59*, pp. 195-198, 2012

[28] Hoznedl, M.; Tajc, J.; Krejcik, J.; Bednar, L.; Sedlak, K.; Linhart, J.: Exhaust Hood for Steam Turbines-Single-Flow Arrangement. ,*Frontiers of Energy and Power Engineering in China, 3(3):321-329, 2009*

[29] Japikse, D.; Baines, N.C.: *Diffuser Design Technology*, Concepts ETI Press, 1998

[30] Kreitmeier, F.; Greim, R.: Optimisation of Blade-Diffuser Interaction for Improved Turbine Performance, in: *5th European Conference on Turbomachinery – Fluid Dynamics and Thermodynamics*, pp. 791–802, 2003

[31] Kumar, D.S.; Kumar, K.L.: Effect of Swirl on Pressure Recovery in Annular Diffusers, in: *Journal of Mechanical Engineering Science, 22(6):305-313,* 2003

[32] Liu, J.J.; Cui, Y.Q.; Jiang, H.D.: Investigation of Flow in a Steam Turbine Exhaust Hood with/without Turbine Exit Conditions Simulated, *Trans. ASME, J. Eng. Gas Turb. Power*, 125:292–299, Jan. 2003

[33] Liu, J.J.; Hynes, T.P.: The Investigation of Turbine and Exhaust Interactions in Asymmetric Flows, Part 1 - Blade-Row Models Applied, in: *Proceedings of ASME TURBO EXPO 2002*, Amsterdam, The Netherlands, June 2002

[34] Liu, J.J.; Hynes, T.P.: The Investigation of Turbine and Exhaust Interactions in Asymmetric Flows, Part 2 - Turbine-Diffuser-Collector Interactions, in: *Proceedings of ASME TURBO EXPO 2002. GT2002-30343*, Amsterdam, The Netherlands, June 2002

[35] MacDonald , A.T.; Fox, R.W.; Van Dewoestine, R.V.: Effect of Swirling Inlet Flow on Pressure Recovery in Conical Diffusers , in: *AIAA Journal, 9(10):2014-2018, 1971*

[36] Maier, R.; Wachter, J.: Shock-Induced Flow Oscillations in Steam Turbine Diffusers, in: *Journal of Turbomachinery, 110(2):173-180, 1988*

[37] Menter, F.; Carregal, F.; Esch, T.; Konno, B.: The SST Turbulence Model with Improved Wall Treatment for Heat Transfer Predictions in Gas Turbines, in: *Proceedings of the International Gas Turbine Congress*, Tokyo, 02–07 Nov. 2003

[38] Menter, F.R.: Influence of Freestream Values on k-ω Turbulence Model Predictions, *AIAA J.*, 30(6):1657–1659, 1992

[39] Menter, F.R.: Performance of Popular Turbulence Models for Attached and Seperated Adverse Pressure Gradient Flows, *AIAA J.*, 30(8):2066–2072, 1992

[40] Menter, F.R.: *Eddy Viscosity Transport Equations and their Relation to the k-ε Model*, Tech. Rep. NASA Technical Memorandum 108854, NASA Ames Research Center, Moffett Field, California, 1994

[41] Menter, F.R.: Two-Equation Eddy-Viscosity Turbulence Models for Engineering Applications, *AIAA J.*, 32(8):1598–1605, Aug. 1994

[42] Menter, F.R.: Turbulence Modelling for Turbomachinery, *QNET-CFD Network Newsletter*, 2(3):18–22, Nov. 2003

[43] Menter, F.R.; Kuntz, M.; Bender, R.: A Scale-Adaptive Simulation Model for Turbulent Flow Predictions, in: *41st AIAA Aerospace Sciences Meeting and Exhibit*, Reno, Nevada, USA, 06–09 Jan. 2003

[44] Menter, F.R.; Kuntz, M.; Langtry, R.: Ten Years of Industrial Experience With the SST Turbulence Model, *Int. Communications in Heat and Mass Transfer*, 4, 2003

[45] Messner, J.; Gretschel, E. Ch.; Wolf, U.: Abstroemung aus der letzten Turbinenstufe durch den Diffusor in den Kondensator,, *Int. final report to the AG-Turbo-Cooperative-Project GuD-Kraftwerk-500 MW auf einer Welle*,ITSM University of Stuttart,Stuttgart, 2003

[46] Mizumi, S.; Ishibashi, K.; Sawamura, Y.: Steam Turbine Exhaust Hood with Swirl Flow Separation Ducts, in: *Proceedings of ASME Turbo Expo*, June 2012

[47] Mizumi, S.; Ishibashi, K.: Design Philosophy and Methodoloy of a Low Pressure Exhaust Hood for a Large Power Steam Turbine , in: *ASME Turbo Expo, San Antonio, Texas, 2013*

[48] Munyoki, D.; Schatz, M.; Vogt, D.M.: Detailed Numerical Study of the Main Sources of Loss and Flow Behavior in Low Pressure Steam Turbine Exhaust Hoods, in: *Proceedings of ASME Turbo Expo 2017: Turbomachinery Technical Conference and Exposition*, June 2017, Charlotte, North Carolina, USA

[49] Munyoki, D.; Schatz, M.; Vogt, D.M.: Numerical Investigation of the Influence of Hood Height Variation on Performance of Low Pressure Steam Turbine Exhaust Hoods, in: *Proceedings of ASME Turbo Expo 2018: Turbomachinery Technical Conference and Exposition*, June 2018, Oslo, Norway

[50] Munyoki, D.; Schatz, M.; Vogt, D.M.: Numerical Investigation of the Influence of Flow Deflection at the Upper Hood on Performance of Low Pressure Steam Turbine Exhaust Hoods, in: *Proceedings of ASME Turbo Expo 2019: Turbomachinery Technical Conference and Exposition*, June 2019, Phoenix, Arizona, USA

[51] Musch, C.: *Beitrag zur gekoppelten Auslegung von Endstufen mit Deckband und anschließendem Diffusor in Niederdruck-Dampfturbinen*, Dissertation, Ruhr Universität Bochum, 2008

[52] Musch, C.; Stuer, H.; Hermle, G.: Optimization Strategy for a Coupled Design of the Last Stage and the Successive Diffuser in a Low Pressure Steam Turbine. Journal of Turbomachinery, 135(1):011013,2013

[53] Owczarek, J.A.; Warnock, A.S.; Bulanowski, E.; Polignano, V.; Rusak V.: Improvement of the Exhaust Hood Flow of a Low-Pressure Turbine. Technical Report, Electric Power Research Inst.,Palo Alto, CA (USA), 1990

[54] Polklas, T.: *Entwicklung eines Numerinchen Verfahrens zur Stroemungsmechanischen Auslegung des Abstroemgehaeuses einer Niederdruck-Dampfturbine*, Dissertation, University of Essen, 2004

[55] Ris, V.; Simoyu, L.; Galaev, S.; Gudkov, N.; Kirillov, V.; Smirnov, E.; Kirillov, A.; Ermolaev, V.: Numerical Simulation of Flow in a Steam Turbine Exhaust Hood: Comparison Results of Calculations and Data from a Full-Scale Experiment, *Journal of Thermal Engineering*, 56(4), 2009

[56] Schlichting, H.: *Boundary Layer Theory*, seventh edn., McGraw-Hill, 1979

[57] Schmiechen, P.: *Traveling Wave Speed Coincidence*, Ph.D. thesis, University of London, 1997

[58] Sieker, O.; Seume, J.R.: Influence of Rotating Wakes on Separation in Turbine Exhaust Diffusers, in: *8th International Symposium on Experimental and Computational Aerothermodynamics of Internal Flows*, Lyon, France, July 2007

[59] Solodov, V.; Gnesin, V.: Three-Dimensional Simulation of Non-Stationary Flow Phenomena in Last Stage Exhaust Hood Compartment, *Journal of Thermal Engineering*, 6(4), 1997

[60] Sovran, G.; Klomp, E.D.: Experimentally Determined Optimum Geometries for Rectilinear Diffusers with Rectangular, Conical or Annular Cross-Section, in: *Fluid Mechanics of Internal Flow, Elsevier Applied Science, 1st edn*, pp. 270–319, 1967

[61] Stanciu, M.; Marcelet, M.; Dorey, J.M.: Numerical Investigation of Condenser Pressure Effect on Last Stage Operation of Low Pressure Wet Steam Turbines, *In ASME Turbo Expo*, San Antonio, Texas 2013. GT2013-94070

[62] Stanciu, M.; Fendler, Y.; Dorey, J.M.: Unsteady Stator-Rotor Interaction Coupled with Exhaust Hood Effect for Last Stage Steam Turbines, *In 9th European Turbomachinery Conference*, Instanbul, Turkey, 2011. B035

[63] Stastny, M.; Ladislav, T.; Kolar, P.; Tucek, A.: Effect of Inlet Swirl on the Flow in a Steam Turbine Exhaust Hood, *Journal of Thermal Science*, 9(4):327–333, 2000

[64] Stein, P.; Pfoster, C.; Sell, M.; Galpin, P.; Hansen, T.: CFD Modeling of Low Pressure Steam Turbine Radial Diffuser Flow by using a Novel Multiple Mixing Plane Based Coupling - Simulation and Validation, in: *Proceedings of the ASME Turbo Expo 2015*, Montreal, Canada, 15–19 June 2015

[65] Szabo, I.: *Einfuehrung in die Technische Mechanik,8th ed., Springer,Berlin,1984*

[66] Tajc, L.; Bednar, L.; Polansky, J.; Gudkov, E.I.: Exhaust Hoods of Double-Flow Arrangement, in: *4th European Conference on Turbomachinery,Firenze, Italy*, 2001

[67] Tajc, L.; Bednar, L.; Sikova, I.; Feldberg, A.; Gudkov, E.I.: The Experimental Investigation of the Influence of the Flow Swirl and Tip Clearance Jet on Aerodynamic Characteristics of Exhaust Hoods, in: *Engineering Mechanics, Pages 1-10,* Svratka, Czech Republic, 2006. SKODA Power

[68] Tanuma, T.; Sasao, Y.; Yamamoto, S.; Niizeki, Y.; Shibukawa, N.; Saeki, H.: Aerodynamic Interaction Effects from Upstream and Downstream on the Down-Flow Type Exhaust Diffuser Performance in a Low Pressure Steam Turbine, *ASME Paper GT2013-95901*, 2013

[69] Tanuma, T.; Sasao, Y.; Yamamoto, S.; Takada, S.; Niizeki, Y.; Shibukawa, N.; Saeki, H.: Numerical Investigation of Exhaust Diffuser Performances in Low Pressure Turbine Casings, *ASME Paper GT2011-45677*, 2011

[70] Taylor, D.; Singh, G.; Hemsley, P.; Claridge, M.: Parametric Experimental and Numerical Study of LP Diffuser and Exhaust Hoods, in: *Proceedings of ASME Turbo Expo 2016: Turbomachinery Technical Conference and Exposition*, June 2016

[71] Thiemann, T.; Polklas, T.; Messner, J.: Abstroemung aus der letzten Turbinestufe durch den Diffusor in den Kondensator, : *Interim Report of the AG-Turbo-Cooperative-Project 500MW auf einer Welle, 8. Statusseminar of the AG Turbo, Sekretariat AG Turbo (Ed.) at Deutsches Zentrum fuer Luft- und Raumfahrt e.V. (DLR)*, Koeln-Porz, 2002

[72] Tindell, R.H.; Alston, T.M.:A Comparison of two Methods for Utilizing Steam Turbine Exhaust Hood Flow Data. Journal of Turbomachinery, 114(2): 398-401, 1992

[73] Tindell, R.H.; Alston, T.M.; Sarro, C.A.; Stegmann, G.C.; Gray, L.; Davids, J.: Computational Fluid Dynamics Analysis of a Steam Power Plant Low-Pressure Turbine Downward Exhaust Hood, *ASME PWR*, 13:43–55, 1991

[74] Tindell, R.H.; Alston, T.M.; Sarro, C.A.; Stegmann, G.C.; Gray, L.; Davids, J.: Computational Fluid Dynamics Analysis of a Steam Power Plant Low-Pressure Turbine Downward Exhaust Hood, Journal of Engineering for a Gas Turbines and Power, 118:214-224, 1996

[75] Truckenmueller, F.: *Stroemungsfeldmessungen am Endstufenversuchsstand,* , Internal Report, ITSM, University of Stuttgart, Stuttgart, 1997

[76] Versteeg, H.K.; Malalasekera, W.: *An Introduction to Computational Fluid Dynamics*, 2nd edn., Pearson Prentice Hall, 2007

[77] Verstraete, T.; Prinsier, J.; Di Sante, A.; Della Gatta, S.; Cosi, L.: Design Optimization of a Low Pressure Steam Turbine Radial Diffuser Using an Evolutionary Algorithm and 3D CFD, in: *Proceedings of ASME Turbo Expo*, June 2012

[78] Voelker, L.; Casey, M.; Neef, M.; Stueer, H.: The Flow Field and Performance of a Model Low Pressure Steam Turbine, : *6th European Conference of Turbomachinery, Fluid Dynamics and Thermodynamic*, Lille, France, 2005

[79] Uvarov, V.; Shkurikhin, I.; Molyakov, V.: Investigation of Joint Operation of Turbine Stages and of a Radial-Annular Diffuser with a Controlled Boundary Layer, in: *Thermal Engineering, 23(5):18-20, 1976*

[80] Wang, H.; Zhu, X.; Du, Z.: Aerodynamic Optimization for Low Pressure Turbine Exhaust Hood using Kriging Surrogate Model. International Communications in Heat and Mass Transfer, 37(8):998-1003,2010

[81] Xu, X.; Kang, S.; Hirsch, C.: Numerical Simulation of the 3D Viscous Flow in the Exhaust Casing of a Low-Pressure Steam Turbine, in: *Proceedings of ASME Turbo Expo: Land, Sea and Air*, no. 2001-GT-0487, June 2001

[82] Yin, M.; Yang, C.; Meng, L.; Yan, W. Zhuhai Z.; Li, J.; Feng, Z.: Numerical Analysis on the Swirl Flows in the Exhaust Hood of Steam Turbine and Optimization Design, in: *Proceedings of ASME Turbo Expo 2016: Turbomachinery Technical Conference and Exposition*, June 2016

[83] Yoon, S.; Stanislaus, F.J.; Mokulys, T.; Singh, G.; Claridge, M.: A Three-Dimensional Diffuser Design for the Retrofit of a Low Pressure Turbine Using In-House Exhaust Design System, in: *Proceedings of ASME Turbo Expo*, June 2011

[84] Zhang, W.; Paik, B.G.; Jang, Y.G.; Lee, S.J.; Kim, J.H.: Particle Image Velocimetry Measurements of the Three-Dimensional Flow in an Exhaust Hood Model of a Low-Pressure Steam Turbine, *Trans. ASME, J. Eng. Gas Turb. Power*, 129:411–419, 2007

[85] Zhou, S.; Liu, J.; Fu, J.: Experimental and Numerical Investigation of Interaction between Turbine Stage and Exhaust Hood, *Journal of Power and Energy, Proceedings of the Institution of Mechanical Engineers*, 2007

[86] Zimmermann, C.: Experimentelle Bestimmung des Stroemungsfeldes im Bereich der Endstufe und des anschliessenden axiradialen Diffusors einer ND-Modellturbine, *Mitteilungen des ITSM , Vol.41, ITSM, University of Stuttgart, Stuttgart*, 1995